AN NMR STUDY OF MEMBRANE TRANSPORT BY IONOPHORIC COMPOUNDS

Sina Sareth

A Thesis Submitted for the Degree of PhD
at the
University of St Andrews

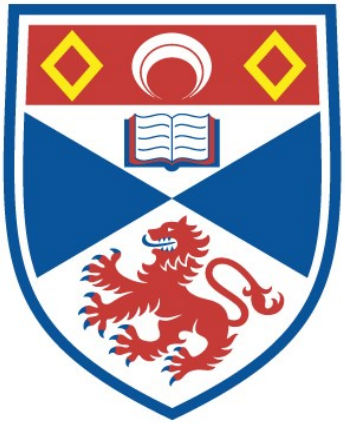

1998

An NMR Study of membrane transport by ionophoric compounds

Sina Sareth

A thesis submitted for the degree of Doctor of Philosophy

Faculty of Science, University of St. Andrews

February 1998

A la mémoire de mes grand-parents

Il existe deux forces dans la Nature:
la force des Hommes et la force des Choses. Rien de bien ne se crée quand ses deux forces s'opposent.

François René de Chateaubriand

Le plus simple écolier d'aujourd'hui sait des vérités auxquelles Archiméde eût sacrifié sa vie.

Ernst de Renan

Acknowledgements

Being a student at the University of St. Andrews has given me the privilege and the opportunity to encounter people who have changed my entire life.
In these following fews lines, I would like to thank Dr. Frank Riddell for his constant support, time and availability through the three years of my PhD.
I am indebted to Prof. G. Jeminet (France), Dr. A-M Delors (France), Prof. Leo Paquette (U.S.A), Prof. A Davis (Ireland) for providing ionophoric compounds for studying throughout this thesis.
Finally, I would like to thank different peoples for their friendship, time, and moral support: Drs. T. Bond, J. Wilkie, C. T. Weller, L. Hill, T. Kahane, M-F Giraud, Janet Esterhuizen and Pui Shan Chou.

Remerciements

Je voudrais en quelques lignes porter mes vibrants et chaleureux remerciements à mes parents et ma sœur Sineth pour le soutien moral et financier, pour l' amour inconditionnel témoigné lors de mon parcours universitaire et social. Comme aimait repéter mon père, la phrase de Jean-Jacques Rousseau disant qu' il n' y a pas de bonheur sans vertus, il n' y a pas de courage sans combats.
Modestement en ces quelques lignes, je voudrais leur témoigner de ma sincère gratitude et de mon profond amour.

Declarations

I, Sina Sareth, hereby certify that this thesis is of my own composition and that it is based upon the results of my own work. Work other than my own is clearly indicated in the text by reference to the relevant researchers or to their pulblications. This thesis has not in whole, or in any part, been previously presented for any other degree or professional qualifications.

I was admitted as a research student in October 1994 and as a candidate for the degree of Doctor of Philosophy in October 1994; the higher study for which this is a record was carried out in the University of St. Andrews between 1994 and 1997.

Date 16/02/98 Signature of candidate

I hereby certify that the candidate has fulfilled the conditions of the Resolution and Regulations appropriate for the degree of Doctor of Philosophy in the University of St. Andrews and that the candidate is qualified to submit this thesis for that degree.

16-02-98

Date Signature of supervisor

Abstract

The first part of this thesis consists of a study of the transport of alkali metal cations across model biological membranes mediated by ionophoric antibiotic cationomycin. The transport rates were measured by ^{23}Na and ^{39}K NMR using large unilamellar vesicles (LUVs) prepared from phosphatidylcholine and were compared with results obtained using red blood cells. These kinetic studies have established that there is a 1:1 complex between alkali cations and the cationomycin during the transport process. The transport rate measured are comparable to those of other ionophoric antibiotics studied previously. Cationomycin transports potassium cation more rapidly than sodium cation, and forms a more stable complex with potassium cation. The rate limiting step in the transport process is release of the cation at the membrane surface.

The second part involves the study of spirotetrahydrofuran analogues as potential alkali cation transporters. A set of new synthetic ionophoric materials designed to resemble to some degree the naturally occuring ionophoric antibiotics was investigated. The kinetic rates of these compounds were measured in phosphatidylcholine LUVs by an NMR study of $^{7}Li/^{23}Na$ exchange. However, these compounds are much poorer transporters than the ionophoric antibiotics which are 10^4 times faster under similar conditions.

The third part of this project deals with the study of the transport of halide anions by steroid-based anionophores. The transport rates of these compounds were measured by an NMR study of $^{35}Cl/^{81}Br$ exchange in phosphatidylcholine LUVs. This preliminary study indicates a close relationship between the lipophilicity of the different anionophores and the transport rates of different halides anions through the model membrane.

The final part of this thesis involves the total assignment of the ^{1}H and ^{13}C NMR spectra of the ionophoric antibiotic tetronasin by utilising two dimensional NMR techniques such as COSY 45, Relay COSY, DQF COSY, TOCSY and HSQC.

Abbreviations

ADP	Adenosine diphosphate
ATP	Adenosine triphosphate
COSY	COrrelation SpectroscopY
CW	Continuous wave
DANTE	Delays Alternating with Nutations for Tailored Excitattion
DEPT	Distortionless Enhancement Polarisation Transfer
DQFCOSY	Double Quantum Filtered Correlation SpectroscopY
HOHAHA	Homonuclear Hartmann-Hahn
HSQC	Heteronuclear Single Quantum Coherence Spectroscopy
I	Quantity of ionophore
i	Current of Na^+ or K^+
IC_{50}	Inhibitory Concentration requires to inhibit parasite growth by 50%
INADEQUATE	Incredible Natural Abundance Double Quantum Transfer Experiment
INEPT	Insensitive Nuclei Enhanced by Polarisation Transfer
k	Kinetic constant of transport
LUV	Large Unilamellar Vesicles
P	Phosphate
PC	Quantity of Phosphatidylcholine
MIC	Minimum Inhibitory Concentrations
$[^mHA]$	Ionophore concentration in the membrane
$[^tHA]$	Analytical ionophore concentration in thw whole suspension
^mV	Volume of the membrane
MW	Molecular weight
NMR	Nuclear Magnetic Resonance
nOe	Nuclear Overhauser Effect
NOESY	Nuclear Overhauser Effect SpectroscopY
RBC	Red Blood Cells
RF	Radio Frequency
rOe	Rotating frame Overhauser Effect
ROESY	Rotating frame Overhauser Effect SpectroscopY
T_1	Spin-lattice or longitudinal relaxation
T_2	Spin-spin or transverse relaxation
TOCSY	TOtal Correlation SpectroscopY

CONTENTS

List of Figures and Tables

Chapter 1

Chapter 2

Chapter4

Chapter 5

Chapter 1

Chapter 2

Chapter 1
General introduction

1.1 Introduction

1.1.1 The structure of the plasma membrane

Biological membranes consist largely of protein and lipid.[1] The lipids are mainly phospholipid (Figure 1.1), the ratio (by weight) of protein to lipid varying from 0.25 in myelin to ~ 3.0 in bacterial membranes. A 1:1 ratio by weight may be regarded as typical. In addition, small amounts of carbohydrates (<5%) are present. Because of its hydrophobic interior, the lipid bilayer is a highly impermeable barrier to most polar molecules and, therefore, prevents most of the water-soluble contents of the cell from escaping. Cells must ingest essential nutrients and excrete metabolic waste products. Many of the membrane proteins mediate these transport processes. They must also regulate intracellular ion concentrations, which means transporting specific ions in or out of the cell.

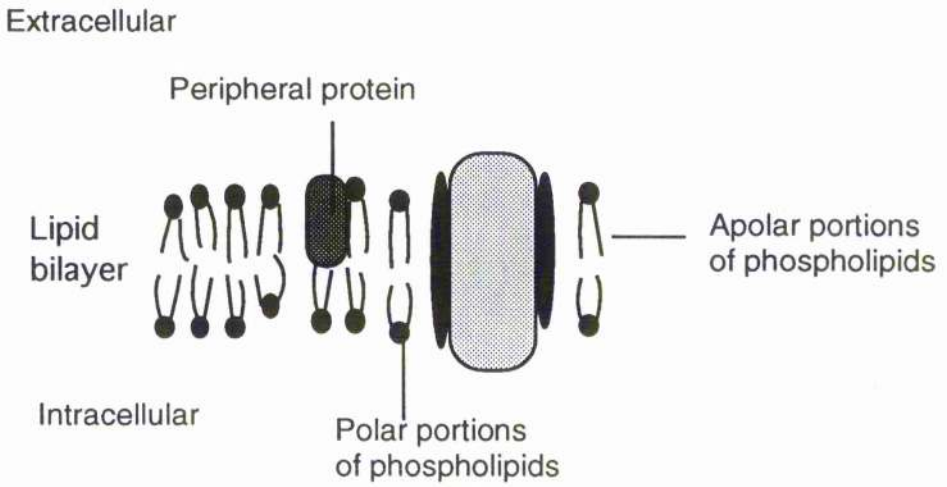

Figure1.1 Schematic diagram of membrane structure.

The distribution of different kinds of lipids[2] varies between membranes. However, phospholipids are always present from 40% to over 90% of the total lipid. Five types of phospholipids predominate: phosphatidylcholine, phosphatidylethanolamine, phosphatidylserine, cardiolipin (diphosphatidyl-glycerol) and sphingomyelin (Figure 1.2).

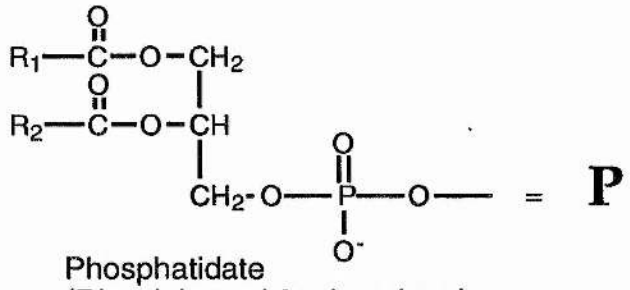

Phosphatidate
(Diacylglycerol 3- phosphate)

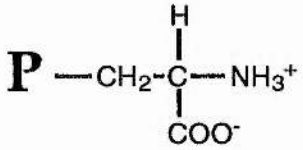

Phosphatidyl serine

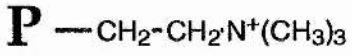

Phosphatidyl choline

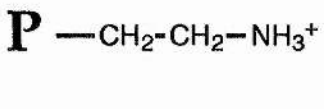

Phosphatidyl ethanolamine

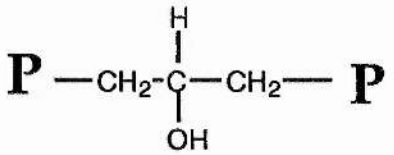

Cardiolipin
(Diphosphatidyl glycerol)

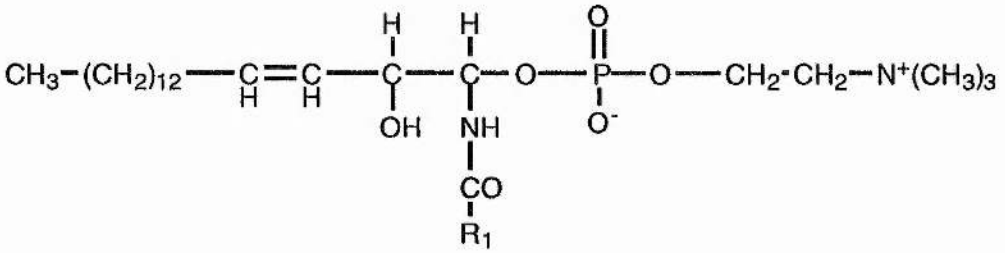

Sphingomyelin

Figure 1.2 Five of the commonly encountered phospholipid groups.

1.1.2 The permeability of the membrane

Given enough time, any molecule will diffuse across a synthetic or biological membrane. However, the rate of diffusion of a molecule depends enormously on its size and its solubility in hydrophobic solvents. In the general case, the smaller the molecule and the more soluble it is in a lipid solvent (that is, the more hydrophobic or nonpolar it is), the more rapidly it will diffuse across a lipid bilayer. Small nonpolar molecules, such as O_2, readily dissolve in lipid bilayers and, therefore, rapidly diffuse across them. Uncharged polar molecules also diffuse rapidly across a bilayer if they are small enough. For example, CO_2, ethanol and urea cross rapidly; glycerol less rapidly; and glucose hardly at all. Importantly, water diffuses very rapidly across lipid bilayers even though water molecules are insoluble in oil. This is because water molecules have a very small volume and are uncharged.

In contrast, lipid bilayers are highly impermeable to all charged molecules (ions), no matter how small: the charge and high degree of hydration of such molecules prevents them from entering the hydrophobic interior of the bilayer.

Components	Intracellular concentration (mM)	Extracellular concentration (mM)
Cations		
Na^+	5-15	145
K^+	140	5
Mg^{2+}	0.5	1-2
Ca^{2+}	10^{-4}	1-2
H^+	$8x10^{-5}$ (pH7.1)	$4x10^{-5}$ (pH7.4)
Anions		
Cl^-	5-15	110

Table 1.1 Comparison of ion concentrations[3] inside and outside of a typical mammalian cell.

Table 1.1 illustrates that the concentrations of Na^+ and K^+ are reversed inside and outside a typical mammalian cell. Therefore, the Na^+ ion tends to enter the cellular cytoplasm and the K^+ tends to move out from the cell. Alkaline earth metals are present in much smaller concentrations than alkali metal cations.

1.1.3 The transport through the membrane

Based on the energy requirements of the process, it is simple to classify two modes of transport. The first type of transport does not involve an input of energy and is called passive transport. The second one involves an input of energy and is termed active transport[4] (see Figure 1.3).

1.1.3.1 Passive transport

If the transported molecule is uncharged, only the difference in its concentration on the two sides of the membrane (its concentration gradient) determines the direction of passive transport.
If the solute carries a charge, however, both its concentration gradient and the electrical potential difference across the membrane (the membrane potential) influence its transport. The concentration gradient and the electrical gradient together constitute the electro-chemical gradient for each solute. All plasma membranes have an electrical potential difference across them, with the inside negative compared to the outside. The potential favours the entry of cations into the cells but opposes the entry of anions.
Passive transport does not need energy and it is possible to distinguish passive transport into two sub-categories: simple diffusion or facilitated diffusion.
Simple diffusion (Figure 1.4) across a biological membrane obeys Fick's first law (Equation 1.1) in which the flux per unit area of a compound through the membrane (J) depends only on the diffusion coefficient of the compound (D) and its concentration gradient across the membrane (dc/dx).

$$J = D\frac{dc}{dx} \qquad \text{Equation 1.1}$$

No term is included for the binding of the substrate to the membrane since discrete binding sites are not involved. Consequently, passive diffusion does not saturate at high substrate concentration.

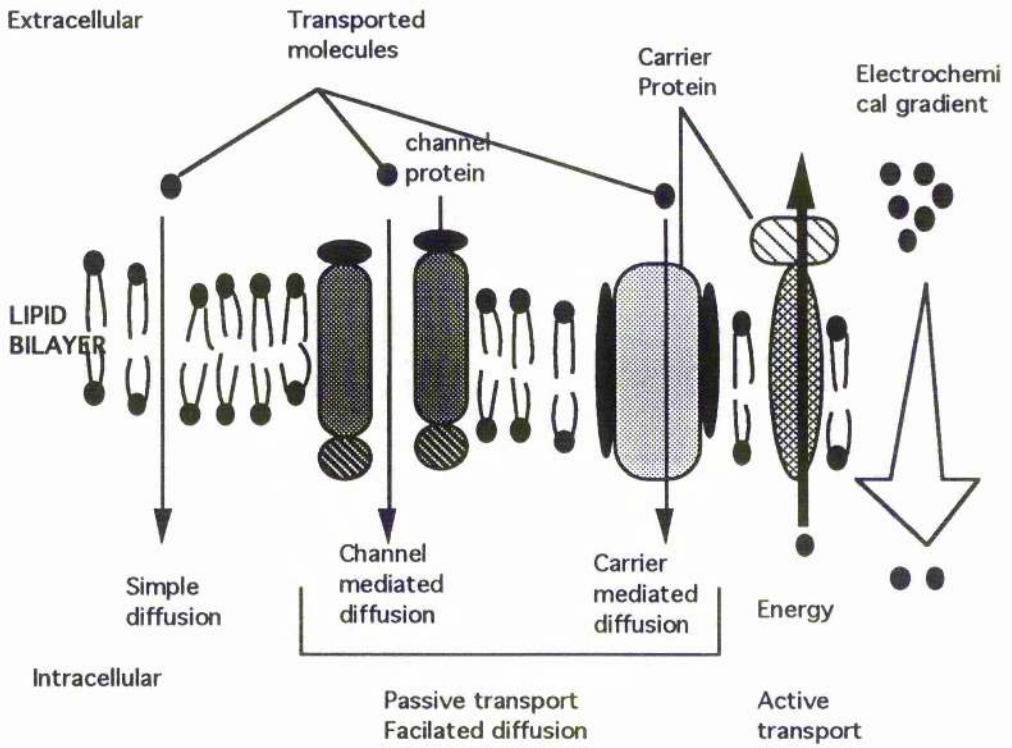

Figure 1.3 Schematic diagram of passive and active transport.[5]

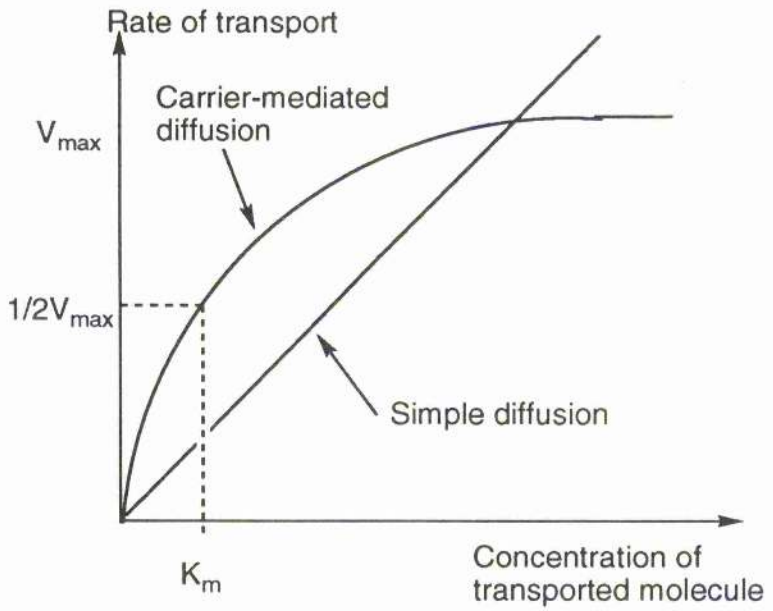

Figure1.4 Kinetics of simple diffusion compared to carrier-mediated diffusion.

In contrast to simple diffusion, facilitated diffusion requires a carrier protein which is specific for each substrate. A carrier protein binds and transfers a solute

molecule across the lipid bilayer, this mechanism resembles an enzyme-substrate reaction, and the carriers involved behave like specialized membrane-bound enzymes. Each type of carrier protein has a specific binding site for its substrates. When the carrier is saturated (that is when all these binding sites are occupied), the rate of transport is maximal and results in a 'plateau'. The rate, referred to as V_{max}, is characteristic of each specific carrier. Each carrier protein has a characteristic binding constant for its solute, K_m, equal to the concentration of solute when the transport rate is half its maximum value.

There are three types of carrier protein (Figure 1.5). The first one is called uniport which transports a single solute from one side of the membrane to the other. The other two carrier proteins are symport and antiport. The symport mediates the transfer of one solute, dependent on the transfer of a second solute molecule in same direction. Of course, the antiport is when the second solute molecule is carried in the opposite direction.

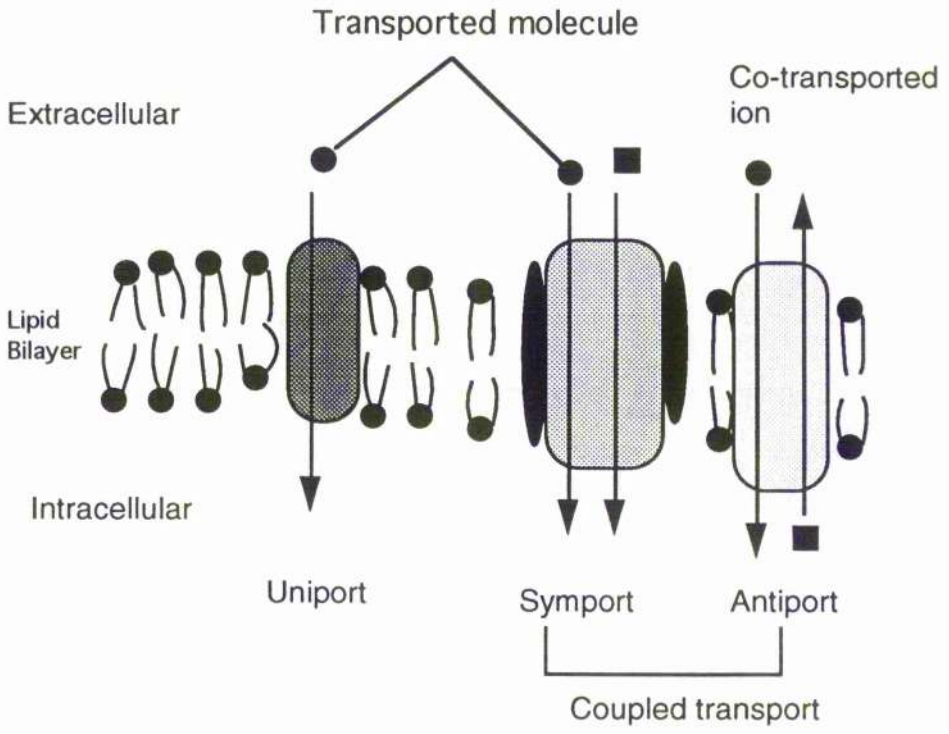

Figure 1.5 Schematic diagram of carrier proteins as uniports, symports and antiports

1.1.3.2 Active transport

This mode proceeds against the electrochemical or concentration gradients and therefore needs an input of energy. Most animal cells have a high concentration of K^+ and a low concentration of Na^+ relative to the external medium (*cf* Table 1.1). These ionic gradients are generated by a specific transport system that is called the Na^+/K^+/ATPase.[3] Indeed, more than a third of the ATP consumed by mammals such as man is used by this enzyme to pump these ions in order to maintain the K^+, Na^+ concentration gradient.

$$ATP + H_2O \xrightarrow{Na^+,\ K^+} ADP + P_i + H^+$$

In vivo, the hydrolysis of ATP is extremely exothermic reaction which releases over 50kJ/mol.

$\Delta G = \Delta G° + RT\ln([ADP][P_i]/[ATP]) \approx -50$ kJ/mol with $\Delta G° \approx -30.5$kJ/mol

The Na^+-K^+ gradient controls cell volume, renders nerve and muscle cells electrically excitable, and drives the active transport of sugars and amino acids. The hydrolysis of one ATP expels $3Na^+$ and allows $2K^+$ into the intracellular medium.

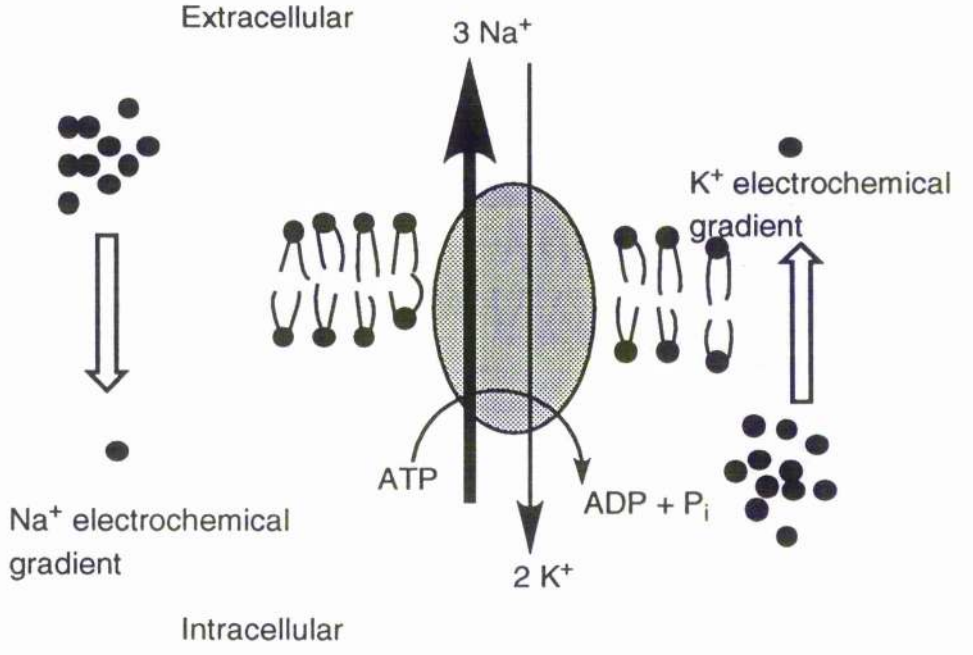

Figure 1.6 The Na^+-K^+ ATPase actively pumps Na^+ out and K^+ into a cell against their electrochemical gradients. For every molecule of ATP hydrolysed inside the cell, three Na^+ are pumped out and two K^+ are pumped in.

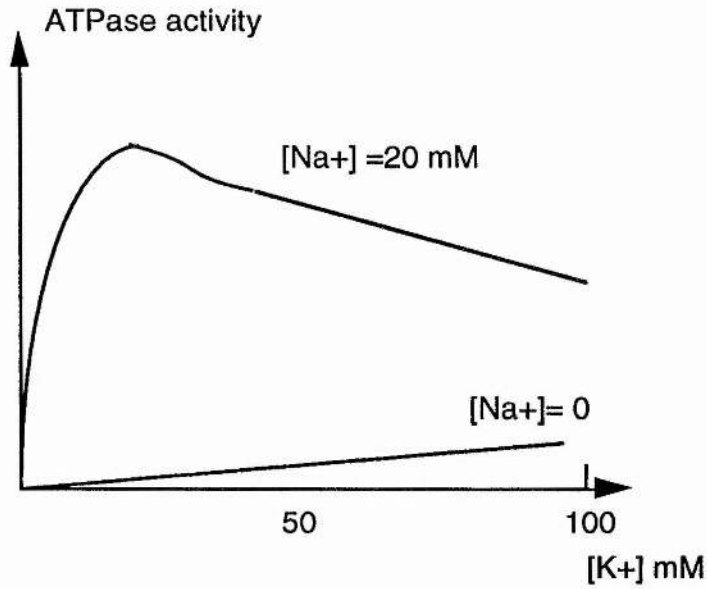

Figure 1.7 The Na^+/K^+/ATPase, a component of the Na^+/K^+ pump, hydrolyses ATP only if both Na^+ and K^+ are present.

For physiological reasons, it is vital to maintain the gradient of concentration of Na^+ and K^+. Figure 1.7 shows that in the absence of Na^+, the activity of the ATPase is negligible. In the presence of Na^+, its activity increases very rapidly in order to remove the excess of Na^+ ion in the intracellular medium. It decreases smoothly when the Na^+ concentration is acceptable.

1.2. General concepts concerning ionophores

Ionophores are compounds of moderate molecular weight (about 200-2000 $g.mol^{-1}$) that form lipid-soluble complexes with cations such as K^+, Na^+, Ca^{2+}, Mg^{2+}. These molecules, in general, may be regarded as molecules with backbones of diverse structure that contain strategically spaced oxygen atoms. The backbone is capable of assuming critical conformations that focus these oxygens about a ring or cavity in space into which a complexible cation may fit more or less snugly. The ligating oxygens are found in various functional groups, such as ether, alcohol, carboxyl and amide. The polar groups of the ionophore complex orient towards the interior, the exterior bristling with various hydrocarbon groupings. The lipid solubility of the resulting complex may be partially explained by the effective shielding of its polar interior, which delocalizes the cation charge.

Two different modes (Figure 1.9) of ionophore mediated transport through biological and artificial membranes have been established: the first mode of transport uses a 'carrier' mechanism, exhibited by neutral ionophores *e.g.* valinomycin and ionophoric antibiotics *e.g.* monensin, cationomycin. The second mode of transport involves a 'channel' mechanism. This mode is subdivided into two different sub-categories: gramicidin type and barrel stave type. The gramicidin type is composed of two dimers and spans through the membrane with one gramicidin on each surface. The barrel stave type formed by *e.g.* alamethicin or peptaibols is composed from single units which traverse the whole membrane as depicted in Figure 1.8.

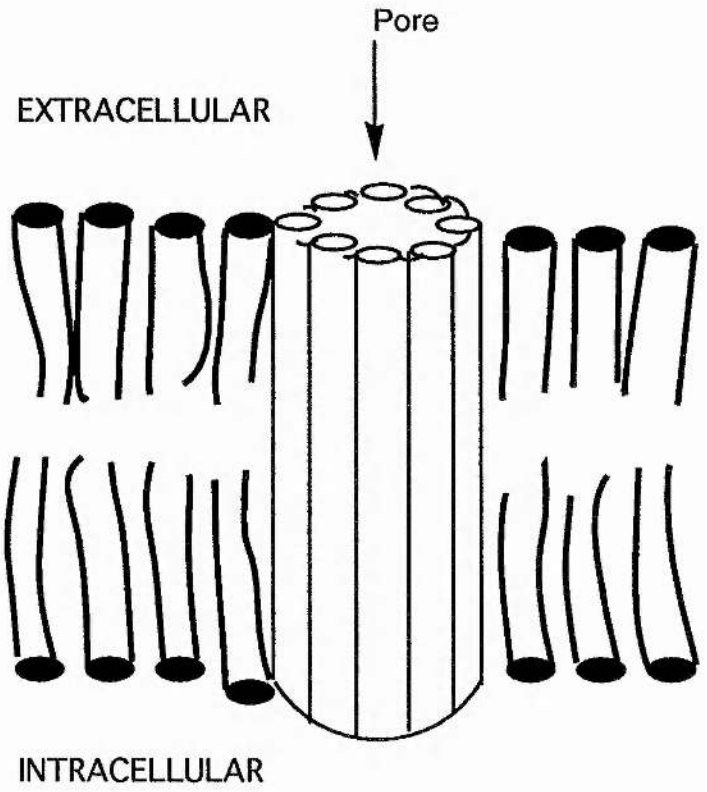

Figure 1.8 Barrel stave type mechanism.

The cation carriers form discrete antibiotic cation complexes at one interface of the membrane which then migrate across to other interface of the membrane where they release the cation. This 'carrier' mode is usually very selective towards the cations, however, it is much slower then the 'channel' mode.

Bamberg[6] and his group have reported that 3 x10^7 K^+ ions per second can be transported by one channel in comparison to 2.5 x10^4 K^+ ions by the valinomycin molecule. However, in the channel mode the molecules must first assemble into the channel which could be the rate determining step.

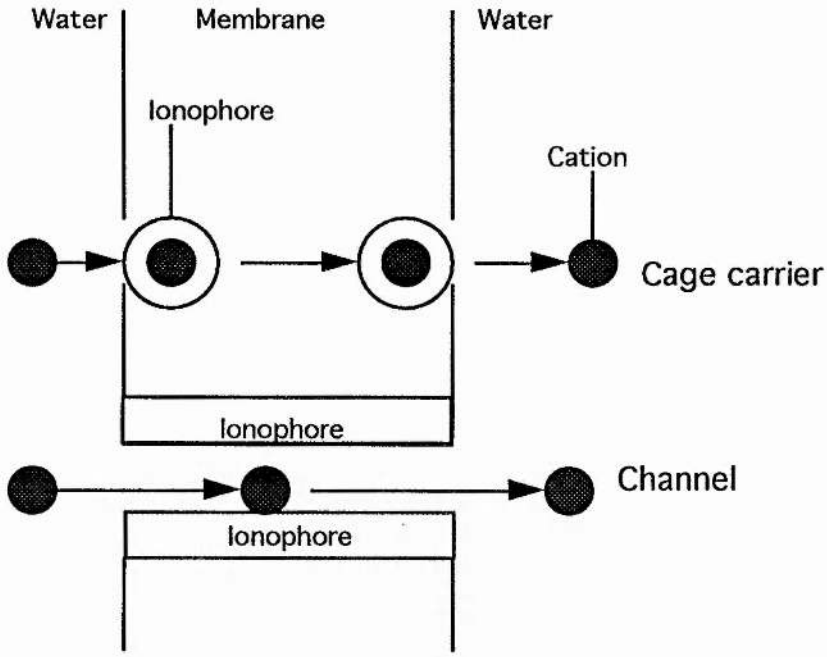

Figure 1.9 Schematic transport by ionophore across the membrane.

In the 'carrier' mode, there are three sub-categories depending on the stoichiometry of cation/ionophore; the 1:1 complex, which is by far the most common for ionophoric antibiotics, 2:1 'sandwiches', and finally 3:2 'stacks' modes (Figure 1.10).

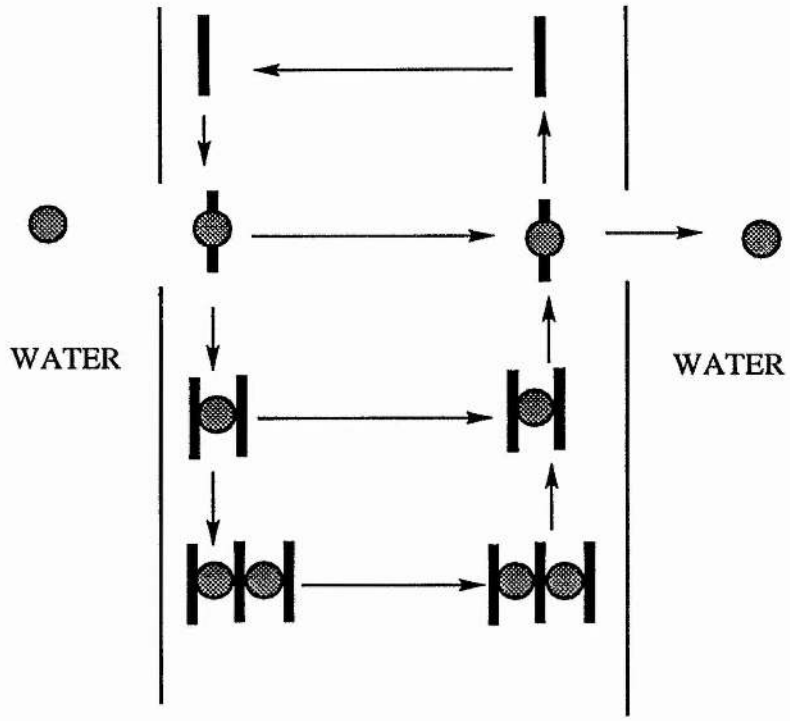

Figure 1.10 Cation transport in the presence of polyether antibiotics.

1.2.1 Classification of ionophores by transport modes

1.2.1.1 Neutral ionophores

Valinomycin[7] (Figure 1.12 and 1.13) is a typical example of this group and was the first of the ionophoric antibiotics to be discovered. It was originally isolated from *Streptomyces fulvissimus* and was found to be a powerful uncoupler of mitochondrial oxidative phosphorylation.[8] Its specialised properties derive from its ability to fold its backbone into a precise conformation to focus six ester carbonyls about a sphere. Valinomycin discriminates between alkali ions in the ratio 10,000:1 in favour of K^+ (radius r=1.33Å) over Na^+ (r=0.95Å).[9-11] X-ray crystallography[12] and Nuclear Magnetic Resonance (NMR)[13] of valinomycin-M^+ complex show independently that the molecule has the shape of a doughnut. A single metal ion is coordinated to several oxygen atoms that surround a central cavity (Figure 1.11). The periphery of the carrier consists of hydrocarbon groups. The roles of the central oxygen atoms and the hydrocarbon exterior are evident. In an aqueous medium, a metal ion such as K^+ binds several water molecules through their oxygen atoms.

A carrier competes with water for binding the ion by coordinating it with several appropriately arranged oxygen atoms in its central cavity. The hydrocarbon periphery makes the ion-carrier complex soluble in the lipid interior of the membranes. In essence, valinomycin catalyses the transport of ions across membranes by making them soluble in lipids.

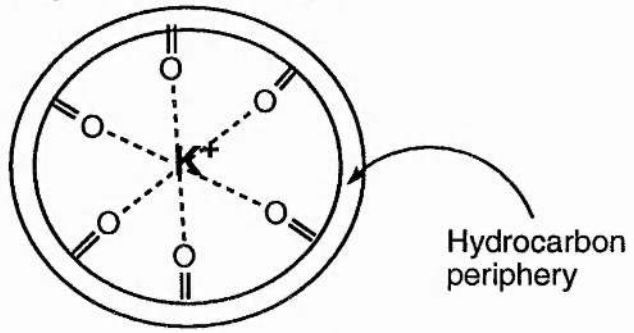

Figure 1.11 Schematic diagram of the chelation of K^+ by oxygen atoms of a carrier transport antibiotic.

A **B** **C** **D**

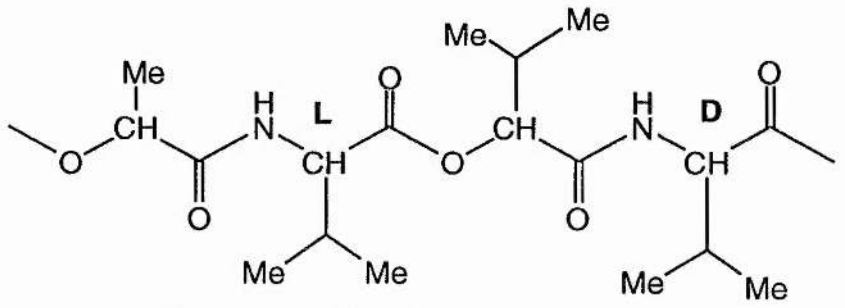

Figure 1.12 Structure of valinomycin.

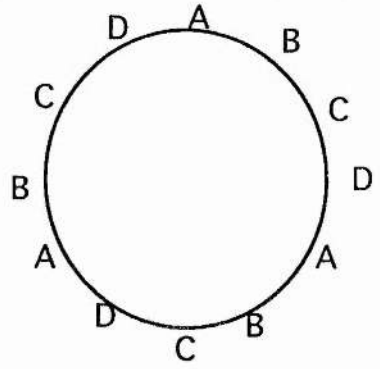

Figure 1.13 Valinomycin is a cyclic molecule made up of repeating L-lactate(**A**), L-valine(**B**), D-hydroxyisovalerate(**C**), and D-valine (**D**) residues.

As a consequence of the spatial constraint, valinomycin accommodates snugly an ion of the dimensions of K^+ (r=1.33Å), Rb^+ (r=1.45Å) or with a little stretching Cs^+(r=1.69Å). The backbone is too rigid to permit snug focusing on smaller ions such as Na^+(r=0.95Å) or Li^+(r=0.60Å).

Solvent	Stability constants of valinomycin complexed with				
	Li^+	Na^+	K^+	Rb^+	Cs^+
Methanol	<5	4.7	$8x10^4$	$18x10^4$	$2.6x10^4$
Ethanol	-	<50	$260x10^4$	$290x10^4$	$65x10^4$

Table 1.2 Stability constants of equimolar valinomycin[14] complexes of alkali cations at 298 K.

In brief, ionophores that engulf their cations in three-dimensional cages show more constraint and therefore higher ionic discrimination than the smaller, more planar ionophores.

1.2.1.2 Transport of cations by neutral ionophores

It is possible to break down into simple steps the transport of a cation through the membrane[15] (Figure 1.14).

- The neutral ionophore within the membrane diffuses to the membrane surface where it encounters a complexible ion.
- When the ion is in a critical position to interact with the ionophore, its solvation water is stripped away by stepwise substitution and replaced by the ligating oxygens of the ionophore.
- The stable complex $(MI)^+$ eventually diffuses from the interface to the interior of the membrane and releases the cation.
- Finally, the empty ionophore diffuses back into the membrane restoring the original condition or transports an ion in the opposite direction.

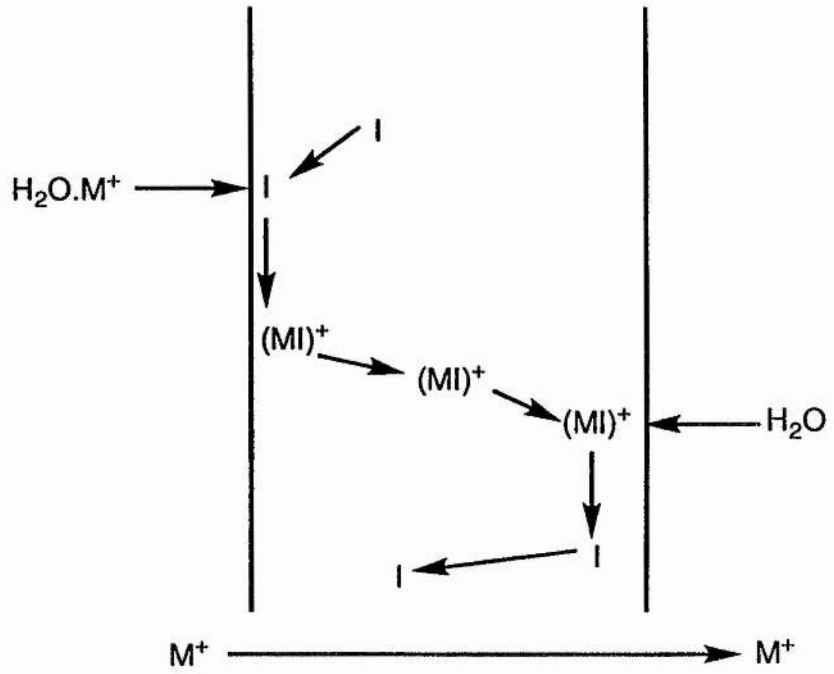

Figure 1.14 Schematic transport of cation with neutral ionophore.

1.2.1.3 Carboxylic ionophores

Carboxylic ionophores appear to be open chains containing oxygenated heterocyclic rings and a single terminal carboxyl. The open chain may lead to confusion since they all form rings by head to-tail hydrogen bonding, although the carboxyl group may (*e.g* in nigericin[16] Figure 1.16) or may not (*e.g* in monensin[17] Figure 1.15) be involved in cation ligating. Carboxylic ionophores will be treated in the next chapter.

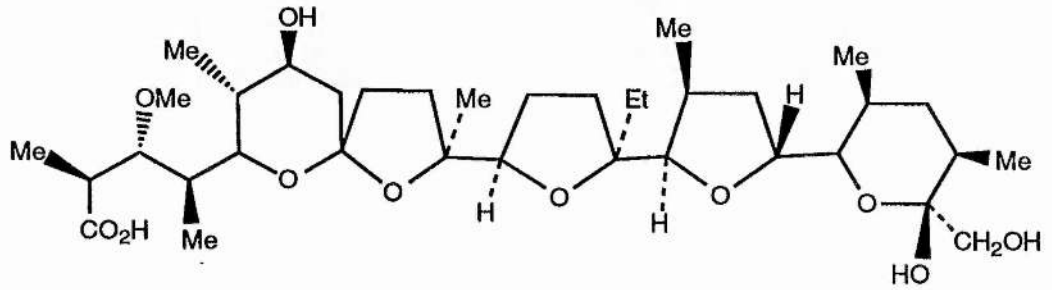

Figure 1.15 Structure of monensin.

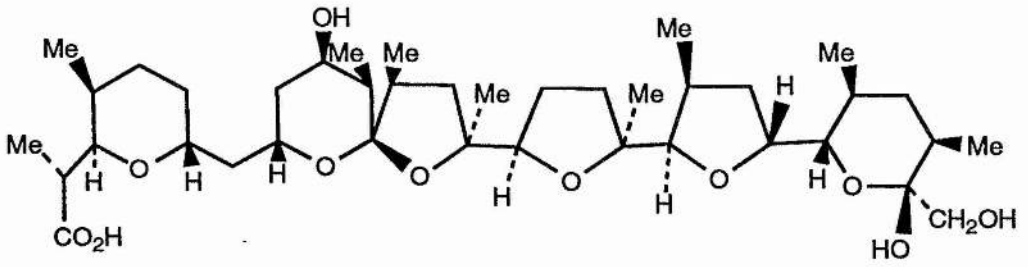

Figure 1.16 Structure of nigericin.

1.2.1.4 Transport of cations by carboxylic ionophores

It is also possible to decompose the transport of cations by carboxylic ionophores[15] into steps (Figure 1.17).

- A protonated ionophore diffuses throughout the artificial or biological membrane to one interface. Then its proton is released at the polar interface.
- The ionophoric anion encounters and engulfs a complexible cation M^+ by stripping away the water of solvation by a stepwise mechanism.
- The zwitterionic complex, its charges internally compensated, is able to break way from the interface, diffuses to the opposite interface and releases its cation, coincident with resolvation.
- Finally, the empty ionophore diffuses back into the membrane restoring the original condition or transports a cation in the reverse direction. The result is the exchange of one cation for another across the membrane with no net charge translocation.

1.2.1.5 Channel forming quasi-ionophores

Channel-forming ionophores differ from other ionophores in that they only interact with metal ions in the presence of a membrane. Molecules such as gramicidin dimerize in the lipid membrane to form channels 2.5-3.0 nm long and 0.4 nm in diameter, which act as ion-conducting channels through the membrane.

A typical example of this group is gramicidin (Figure 1.18) which is an open-chain polypeptide consisting of fifteen amino acid residues. It forms a coiled structure[18] inside the membrane which then dimerises as depicted in Figure 1.19 to form a channel capable of conducting cations and virtually impermeable to

anions. Again, the hydrophobic groups are on the outside and polar groups are on the interior of the channel. Cations enter such a channel at one surface of the membrane and diffuse through it to the other side of the membrane.[7] The dimer is large enough to traverse the lipid bilayer membrane.

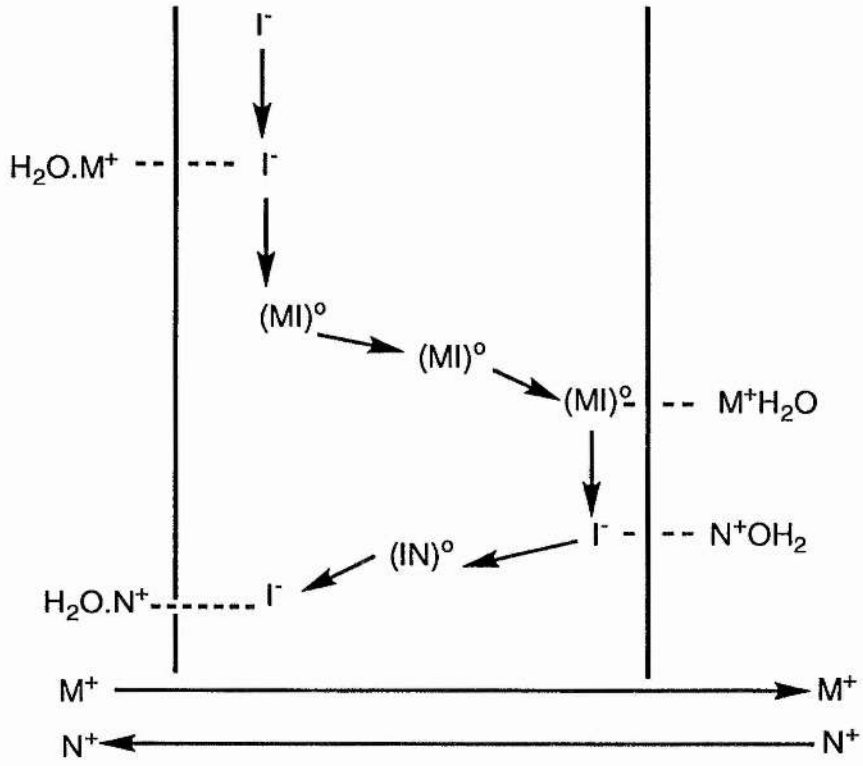

Figure 1.17 Schematic transport of a cation by carboxylic ionophore.

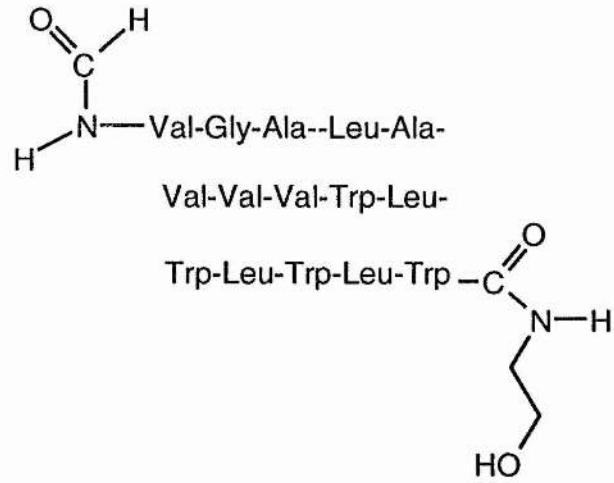

Figure 1.18 Structure of gramicidin A.

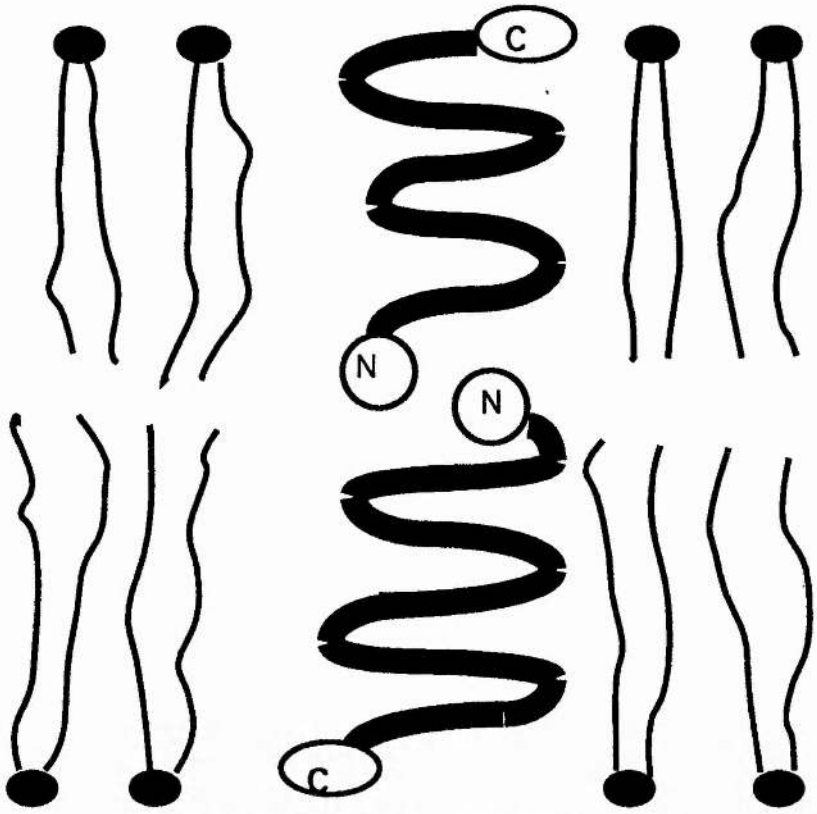

Figure 1.19 Schematic diagram of gramicidin-A channel formed by the association of two polypeptides[8] at their N-formyl ends.

In order to explain the experimental conductance effects, Urry has proposed a field dependent equilibrium between conducting and non-conducting gramicidin conformations[18,19] which is shown schematically in Figure 1.20. Structure **B** represents the conducting helical conformation. In this conformation, the molecule has an internal cavity which can accommodate metal ions, and has a net dipole moment along the helix axis. Structure **A** shows the non conducting, spiral conformation. The internal cavity of this form is closed by two intramolecular hydrogen bonds per turn and there is no net dipole moment along the spiral axis. Therefore structure **A** prevents the entry of cations through the membrane.

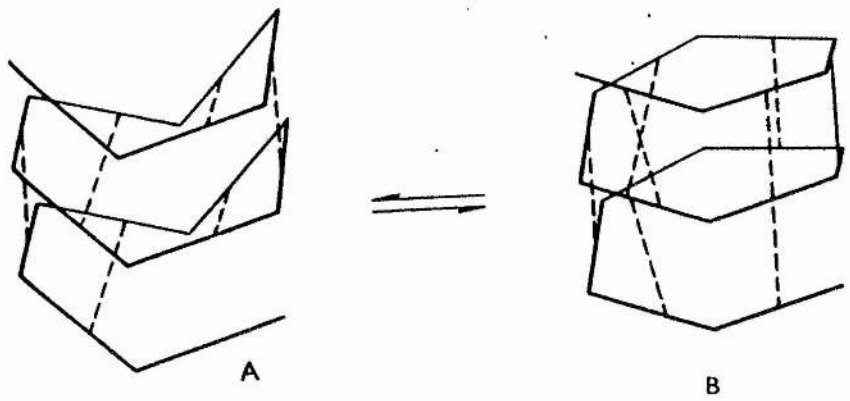

Figure 1.20 Schematic representation of an equilibrium between non-conducting (**A**) and conducting (**B**) helical conformations of gramicidin A. Intramolecular hydrogen bonds are shown as dashed lines.

References to chapter 1

1. E. F. Caldin, in 'Fast reactions in solution', Wiley, New-York (USA), 1964.
2. W. P. Jencks, in 'Catalysis in chemistry and enzymology' McGraw-Hill, New-York (USA), 1964.
3. B. Alberts, D. Bray, J. Lewis, M. Raff, K. Roberts, J. D. Watson in ' Molecular biology of the cell' Garland Publishing, New York (USA), 1989.
4. J Kyte, *Nature*, 1981, **292**, 201.
5. L. Stryer, in 'Biochemistry', W.H. Freeman & Company, New-York (USA), 1988.
6. E. Bamberg, P. Lauger, *J. Membr. Biol.*, 1973, **11**, 177.
7. H. Brockmann, G. Schmidt-Kastner, *Chem. Ber.*, 1955, **88**, 57.
8. W. McMurray, R. W. Begg, *Arch. Biochem. Biophys.*, 1959, **84**, 546.
9. C. Moore, B. C. Pressman, *Biochem. Biophys. Res. Commun.*, 1964, **15**, 562.
10. B. C. Pressman, *Proc. Natl. Acad. Sci. USA*, 1965, **53**, 1076.
11. B. C. Pressman, *Fed. Proc.*, 1968, **27**, 1283.

12. M. Pinkerton, L. K. Steinrauf, P. Dawkins, *Biochem. Biophys. Res. Commun.*, 1969, **35**, 512.

13. V. T. Ivanov, I. A. Laine, N. D. Abdullaev, L. B. Senyavina, E. M. Popov, Y. A. Ovchinnikov, M. M. Shemayakin, *Biochem. Biophys. Res. Commun.*, 1969, **34**, 803.

14. Y. A. Ovchinnikov, *Eur. J. Biochem.*, 1979, **94**, 321.

15. B. C. Pressman, *Annu. Rev. Biochem.*, 1976, **45**, 501.

16. L. Steinrauf, M. Pinkerton, J. W. Chamberlin, *Biochem. Biophys. Res. Comm.*, 1968, **33,** 29.

17. A. Agtarap, J. W. Chamberlin, M. Pinkerton, L. Steinrauf, *J. Am. Chem. Soc.*, 1967, **89**, 5737.

18. D. W. Urry, *Proc.Nat. Acad. Sci. USA*, 1971, **68**, 672.

19. D. W. Urry, *Proc.Nat. Acad. Sci. USA*, 1972, **69**, 1610.

Chapter 2
Cation transport mediated by ionophoric antibiotics

2.1 History of ionophoric antibiotics

The first three ionophoric antibiotics were reported as early as 1951,[1,2] but little attention was given to this new group of antibiotics until the isolation and structure elucidation of monensin[3] (Figure 1.15) in 1967.

The remarkable increase in interest toward polyether antibiotics was due to two main reasons :

- the first one was the recognition that acid ionophores were an excellent tool for biochemists to investigate cation transport through biological and artificial membranes

- the second one was the discovery of the potent anticoccidial activity of the polyether antibiotics for poultry together with their ability to improve feed nutrition for ruminant animals which meant a potential world-wide market of $100 million.

Figure 2.1 illustrates the evolution of the number of known polyether antibiotics with time and it shows how economic interest in the compounds is a driving force in this research.

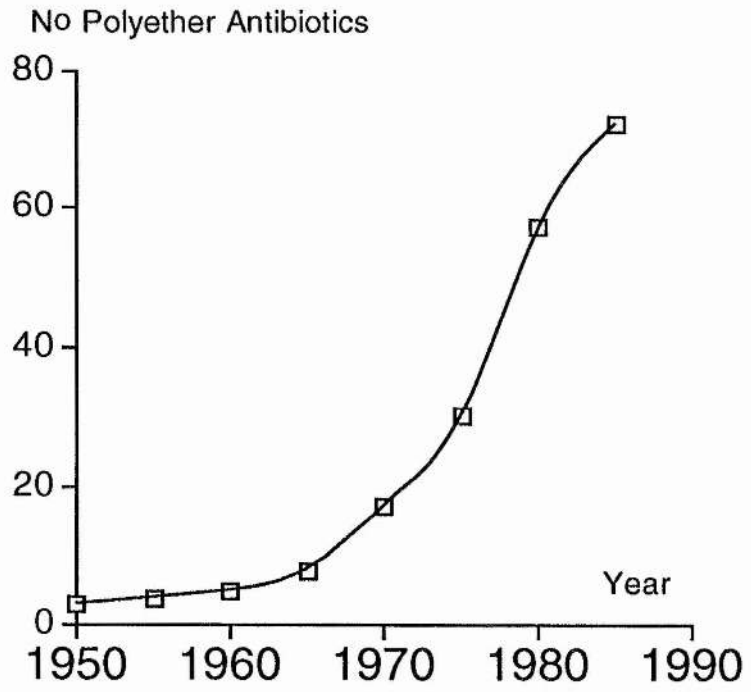

Figure 2.1 Evolution of number of polyether antibiotics known versus time.

2.2 Biological activities

Bacteria are subdivided according to whether or not they are able to retain the violet dye which is composed of alcohol or acetone and iodine (the Gram stain). Gram-positive bacteria retain the dye, and Gram-negative ones do not. Polyether antibiotics are highly effective against Gram-positive bacteria and a number of anaerobic bacteria but exhibit no activity against any of the Gram-negative aerobes tested.

Gram-positive bacteria have little or no lipid, and a high content of amino sugars in the composition of their biological membranes.
On the other hand, Gram-negative bacteria have a high lipid and low sugar composition. This high concentration of lipid prevents the penetration of hydrophobic molecules of high molecular weight such as polyether antibiotics as shown in Table 2.1.

Polyether antibiotics	Molecular weight ($g.mol^{-1}$)
Monensin	671
Nigericin	725
Cationomycin	851
Tetronasin	602

Table 2.1 Polyether antibiotics and their molecular weights.

2.2.1 Mode of action of polyether antibiotics

Polyether antibiotics interact with the cytoplasmic membrane and cause the leakage and depletion of alkali cations from the bacterial cell and then acidification of the cytoplasm leads to the death of bacteria.
It is possible to distinguish two groups of carboxylic ionophores in relation to their relative transporting ability of alkali cations across the artificial or biological membrane.
The first one (Figure 2.2) involves ionophores with higher transporting ability for Na^+ than K^+ such as monensin which produces an initial Na^+_{in}/H^+_{out} exchange followed by re-equilibration of pH through a H^+_{in}/K^+_{out} exchange.

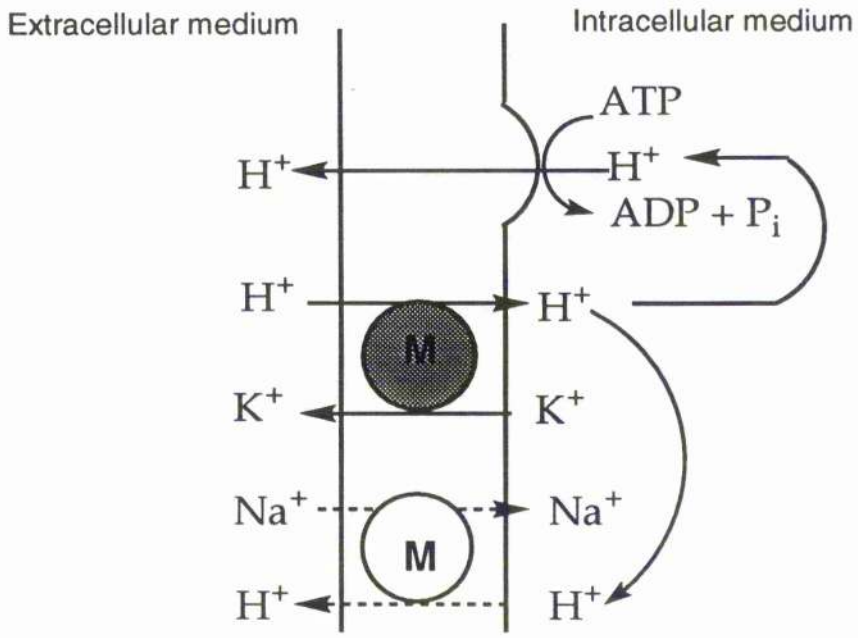

Figure 2.2 Schematic representation of mode action of monensin type.

The second group (Figure 2.3) involves ionophores with a greater transporting ability for K^+ than Na^+, such as nigericin or cationomycin, which produce an initial H^+_{in}/K^+_{out} exchange, followed by reequilibration of pH through a secondary Na^+_{in}/H^+_{out} exchange.

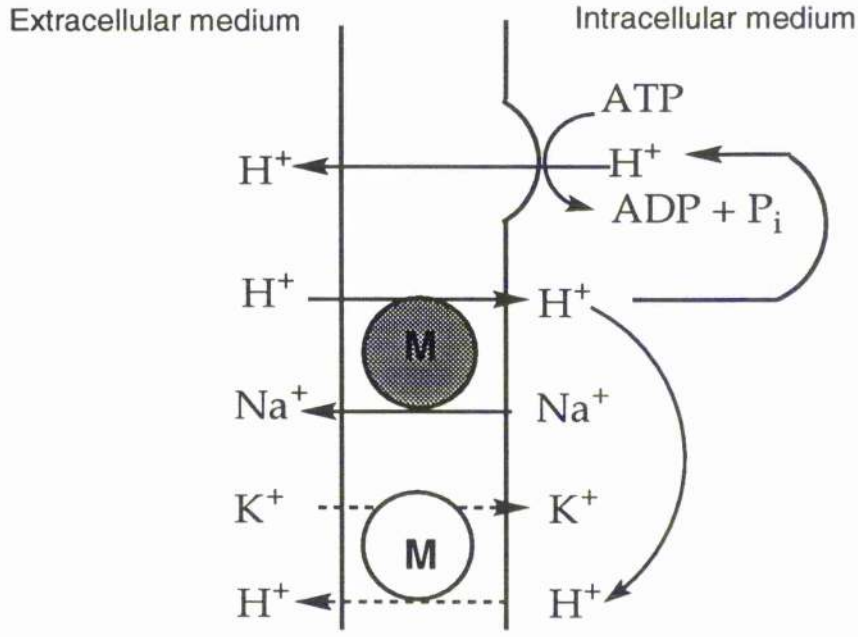

Figure 2.3 Schematic representation of mode action of cationomycin or nigericin type .

Guffanti[4] and his team carried out studies of the effect of nigericin on the acidophilic bacterium *Bacillus acidocaldarius.* They showed that, at an external pH 3.5 (the pH of the medium in which the organism was grown), the nigericin-type abolishes the transmembrane proton gradient (due to electroneutral H^+/K^+ exchange), causing a rapid acidification of the cytoplasm (from pH 6.0 to 3.5). This led to a marked decline in respiratory activity and rapid decrease of cytoplasmic ATP content. Nigericin-induced death of *Bacillus acidocaldarius* was due to the acidification of the cytoplasm rather than loss of K^+ from the cell, since no loss of viability was observed when the pH gradient was abolished by elevation of the external pH with buffer containing no K^+.

As was mentioned in Chapter 1, it is vital to establish a concentration gradient for Na^+ and K^+ between the intra- and extracellular medium. The Na^+/K^+/ATPase pump maintains this gradient. Carboxylic antibiotics disrupt alkali metal ion and proton electrochemical gradients (Figures 2.2 and 2.3) with the proton electrochemical gradient serving as an energy source for the synthesis of ATP. In order to preserve Na^+/ K^+ gradients, the Na^+/K^+/ATPase pump is activated until all the ATP is consumed leading inevitably to cell death.

2. 3 Spatial structures of some carboxylic antibiotics

X-ray diffraction and NMR are extremely powerful techniques for establishing the spatial structure of biomolecules. In general, the architecture of biomolecules in the solid state (given by X-ray diffraction) does not differ greatly from the structures produced by NMR. This section aims to establish the relationship between the general architectural features of the conformation adopted by these ionophoric antibiotics and the transport of cations through bilayer membranes.

2.3.1 Origin and structure of monensin

The polyether antibiotic monensin (Figure 2.5) is produced by a strain of *Streptomyces cinnamonensi.* This antibiotic induces monovalent cation permeability, exhibits selectivity[5] for Na^+ over K^+, and has a greater stability constant with Na^+ than K^+. This selectivity for sodium rather than potassium is rare.

Different X-ray studies[6,7] have established that the spatial structures of the complexes of monensin with different cations are similar to each other.

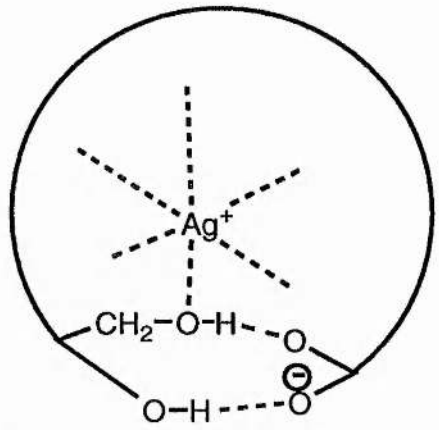

Figure 2.4 Schematic structure of monensin Ag^+.

These analyses showed that the complex molecule (Figure 2.4) forms a macrocycle[8] secured by a pair of hydrogen bonds to the negatively charged oxygen atoms of the molecule. The outside of the complex is formed by side chains and CH_2 groups of the rings and is, on the whole, hydrophobic.

The cation enclosed in the resulting cavity is coordinated to six oxygen atoms at distances of 2.3-2.8 Å in an irregular arrangement (Table 2.2).

Two of these, O-(4) and O-(11), are from hydroxyl groups, three are ether oxygens from the five-membered rings B, C and D, and the sixth is from the six-membered ring A.

	Ag^+ salt.H_2O	Na^+ salt.H_2O	Na^+ anhydrous	Free acid	K^+ salt.H_2O
X-O(4)	2.43	2.34	2.35	3.48	2.65
X-O(6)	2.41	2.36	2.41	3.40	2.66
X-O(7)	2.69	2.54	2.53	2.85	2.79
X-O(8)	2.58	2.44	2.41	3.77	2.72
X-O(9)	2.56	2.45	2.51	3.73	2.80
X-O(11)	2.46	2.45	2.38	2.64	2.79
X-O(1)	3.86			2.90	
X-O(2)	3.84			3.84	

Table 2.2 Distances (Å) with different cations and free acid for monensin.[9,10]

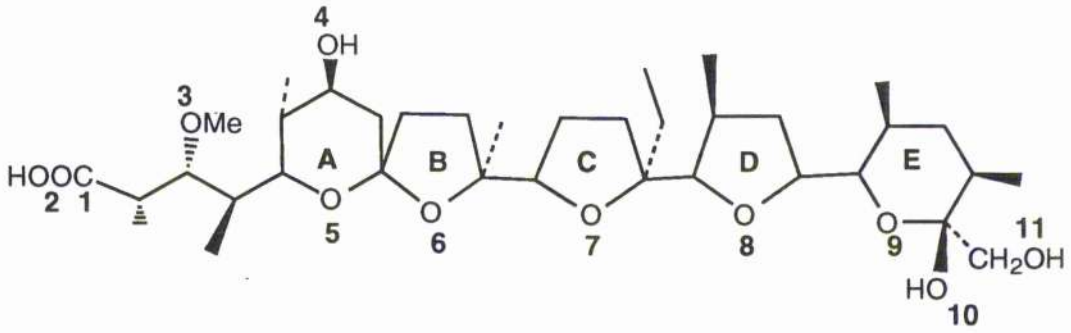

Figure 2.5 Structure of monensin.

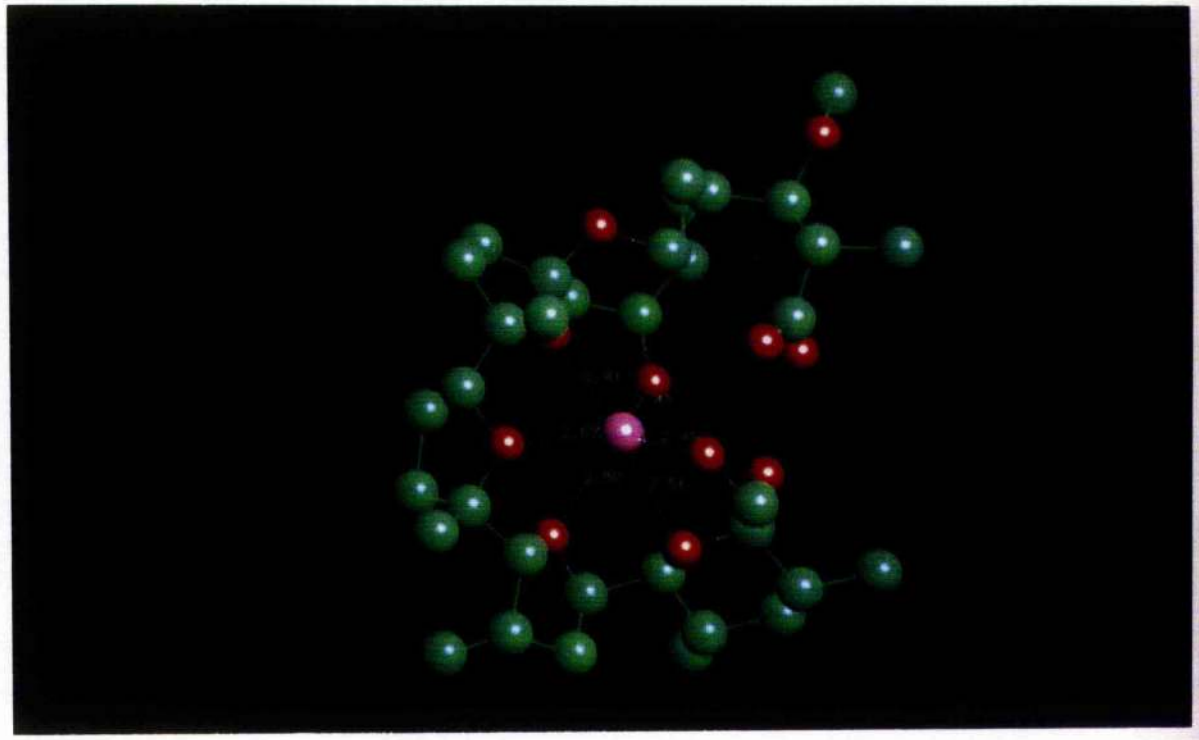

Figure 2.6 Photograph of monensin-Ag^+.

2.3.2 Origin and structure of nigericin

In 1965, nigericin was the first of this type of carboxylic antibiotic to be studied, and many of the early biological experiments were carried out by Graven and his group.[11] Nigericin is produced by a strain of *streptomyces hygroscopicus*. Some early kinetic studies revealed that nigericin transports K^+ more efficiently than Na^+. The structure of the nigericin Ag^+ salt was determined by two independent teams[12,13] and both studies were published at the same time. The overall similarity to the monensin complexes is striking as depicted in Figure 2.7.

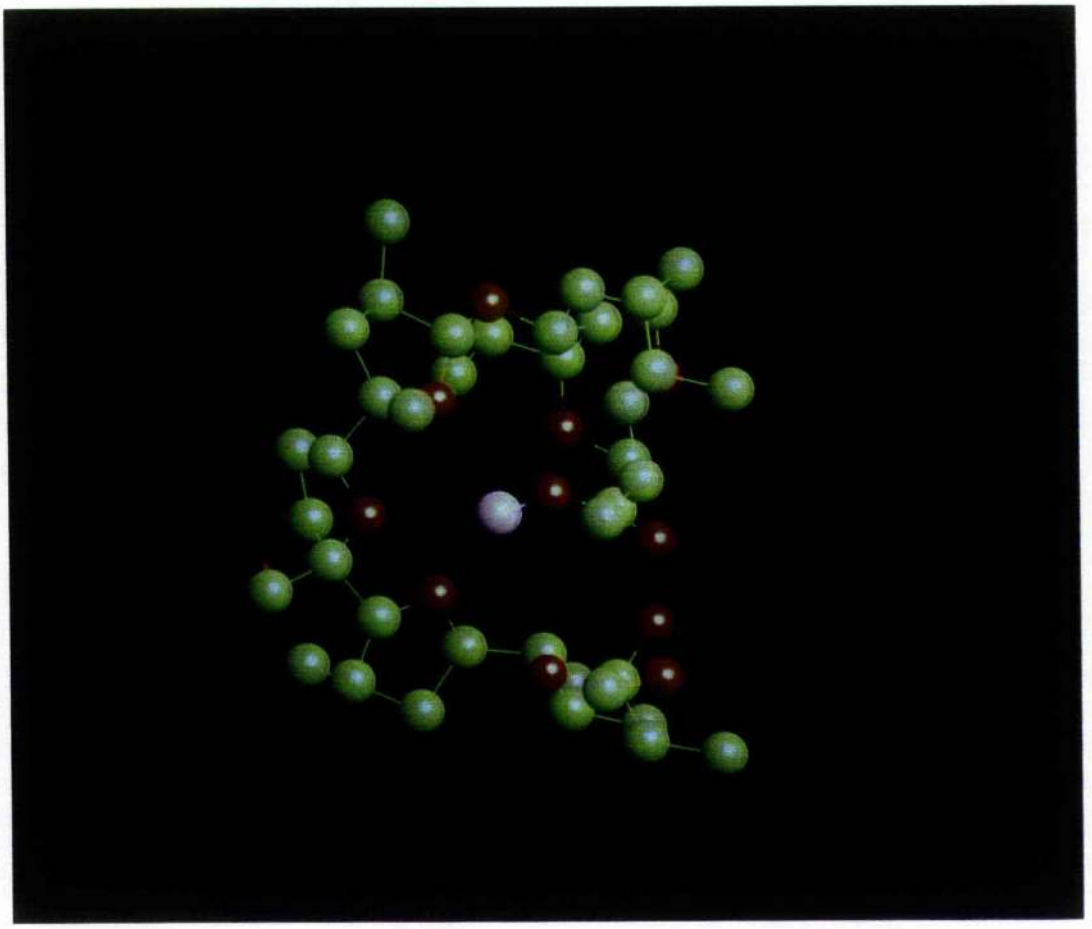

Figure 2.7 Photograph of nigericin-Ag^+.

However, differences occur in the coordination of the metal ion and the hydrogen bonding scheme. In nigericin the cation is coordinated to only five oxygens (Figure 2.8) (four of them are ether oxygens and the fifth is one of the carboxyl oxygens atoms) compared with six in the case of monensin. The conformation of the salt has the usual features: a nonpolar exterior and a polar interior, and the circular conformation held together by head to tail hydrogen bonding. Table 2.3 shows that the silver ion is coordinated by five oxygen atoms with Ag-O distances from 2.26 to 2.66 Å.

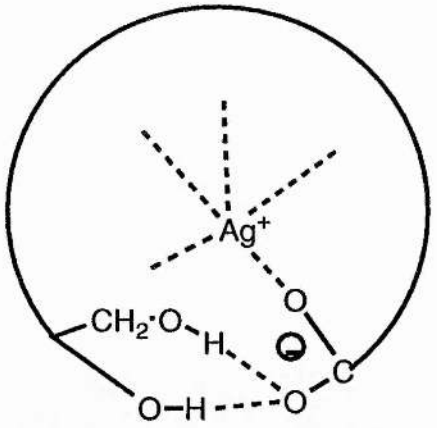

Figure 2.8 Schematic structure of nigericin Ag^+.

Ag^+-O(X)	Distance (Å)	Ag^+-O(X)	Distance (Å)
Ag^+-O(1)	2.26	Ag^+-O(11)	2.62
Ag^+-O(7)	2.47	Ag^+-O(6)	2.66
Ag^+-O(5)	2.60		

Table 2.3 Ag^+-O Distances in the Ag^+-nigericin salt.[13]

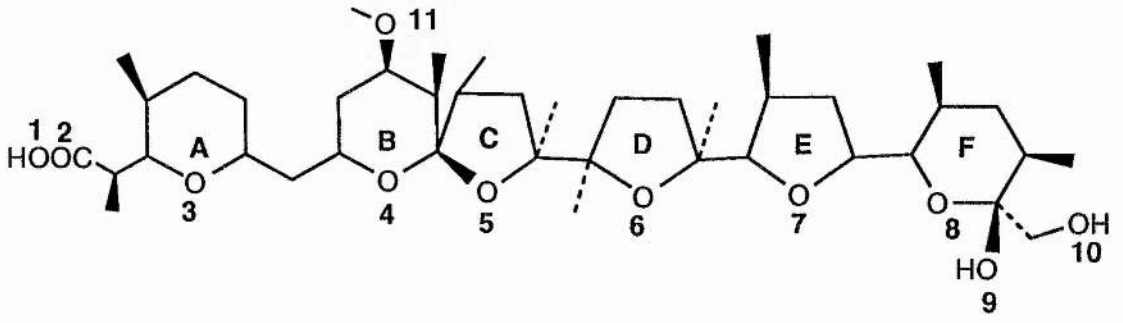

Figure 2.9 Structure of nigericin.

2.3.3 Origin and structure of cationomycin

Cationomycin (Figure 2.10) is a carboxylic polyether antibiotic isolated[14] from *Actinomadura azurea*. Its biosynthesis was studied using ^{13}C-acetate.[15] Cationomycin transports cations across biological membranes, as a mobile carrier, by a proposed mechanism of H^+/cation exchange (see Chapter 2 section 2.2.1). The structure of the thallium salt[16] of this molecule from X-ray diffraction is rather similar to the conformations obtained in solution by NMR[17] of the acid form and the complexes with K^+, Rb^+, Na^+, Li^+ , Cs^+ and NMe_4^+.
Cationomycin induces monovalent cation permeability, exhibits selectivity[18] for K^+ over Na^+, and has a greater stability constant for complexation of K^+ than Na^+. The molecule has a tadpole shape (Figure 2.11) in the thallium complex with a planar tail. The backbone (27 carbons atoms) starts from the carboxyl group and forms a circular conformation around the thallium ion. The end of the side is connected by a hydrogen bond between the terminal hydroxy group O(12) and one of the oxygens O(2) of the carboxyl group. The thallium ion is coordinated by seven oxygen atoms with Tl-O distances from 2.79 to 3.07 Å (Table 2.4). The exterior surface of the head of the molecule consists of hydrophobic groups.

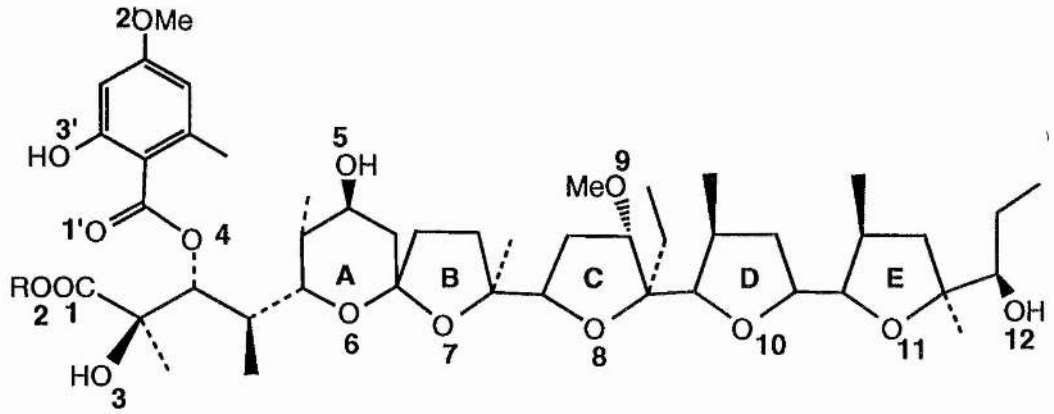

Figure 2.10 Structure of cationomycin.

Tl^+-O(X)	Distance (Å)	Tl^+-O(X)	Distance (Å)
Tl^+-O(1)	3.00	Tl^+-O(8)	3.07
Tl^+-O(6)	2.79	Tl^+-O(10)	3.04
Tl^+-O(7)	2.82	Tl^+-O(11)	2.85
Tl^+-O(12)	3.00		

Table 2.4 Tl^+-O Distances in the cationomycin salt.[16]

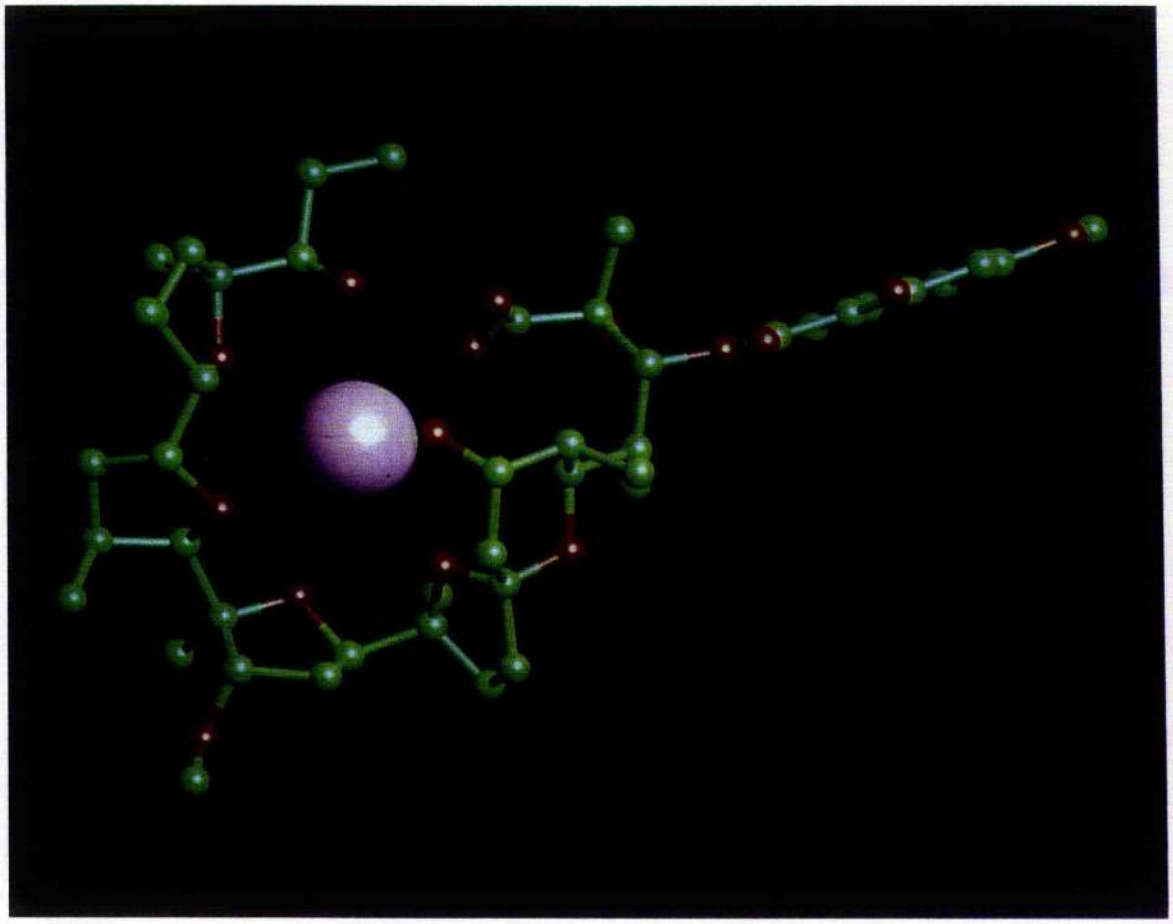

Figure 2.11 Photograph of cationomycin -Tl^+.

2.3.4 Origin and structure of tetronasin (M139603)

Tetronasin or M139603 (Figure 2.12) is a different type of carboxylic antibiotic[19] isolated from the aerobic fermentation of *Streptomyces longisporoflavus*. The X-ray structure reveals a similar shape to other ionophoric antibiotics such as monensin and cationomycin. The cation is enclosed in the pseudo-cyclic cavity with the hydrophobic side pointing outside. The Na^+ ion is coordinated to five oxygens O(3), O(4), O(6), O(7), and O(8), at distances from 2.31 to 2.73Å (Table 2.5) and it is also coordinated to a solvent molecule. The five ligating oxygens form a very unsymmetrical array around the central metal ion as depicted in Figure 2.13.

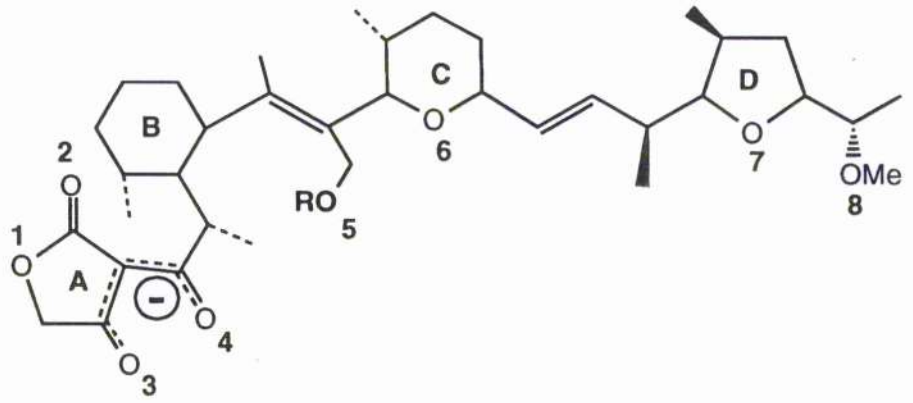

Figure 2.12 Structure of tetronasin.

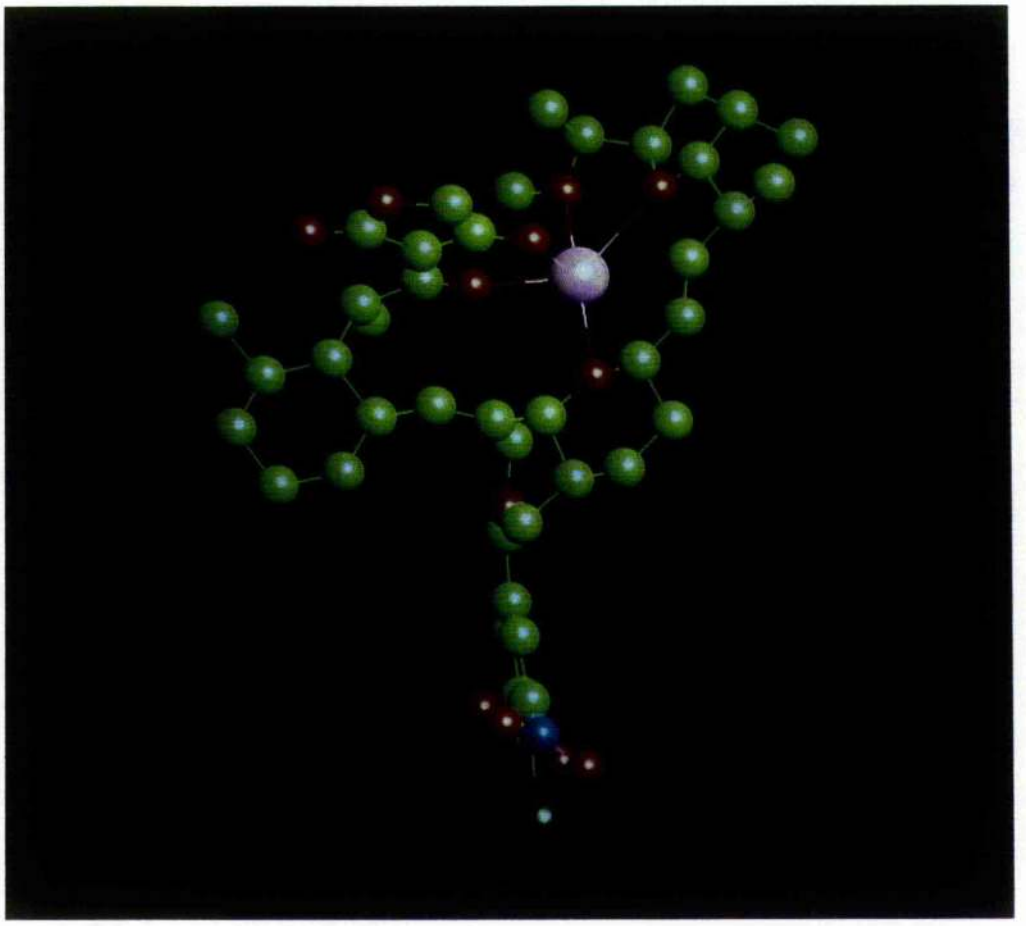

Figure 2.13 Photograph of tetronasin-Na^+.

Na^+-O(X)	Distance (Å)	Tl^+-O(X)	Distance (Å)
Na^+-O(3)	2.31	Na^+-O(7)	2.55
Na^+-O(4)	2.33	Na^+-O(8)	2.73
Na^+-O(6)	2.56		

Table 2.5 Na^+-O distances in the Na^+ tetronasin salt.[19]

2.3.5 General architectural features

From the studies of these four ionophoric antibiotics, it is possible to draw up a list of general architectural features. Ionophores must possess a set of functional and structural characteristics in order to function as efficient mobile carriers within natural or artificial membranes.

(i) The ionophores must have polar and non-polar groups. The polar groups function as ligands which replace the solvent molecules in the primary solvation sphere of the complexed ion. In order to compete with the ionic solvation sphere, the ionophore should contain five to eight but not more then twelve liganding polar groups. The most stable ionophore-alkali ion inclusion complexes have a coordination number of six, while the larger alkaline earth cations prefer a coordination number of eight.

(ii) The ionophore must be able to assume a stable conformation which directs the polar ligating moieties into a central cavity suitable for enclosing the cation. High ion complexation selectivities are achieved by locking the coordination sites into a rigid arrangement around the cavity. Rigidity is generally achieved by intramolecular hydrogen bonding, extended spirane systems and substituents (alkyl groups) which limit free rotation about key bonds. These alkyl groups must insulate the internal ligating cavity sufficiently to ensure the stability of the ion while crossing the apolar membrane interior.

(iii) Ion complexation-decomplexation reactions must proceed at a sufficiently rapid rate in order for the ionophore to function as an efficient carrier. This is only possible when the ionophore is flexible enough to allow a stepwise rather than a concerted substitution of ligating moieties for solvent molecules. Thus, in order to be an effective ionophore a compromise between ion affinity and ion exchange kinetics must exist.

2.4 Introduction to ion transport studies using NMR

The alkali metal cations Na^+ and K^+ and the alkaline earth metal cations Mg^{2+} and Ca^{2+} are ubiquitous in living systems. Sodium and potassium are present as free aquo cations, and the essence of their biochemistry lies in their unequal distributions across cell membranes.

The concentrations, electrochemical gradients, and transmembrane fluxes of Na^+ are of fundamental importance in a variety of vital cell functions. Changes in the intracellular concentration of sodium are often an indication of tissue disease or malfunction, and have been associated with cancer,[20] hypertension,[21] diabetes,[22] and sickle cell disease.[23]

The idea of using NMR (Nuclear Magnetic Resonance) to study the effect of complexation on the CW signal of ^{23}Na started with Jardetsky[24] and Wertz[25] in 1956. However, the success of studies was made possible to a large extent by the advent of Fourier Transform into NMR spectroscopy.[26] The main asset of NMR compared to other traditional spectroscopic techniques is that it is non invasive, so that ionic and metabolic changes in the cellular environment can be observed as they take place within the living system.

2.4.1 NMR spectroscopy of metal cations

NMR techniques enable us to study alkali and alkaline earth cation exchange without destroying the cell. Fortunately, there are isotopes for each of these ions, which have nuclear magnetic moments and therefore, are NMR active so NMR can provide information about the physical state of the cations.

Nuclide	I	Natural Isotopic Abundance (%)	NMR receptivity¥	BIONMR receptivity*
^{1}H	1/2	100	100	100
^{31}P	1/2	100	6.65	25.7×10^{-3}
^{23}Na	3/2	100	9.27	4.08×10^{-3}
^{39}K	3/2	93.1	0.48×10^{-1}	0.23×10^{-4}
^{25}Mg	5/2	10.1	2.72×10^{-2}	5.71×10^{-6}
^{43}Ca	7/2	0.15	8.67×10^{-4}	3.24×10^{-6}

Table 2.6 NMR sensitivities of biological magnetic nuclides.[27]
(¥relative to ^{1}H=100 at natural abundance, * relative to ^{1}H=100 in human body)

The NMR receptivity is a measure of the sensitivity of the NMR signal of that nucleus, present at natural abundance, relative to that of the proton, which is assigned the value of 100. The BIONMR receptivity is the product of the NMR receptivity and the concentration of the element in the human body, normalised to a proton value of 100 (see Table 2.6).
Although ^{31}P formally has the second-highest BIONMR receptivity, its signal is normally dispersed into multiple resonances in nature.
^{23}Na is by far the second most NMR sensitive nucleus in biological systems and it has a very short relaxation time of 1-60 ms. While the signal produced by the ^{23}Na nucleus following a single RF pulse is an order of magnitude smaller than that generated by protons, its relaxation times are often two orders of magnitude shorter than those of protons in a similar environment. Therefore, in time-averaging experiments, the ^{23}Na NMR signal acquired per unit time is comparable to that resulting from a similar population of protons.
It is possible to carry out NMR experiments with ^{39}K NMR, however, it tends to be more difficult to study due to its low BIONMR receptivity which is 180 times less then ^{23}Na NMR signals.
Unfortunately, the real sensitivities of ^{25}Mg and ^{43}Ca are so low that Mg^{2+} and Ca^{2+} at natural abundance are extremely difficult to study by NMR techniques.

2.4.1.1 Isochronicity of compartmental resonances

Two problems arise in the use of NMR techniques with biologically important quadrupolar nuclei : isochronicity and the possible invisibility of cations.

The first problem is that the ^{23}Na and ^{39}K signals from the various compartments are isochronous. This means the ^{23}Na signals from the intra- and extracellular compartments occur at precisely the same chemical shift. This is presumably because Na^+ is present mostly as hydrated cations and therefore the chemical environment or chemical shift of the ^{23}Na nucleus (which is dependent on its immediate electronic environment) remains unaltered in different compartments.[28-30] Therefore, the more interesting, smaller ^{23}Na resonance of intracellular ions is masked by the less interesting but much larger resonance of extracellular ions.

2.4.1.2 Invisibility of sodium and potassium signals

The second problem is the finding of partial NMR invisibility of ^{23}Na and ^{39}K signals from tissues. This is the term most often used for the situation in which the integrated ^{23}Na or ^{39}K spectral intensity, obtained under relatively high resolution conditions, is less than that expected for the total amount of Na^+ or K^+ known to be present from chemical analyses (Table 2.7). This arises when $^{23}Na^+$ or $^{39}K^+$ are subject to quadrupolar interactions from being bound to slowly tumbling cell components such as proteins or membranes

The clearest explanation of this invisibility phenomenon is given by Berendsen and Edzes.[31]

The NMR invisibility of the ^{23}Na and ^{39}K in tissues is due to the presence of static and/or dynamic quadrupolar effects caused by the microenvironments of the Na^+ and K^+ ions in tissue. Table 2.6 reveals that most of the biological magnetic nuclides have electric quadrupole moments (Q) (the nuclear spin quantum number is ≥ 1). Therefore, the nucleus distorts, and instead of a spherical distribution of charge, we have a prolate or oblate ellipsoidal distribution of charge.

	Volume of the sample (ml)	Na^+ content (mmol)	
	Flame photometry	NMR	Ratio
Incubated in 1 mM	7.8	268	117	0.43
Incubated in 5 mM	8.2	307	123	0.40

Table 2.7 State of Na^+ in the frog skin.[32]

In the presence of an electric field gradient at the nucleus (eq), the distribution of electric charges is asymmetric as depicted in Figure 2.14. The product $\chi = (eQ.eq)/\hbar$ is called the quadrupole coupling constant, and in the case of the ^{23}Na nucleus is of the order of 1 MHz in aqueous solution.

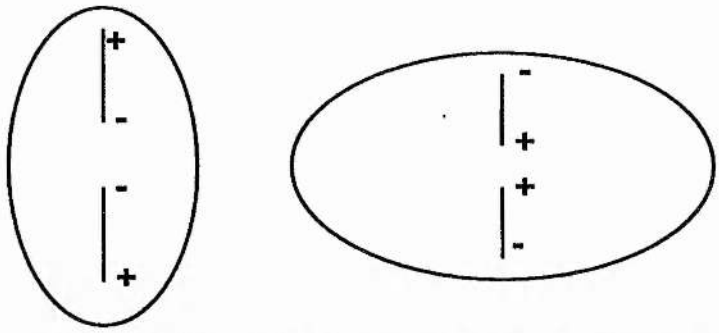

Figure 2.14 Charge distribution in asymmetrical nuclei.

With a spin number I=3/2 the ^{23}Na can assume 2I+1= four orientations in a magnetic field $\mathbf{B_0}$. The projections of the spin vector I along the $\mathbf{B_0}$ axis have the values m_I= -3/2, -1/2, +1/2, and +3/2. The transitions between the corresponding energy states are degenerate in the absence of an electric field gradient at the nucleus (q=0). The degeneracy is lifted by the quadrupolar interaction ($q \neq 0$) (Figure 2.15).

The resultant three transitions should show up as three equidistant lines, the central line with 40% of the total intensity, and the outer lines having each 30% of the total intensity. However, there are two types of interactions: static quadrupolar effects and dynamic quadrupolar effects which make the two quadrupolar transitions (3/2->1/2) and (-1/2->-3/2), disappear from the spectrum, we would therefore observe only 40 % of the expected intensity.

Further details of these phenomena are described in Lindblom and Lindman's article.[33]

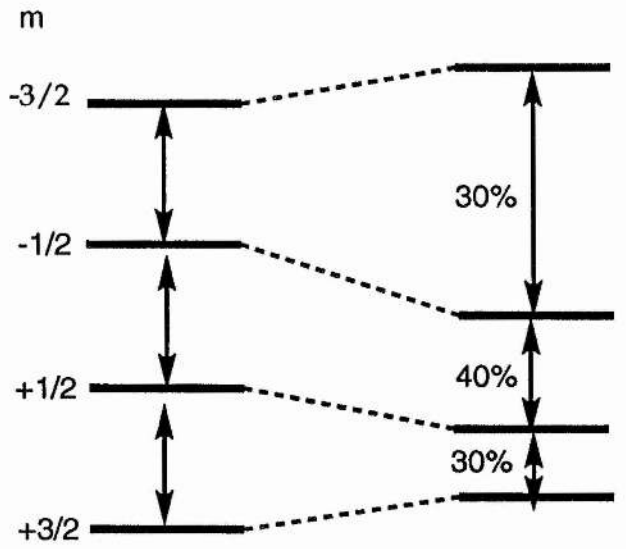

Figure 2.15 Energy states of spin 3/2 nucleus in the absence (left) and in the presence (right) of a quadrupolar interaction.

2.4.2. The use of contrast reagents for metal cations

As already mentioned, the lack of spectral discrimination between intra- and extracellular alkali cation resonances has restricted the use of NMR.
However, since 1982[34] it has been possible to distinguish between the two by using two different means: the first method involves the use of chemical shift reagents which rely on interaction between the cation and a paramagnetic lanthanide such as dysprosium or terbium.
The second method involves the use of relaxation reagents which rely on placing the cations in a region where they are subject to a large quadrupolar or paramagnetic interaction and are thereby relaxed.

2.4.2.1 Shift reagents for cation NMR

The shift reagents used are anionic chelate complexes of paramagnetic lanthanides (Dy^{3+}, Tm^{3+},Tb^{3+}). The binding of a paramagnetic ion to a molecule causes the resonances from the nuclei close to the binding site to shift and broaden as a result of the interactions between the unpaired electron density associated with the paramagnetic ion and the nuclear spin.
The resonance from the intracellular Na^+ is not affected because the lanthanide complexes do not penetrate the biological or artificial membrane.

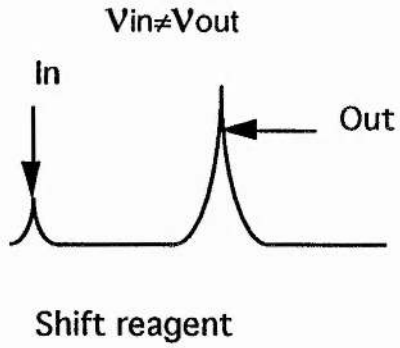

Figure 2.16 Effect of chemical shift reagents.

Shift reagent	Acid anion	
$[Dy(PPP)_2]^{7-}$	Tripolyphosphate	$(P_3O_{10})^{5-}$
$[Dy(DPA)_3]^{3-}$	Dipicolinate	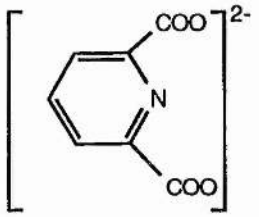
$[Dy(NTA)_2]^{3-}$	Nitrilotriacetate	$[N(CH_2COO)_3]^{3-}$
$[Dy(CA)_3]^{6-}$	Chelidamate	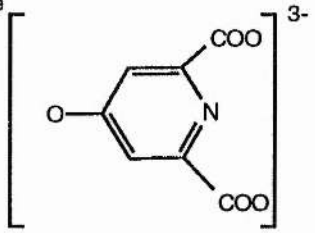
$[Dy(THHA)]^{3-}$	Triethylenetetraminehexaacetate	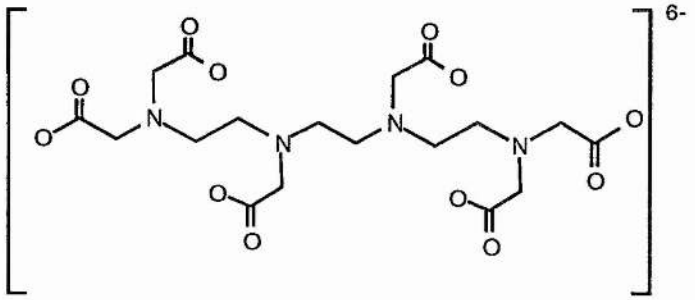
$TmDOTP^{5-}$	Thulium 1,4,7,10-teraazacyclodecane-1,4,7,10-tetrakismethylenephosphonate	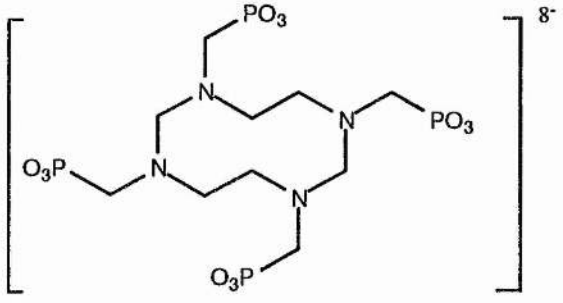

Figure 2.17 Structure of ligands of the lanthanide shift reagents.

2.4.2.2 Relaxation reagents for cation NMR

In contrast to the chemical shift reagents, relaxation reagents increase the linewidth of the resonance from the cation in the same environment until the signal is no longer visible, as shown in Figure 2.18.

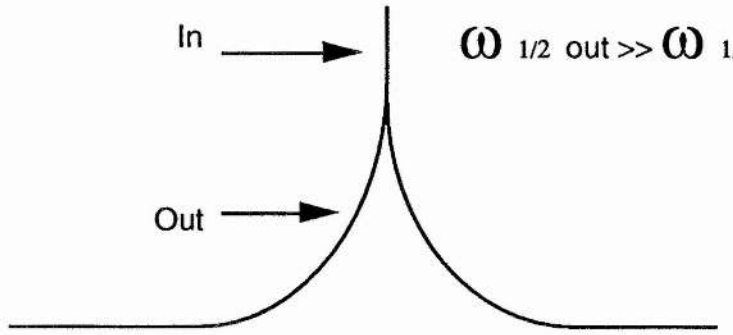

Figure 2.18 Relaxation shift reagents.

2.4.3 The use of NMR to study ion transport

2.4.3.1 Kinetics of the transport process

Previous work from this research group has involved the study of the transport of alkali metal ions mediated by ionophoric antibiotics in large unilamellar vesicles (LUV). These vesicles were made from egg yolk phosphatidylcholine suspended in a dilute aqueous salt soultion and were grown by dialytic detergent removal. The ionic strength and cation concentration were identical inside and outside of the vesicles. No osmotic pressure or ion gradients were involved in the rate equation. The model shown in Figure 2.19 was proposed by Pressman.[35] The rate of formation and dissociation are multistep processes but are represented by a single rate constant.[36-38]

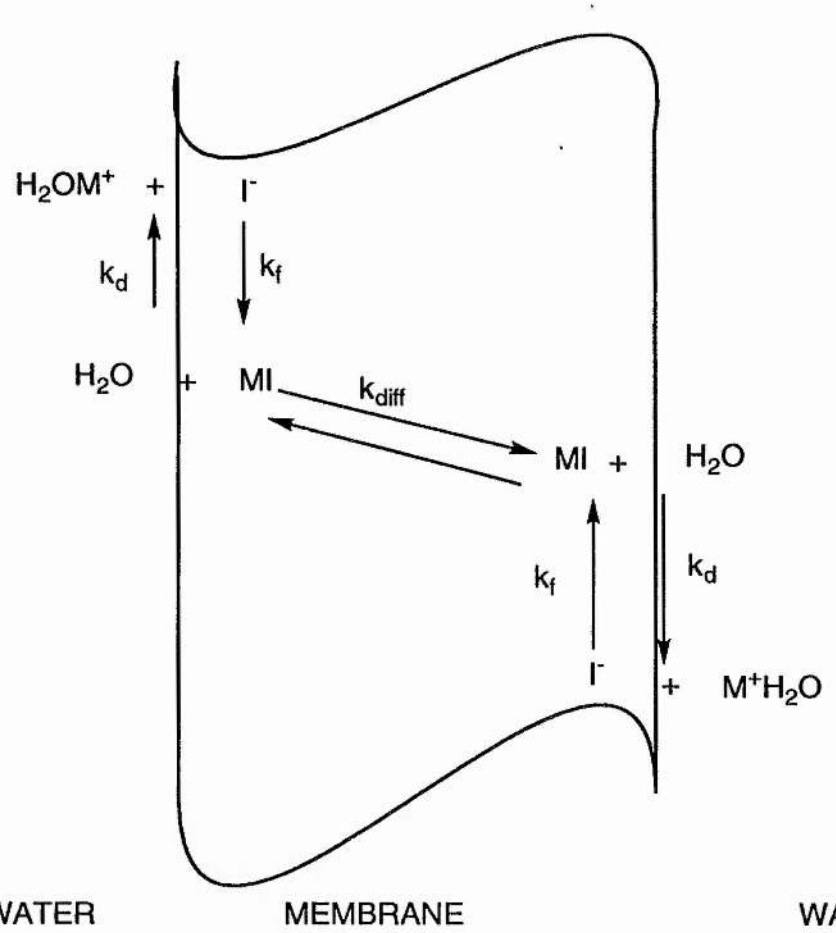

Figure 2.19 Model used to describe ionophore mediated ion transport through phospholipid bilayers.

This model gives rise to the following rate equation for exchange in vesicle systems.

$$\frac{1}{\tau_{M^+_{In}}} = \frac{A.k_{diff}.k_d.[L]_T}{V_{In}.(k_d + 2k_{diff}).([M^+] + k_d / k_f)} \quad \text{Equation 2.1}$$

where:

$\tau_{M^+_{In}}$ Lifetime of M^+ inside a vesicle

A Surface area

V_{In} Internal volume

$[L]_T$ Total concentration of ionophore

k_f Rate of formation of the complex

k_d Rate of dissociation of the complex
k_{diff} Diffusion coefficient of the complex
$[M^+]$ Metal ion concentration

This equation can be simplified by the introduction of two terms:

$$K_m = \frac{k_d}{k_f} = K_S^{-1} \qquad \text{Equation 2.2}$$

$$V_m = \frac{k_{diff}.k_d}{(k_d + 2k_{diff})} \qquad \text{Equation 2.3}$$

Where K_S is the stability constant of the ionophore.
Substituting these into equation 2.1 gives the simplified version.

$$\frac{1}{\tau_{M^+_{In}}} = \frac{A.V_m.[L]_T}{V_{In}.(K_m + [M^+])} \qquad \text{Equation 2.4}$$

From this equation it can be seen that the process will be first order in ionophore concentration with a rate constant.

$$k_2 = \frac{A.V_m}{V_{In}.(K_m + [M^+])} \qquad \text{Equation 2.5}$$

A plot of $1/k_2$ versus $[M^+]$ will have a gradient of $V_{in}/ A.V_m$ and an intercept of $V_{in}.K_m/ A.V_m$. Therefore, the ratio of slope to intercept is the stability constant of the membrane bound complex.
There are two limiting conditions depending on whether the diffusion coefficient is small or large with respect to the rate of dissociation.

- If $k_{diff} >> k_d$ then $V_m = k_d/2$
  Therefore the slope is proportional to $1/k_d$ and the intercept to $1/k_f$.
- If $k_{diff} << k_d$ then $V_m = k_{diff}$
  Therefore, the slope is proportional to $1/k_{diff}$ and the intercept to K_m/k_{diff}.

If neither of these conditions hold then these equations are too complex and they are out of the scope of this thesis.

2.4.3.2 NMR measurement techniques

The rate of exchange across the vesicle membrane is measured by different NMR techniques such as dynamic line broadening, magnetisation transfer and isotope exchange.

2.4.3.2.1 Dynamic line broadening

This technique relies on the coalescence of signals from rapidly exchanging sites into a single peak in the NMR spectrum. It works when the rate of exchange is similar to the chemical shift differences between the sites expressed in Hz. Near the fast and slow exchange limits, the line broadening is proportional to the rate of exchange between the two sites.

It is possible to distinguish between three exchange regimes depending on the velocity of this process, as depicted in Figure 2.20.

(i) Slow exchange. If the rate of exchange is slow (on the NMR time scale) then the NMR spectrum shows two separate peaks.

(ii) Fast exchange. If the rate of exchange is fast, the NMR spectrum observed is one 'averaged' spectrum in which a single peak represents the weighted averages of the two peaks.

(iii) Intermediate rates of exchange. In this case we observe broad lines in the NMR spectrum.

Therefore, this technique is suitable for studying the rate of exchange of Na^+ and K^+ mediated by ionophoric antibiotics such as cationomycin. This method requires a good separation between the 'in' and 'out' signals to be of use.

This technique enables the calculation of k_2 from a single set of vesicles by following the changes in linewidths as successive aliquots of ionophore are added.

Typically speaking, the rate of exchange measured with this method is in the range 5-100 s^{-1}.

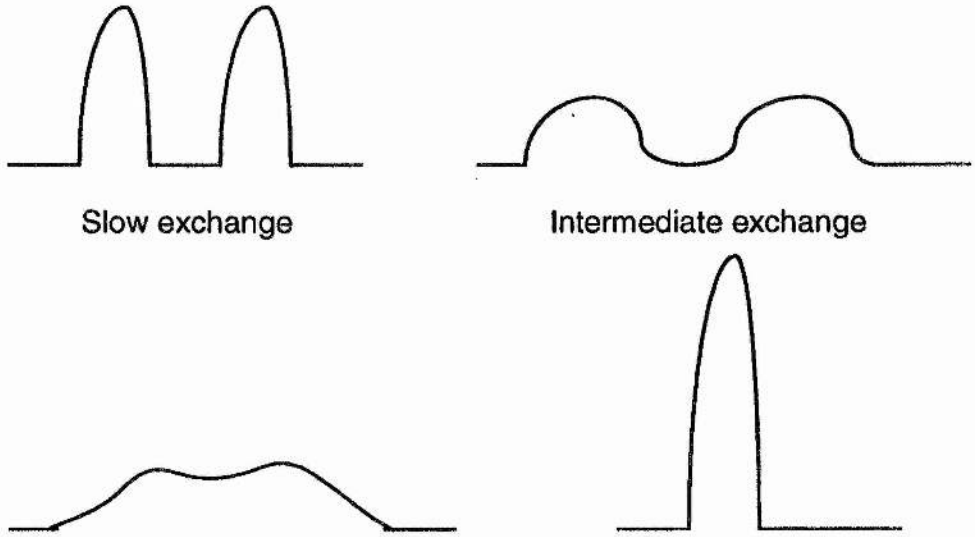

Figure 2.20 The effect of line broadening.

2.4.3.2.2 Magnetisation transfer

One-dimensional magnetisation transfer NMR experiments rely on the spins at one of the exchange sites being either selectively inverted or selectively saturated. In order to obtain such a frequency selective excitation, either a long, 'soft' pulse or a long duration train of short, 'hard' pulses, termed DANTE[39,40] (Delays Alternating with Nutations for Tailored Excitation) sequence or specific site inversion is usually necessary.

The technique commonly used in our group relies on placing a magnetic label at one site by inverting the spin population (inverted signal), and then following the intensity at the other site as the inverted signal relaxes back. If there is chemical exchange on the time scale of the relaxation process a reduction in intensity of the monitored signal will be observed.
Successful application of magnetisation transfer depends entirely on having the the shortest possible delay. If the magnitude of the delay is too large, then the spins will have begun to relax transversely and longitudinally before the last two 90° pulses are applied. In the extreme narrowing region, the longitudinal and transverse relaxation times are of the same magnitude. The longitudinal

relaxation is determined by the conventional technique, which is the inversion recovery technique.[40]

As we have seen, magnetisation transfer requires a long relaxation time in order to operate at the optimum condition. Therefore this method[41] is suitable for nuclei such as ^{6}Li (T_1 typically 10 to 80 s). and ^{7}Li (T_1 0.3 to 3 s) and less suitable for nuclei such as ^{23}Na (T_1 0.06 s) and ^{39}K (T_1 2 x10^{-2} s).

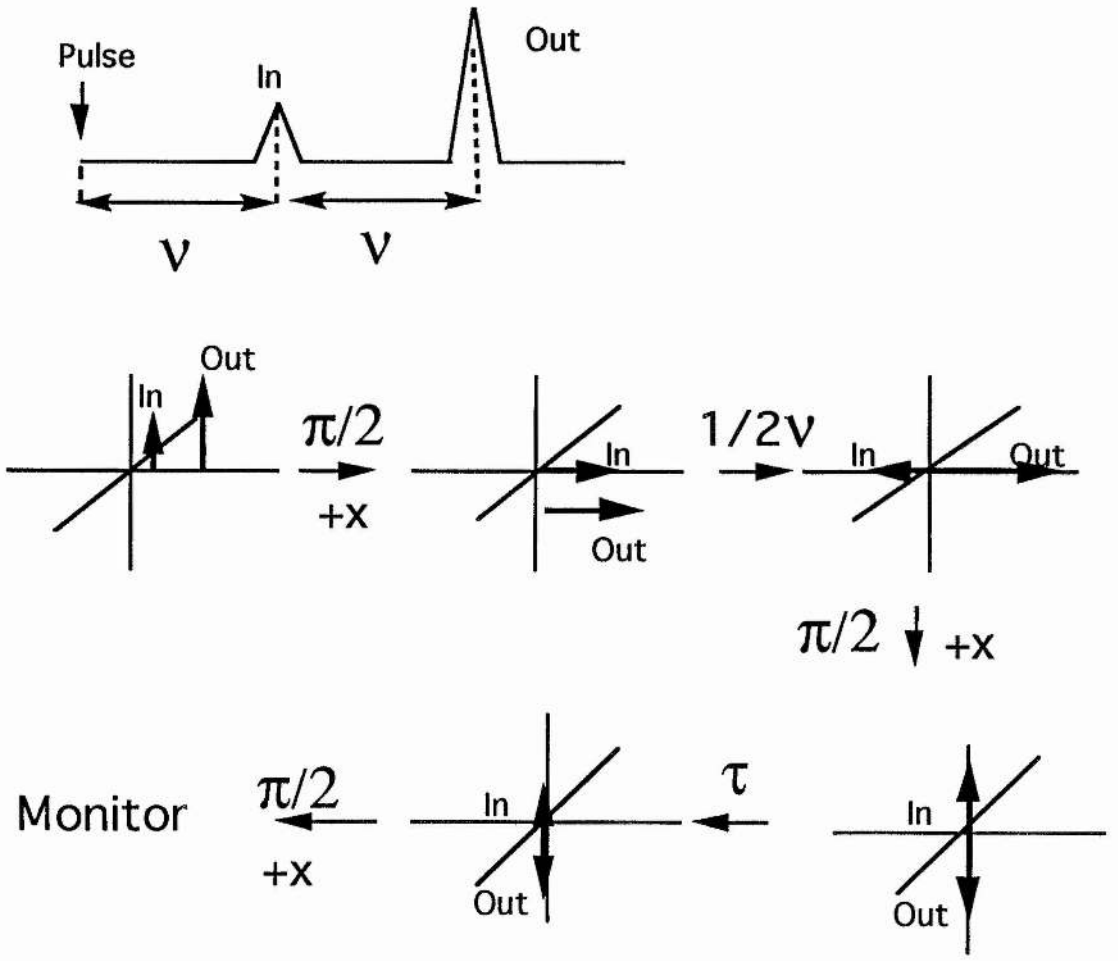

Figure 2.21 The pulse sequence used for magnetisation transfer experiments.

2.4.3.2.3 Isotope exchange

Isotope exchange is the simplest method used, and relies on following the decrease of the peak-intensity after adding an aliquot of ionophore. It relies on having different isotopic compositions on either side of the membrane *e.g* $^{7}Li/^{6}Li$ or $^{39}K/^{23}Na$. Three types of rate have to be considered: the leakage rate which is the exchange rate without the ionophore's contribution, the transport rate is the rate owing solely to the ionophore, and the diffusion rate is the sum of the leakage rate and transport rate. The area of the 'in' peak is obtained by integration usually expressed as a ratio of the inside/ outside peaks or by a factor which is the ratio between the first peak intensity at t=0 and the peak intensity at time t. Spectra are acquired at regular intervals after the addition of ionophore. The data are analysed using straightforward kinetic methods applicable to a first order process. The transport rate is then calculated from a plot $\log(I_t-I_\infty)$ versus time where I_t is the peak intensity after time t and the I_∞ the final peak intensity is obtained rapidly after adding a powerful ionophore such as monensin. The transport rate constant is obtained directly from the plot of rate against the concentration of ionophore in the membrane.
This method is suitable for slow exchange rate constants. Typically, the rates of exchange measured are in the range of 10^{-4}-10^{-5} s^{-1}.

2.4.3.2.4 Treatment of data

The dynamic line broadening method was used in order to calculate the rate and stability constants (k_f, k_d, K_s) from the kinetic data for cationomycin. Two different graphs were required, the first graph plots rate ($1/\tau_{M+in}$) versus I/PC. I/PC represents the ratio between the quantity of ionophore and phosphatidylcholine. It is preferable to plot I/PC rather than $[L]_t$ since it is normalised and allows comparison with other experiments. The gradient of this line is the first order rate constant for efflux: k.
In the case where the diffusion coefficient is much greater than the dissociation rate constant of the metal/ ionophore complex the second graph plots 1/k versus metal ion concentration. The rates of dissociation (k_d) and formation (k_f) of the complex are inversely proportional to the slope and intercept respectively.

2.4.3.2.5 Concluding remarks to NMR measurement techniques

NMR offers a unique and powerful technique to study the rate of exchange without disturbing the artificial or biological system. As already mentioned, the choice of these techniques depends on the time scale of the process.
Dynamic line broadening is designed to be used for very rapid exchange rates where the rate is greater than 5 s^{-1}. The magnetisation transfer technique is suitable for intermediate rates, where the exchange rate is comparable to the NMR relaxation time 10^{-1}-$1s^{-1}$. Finally, isotope exchange measures the very slow exchange rates in the range of 10^{-4}-$10^{-5}s^{-1}$ between the same or different nuclei.
In principle, it is possible to investigate *in vivo* ionic transport phenomena within the human body, such as the kinetics of Na^+/K^+/ATPase. However, there are two main problems which restrain the use of these techniques.
The first one is due to the toxicity of the lanthanide shift reagents to cellular systems. The second one[42] is because the shift reagent induced hyperfine shifts are pH dependent and inversely proportional to the amount of divalent cations present. $Dy(PPP)_2^{7-}$, for example, has maximum shifting power in the absence of Mg^{2+} or Ca^{2+} and near pH 8. Most transport enzymes require the presence of Mg^{2+} and a pH near 7 for maximum activity.

2.5 Kinetic studies of cationomycin

Cationomycin, isolated from *Actinomadura azurea* , presents higher antibacterial activity, displays selectivity of complexation and transport for K^+, and furthermore shows a lower toxicity in mice[14] compared with other ionophores of the group. From a study of the literature it appears that very little information is available on the transport abilities of cationomycin and its derivatives. The only data concerns bulk Na^+ transport across a CCl_4 layer.[18] No data has been collected for K^+ transport.
The present studies of the ionophoric properties of cationomycin were carried out in close collaboration with the University of Clermont-Ferrand (France) using two different systems: large unilamellar vesicles and human erythrocytes or Red Blood Cells (RBCs).

Large Unilamellar Vesicles (LUVs) are excellent models for studying the transport of metal ions through phospholipid bilayers and these kinetic studies were performed at the University of St. Andrews (UK).
In a typical experiment, LUVs are prepared by the dialytic detergent removal technique introduced by Reynolds[43] and employed in our previous studies[36-38] with equal concentrations of metal ions inside and outside the vesicle. A chemical shift difference for the alkali metal ion is established by the use of an aqueous shift reagent and a dynamic line broadening technique is used to obtain transport rates as the ionophore is added. The classical mobile carrier system presented by Painter and Pressman[44] is satisfactory to account for the observed kinetics. A series of equations has been developed to allow dissection of the rate data into the formation rate of the metal ion at the membrane surface (k_f) the dissociation rate (k_d) and the diffusion coefficient (k_{diff}).[36]

In contrast to LUVs, erythrocytes present a real biological membrane structure with ion gradients on both sides. Modifications of the Na^+ gradients induced by cationomycin on red blood cells (RBCs) were studied by ^{23}Na NMR in the presence of $[Dy(PPP)_2^{7-}]$ as external shift reagent. This technique has been successfully applied for the study of erythrocytes.[34,44-51] Concomitant K^+ movements were measured by potentiometry in the external medium. Kinetic constants were determined and compared to those of monensin, a well-known ionophoric antibiotic whose selectivity is in favour of Na^+ versus K^+,[32,45-46,54-60] under the same experimental conditions. The experiments on erythrocytes were conducted in Clermont- Ferrand (France).

2.5.1 Selectivity of cationomycin

Polyether antibiotics present different affinities for diverse ions and therefore transport them at various rates. In this section, we try to establish the key element for better affinity towards Na^+ or K^+ cations.
Molecular mechanics calculations[10] show that the monensin ligand is more strained in its K^+ complex than its Na^+ complex, and that this extra strain in the K^+ complex is localised in the spiroketal group.

Polyether antibiotics	Selectivity Sequence
Monensin	$Na^+>K^+>Rb^+>Li^+$
Nigericin	$K^+>Rb^+>Na^+>Li^+$
Cationomycin	$K^+>Rb^+>Na^+>Li^+$

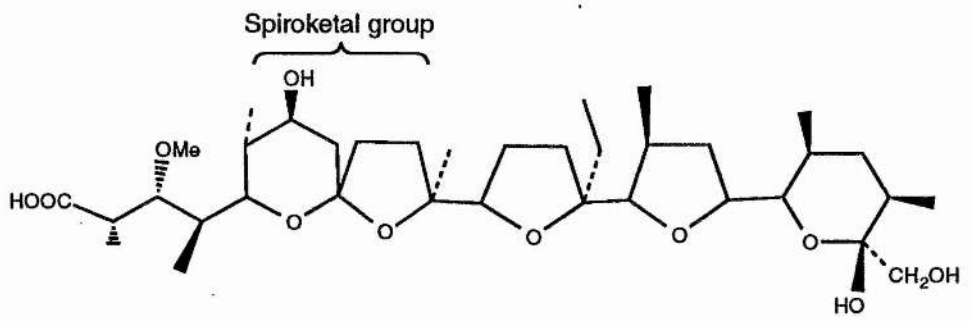

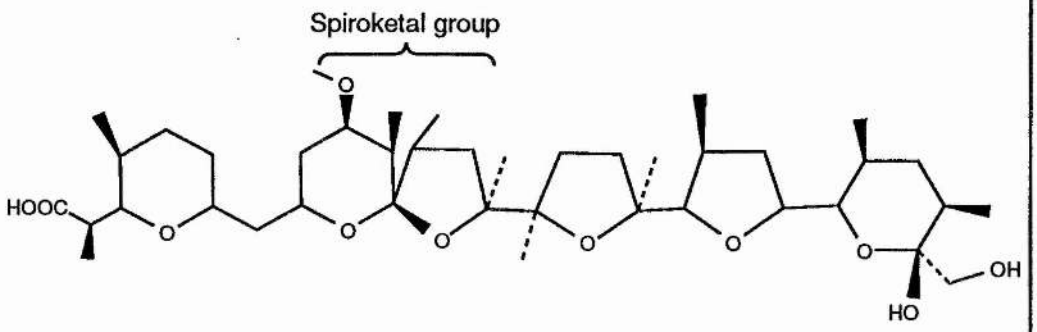

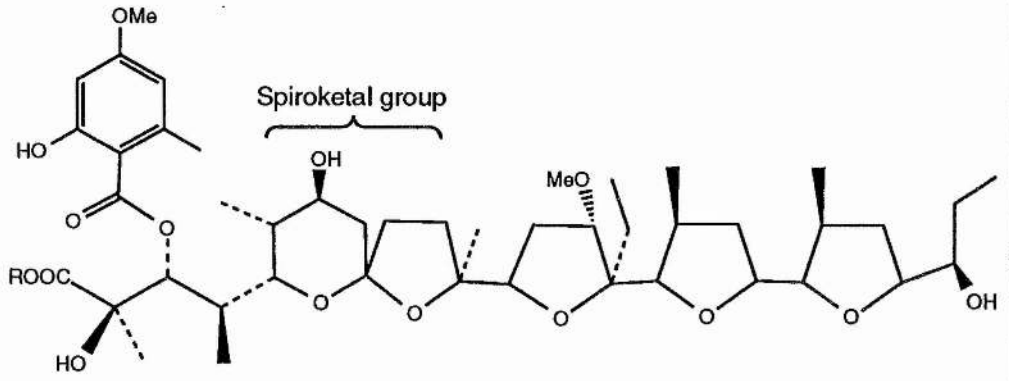

Figure 2.22 Selectivity sequence[9,18] of polyether antibiotics.

Looking at the spiroketal group in the crystal structure of its complex with K^+ shows that it coordinates to the metal ion to give a reinforced six membered chelate ring. Therefore the spiroketal group provides a rigid reinforced six membered chelate ring which should greatly promote selectivity for smaller metal ions. Furthermore, there exist several methyl groups situated on the spiroketal group of nigericin in such a way that coordination of the spiroketal group to the alkali ion will be sterically hindered.
Cationomycin has similar spiroketal group structures to monensin. However, cationomycin reveals a better affinity[18] towards K^+ rather then Na^+ ions. The influential factor seems to be the presence of the aromatic ring.

2.5.2 Sodium and potassium transport mediated by cationomycin

All experimental details are reported in Chapter 6 (section 6.1).

2.5.2.1 Results and discussion: Transport study with LUVs

The results for the ionophore mediated transport of sodium and potassium by cationomycin are given in Figure 2.24 and Figure 2.25 respectively.
As we have previously observed for other ionophoric antibiotics (Riddell *et al.* [36,37,53,61]) adding small aliquots of cationomycin to the vesicle preparation containing the same concentration of metal inside and outside the vesicle broadens both lines in the spectra in a fashion consistent with a dynamic exchange process between the M^+_{in} and M^+_{out} populations. For every sodium or potassium concentration studied the transport rate in the direction 'in' to 'out' varies linearly with the cationomycin/PC ratio, indicating a first-order relationship between cationomycin and the transport rate.
These findings present a strong confirmation that our model for ionophore mediated ion transport also applies to cationomycin, involving a 1:1 complex between sodium or potassium and the cationomycin during the transport process.
These graphs (Figures 2.24, 2.25, 2.26) allow the extraction of the rate constants for complex formation in the membrane surface (k_f=1/intercept) and for dissociation (k_d=1/slope) (see Table 2.8). The ratio of slope to intercept gives the stability constant of the metal/ ionophore complexes in the membrane surface (Table 2.8) and it is the K^+ complex that is the more stable.

The values obtained are typical of the other ionophoric antibiotics that we have studied previously. It is worth noting that cationomycin transports Na^+ more slowly than monensin and forms a lower stability complex with Na^+ because of the lower formation rate for the complex in the membrane surface (Table 2.8). The values for K^+ are lower than those for Na^+ showing more rapid transport of K^+ at all concentrations studied (Figure 2.26). Cationomycin both transports K^+ more rapidly then Na^+ and forms a more stable complex with K^+. In biological systems cationomycin will be almost exclusively involved in K^+ transport.
Cationomycin (MW 851 $g.mol^{-1}$) is a larger ligand then monensin (MW 671 $g.mol^{-1}$) or nigericin (MW 725 $g.mol^{-1}$) and therefore the K-cationomycin and Na-cationomycin complexes should diffuse more slowly than the corresponding M-monsensin and M-nigericin complexes. In fact the slopes for the M-cationomycin complexes are comparable to those for the other ligands. This would not be the case were diffusion the rate limiting step. In addition the derived dissociation rates (*ca* 0.16×10^{4} $M.s^{-1}$) which might be interpreted as diffusion coefficients are greater than that for K-nigericin (0.10×10^4 $M.s^{-1}$). We believe, therefore, that dissociation not diffusion is the rate limiting step.

	Sodium			Potassium		
Ionophore	k_f	k_d	K_s	k_f	k_d	K_s
	10^4 s^{-1}	$10^4 Ms^{-1}$	M^{-1}	10^4 s^{-1}	$10^4 Ms^{-1}$	M^{-1}
Cationomycin	1.88	0.16	12.1	10.5	0.17	62.9
Tetronasin	20.52	0.86	24.0	5.65	0.80	7.0
Monensin	4.88	0.15	32.6	2.30	0.43	5.3
Nigericin	7.84	0.35	22.0	9.61	0.10	96.0
Salinomycin	2.61	0.43	6.1	28.3	1.39	20.4
Narasin	5.86	0.54	11.0	14.7	1.67	8.8

Table 2.8 The dissociation, formation and stability for some polyether antibiotics with sodium and potassium.[62]

Cationomycin vs [K+] at 200mM

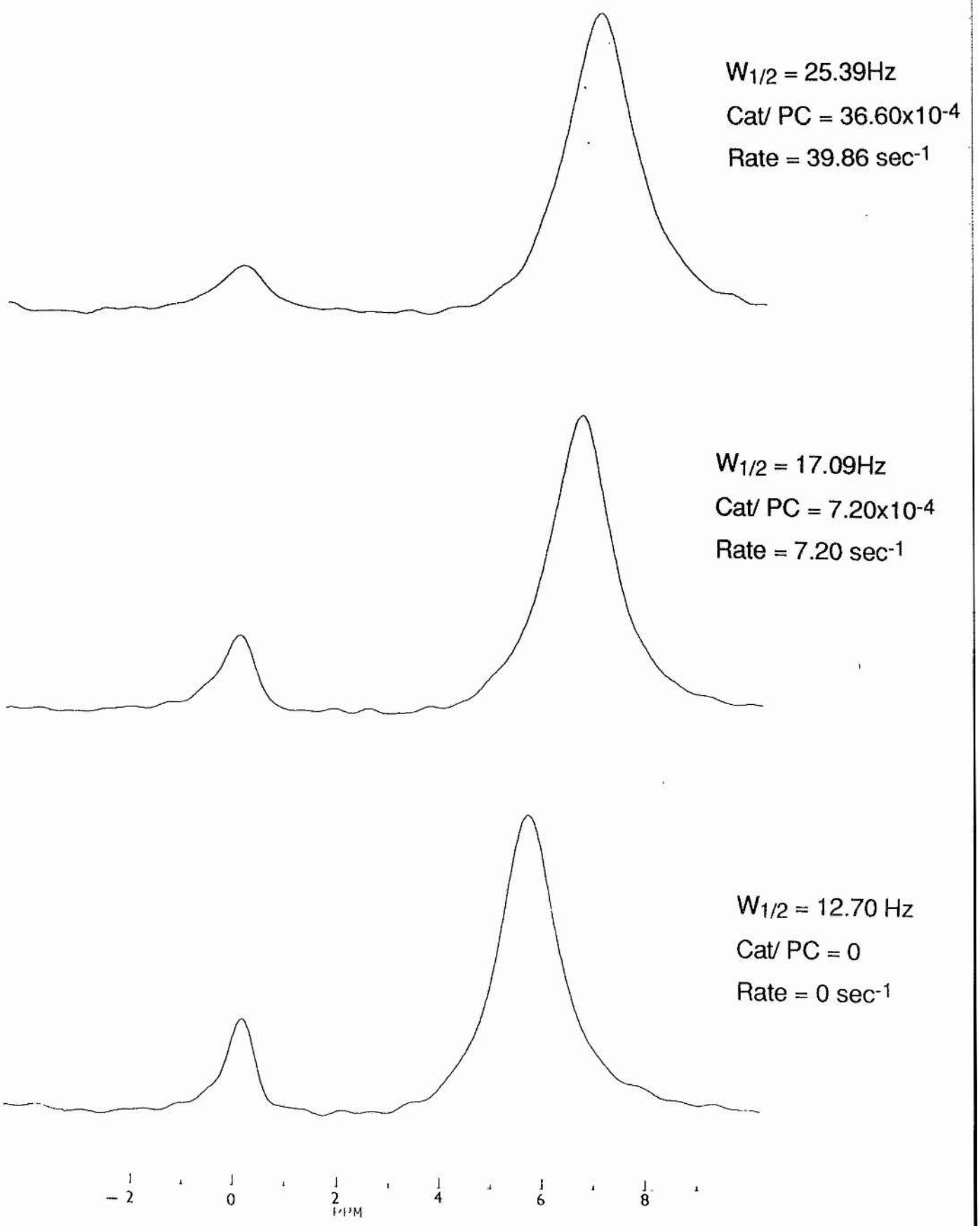

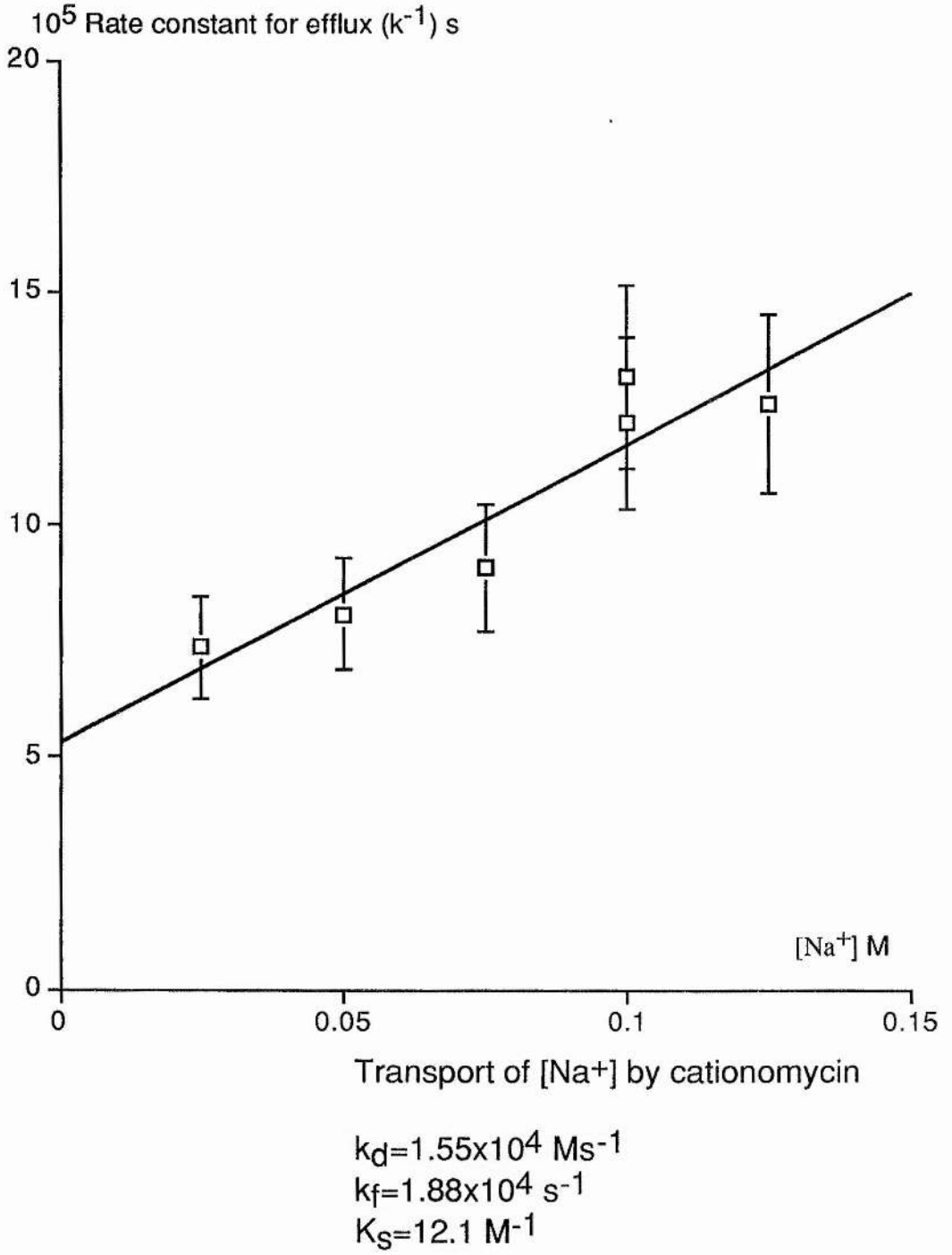

Figure 2.24 Graph showing the linear relationship between k^{-1} and [Na+] from which the values of k_f and k_d are obtained .

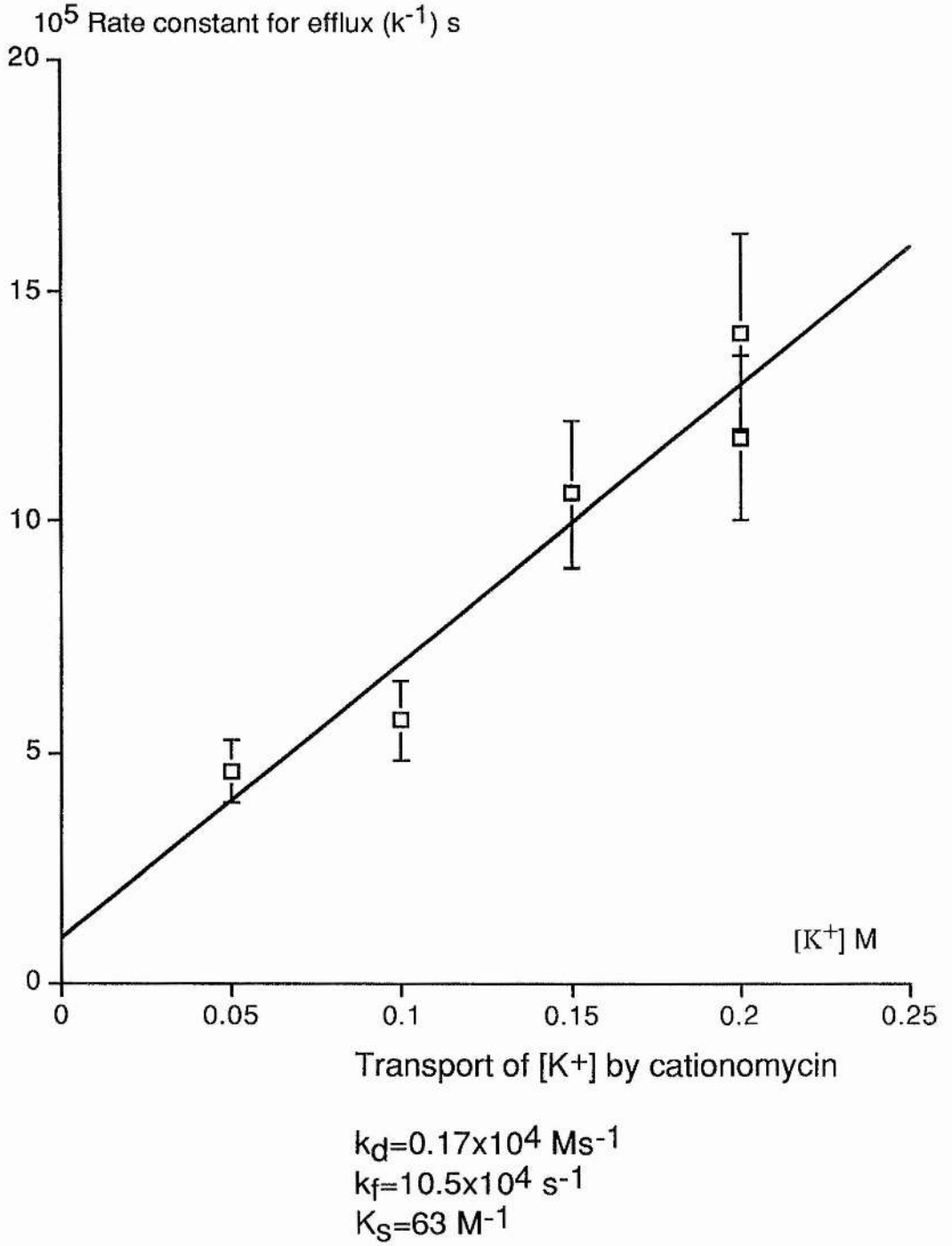

Figure 2.25 Graph showing the linear relationship between k^{-1} and $[K^+]$ from which the values of k_f and k_d are obtained .

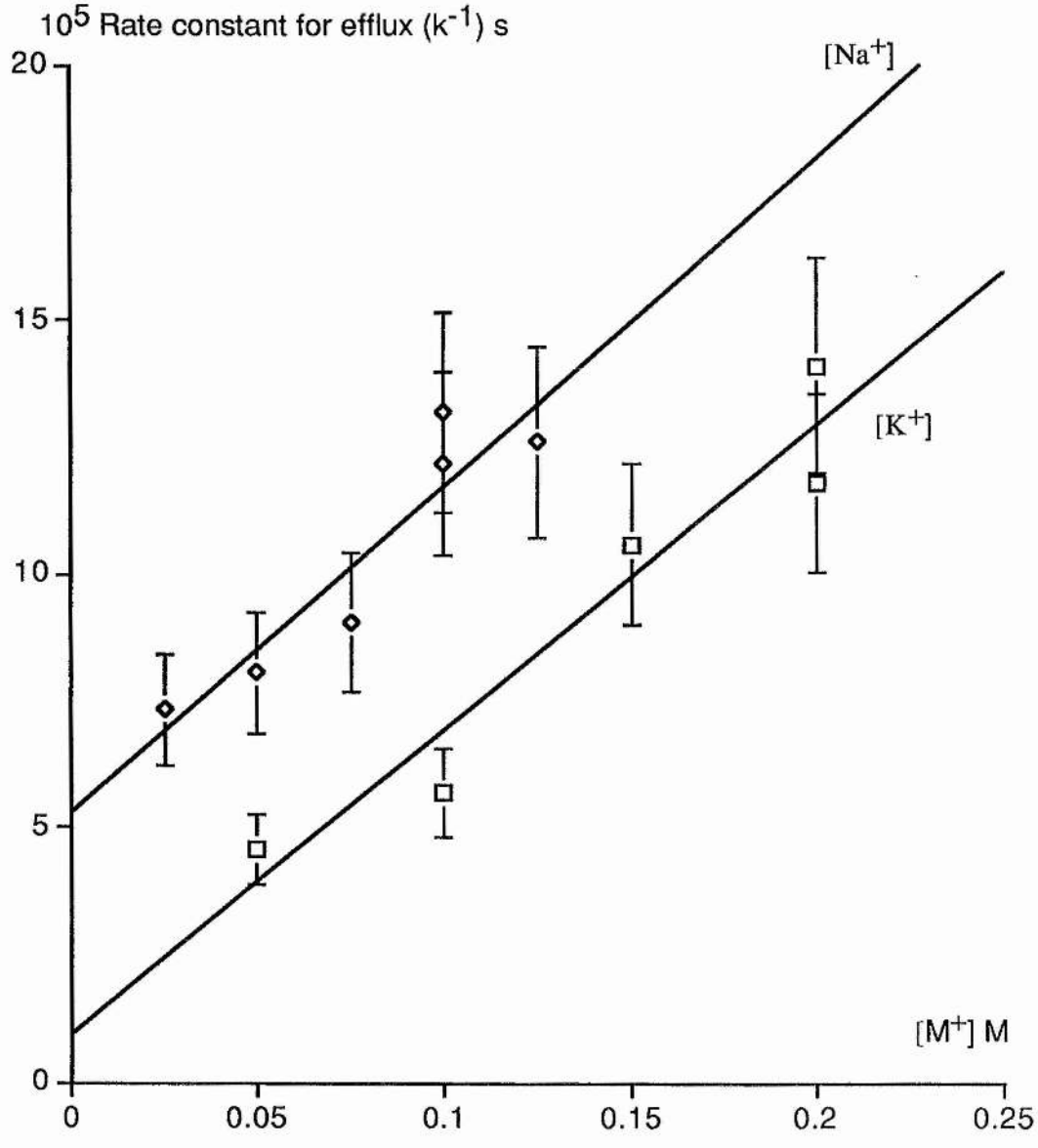

Figure 2.26 Graph showing the linear relationships between k^{-1} and $[M^+]$ from which k_f and k_d are obtained.

2.5.2.2 Results and discussion: Modifications of sodium and potassium gradients in human erythrocytes

Under physiological conditions, human erythrocytes show ionic concentrations on both sides of the membranes that are those encountered for living cells: $[Na^+]_{in}$ (~10 mM) << $[Na^+]_{out}$ (~150 mM); $[K^+]_{in}$ (80 mM) >> $[K+]_{out}$ (<1 mM). They make interesting models to study the ionophoric properties of cationomycin, especially with respect to its cation carrying efficiency, Na^+/K^+ transport selectivity, and pH modifications.

For several technical reasons, mainly linked to the NMR method (*e.g.* sensitivity, homogeneity of the medium), the experimental conditions for ^{23}Na NMR studies (hematocrit 40%) were slightly different from those for potentiometric measurements (hematocrit 20 %). For the sake of consistency, the ionophore concentrations were expressed not in the whole suspension but in the membrane [^{m}HA]: (these compounds are not soluble in the water phase). The volume of the membrane (mV) was estimated from the number of red cells, their volume and the thickness of the membrane (see Chapter 6 section 6.1.2).
The time dependence for the variation of the internal sodium content (ΔNa^+) and of the external potassium content (ΔK^+) in the presence of increasing cationomycin concentrations are reported in Figures 2.27 and 2.28 respectively. Note that in the absence of the ionophore, the erythrocytes maintained fairly constant Na^+ and K^+ gradients.
These experiments clearly help to characterise Na^+ and K^+ transporting abilities of cationomycin. The currents of transport for Na^+ ($i_{Na}+$) and K^+ (i_K+) were determined from the initial rates in Figure 2.28. These ionic currents (i) are expressed in 10^{-6} moles.min^{-1} by ml of erythrocyte suspensions. They are plotted as a function of ionophore concentration in the membrane [^{m}HA] (Figure 2.29 A and B). The relationship was linear i=k.[^{m}HA] which allowed the determination of the (first order) rate constants (k) for the transport process of Na^+ and K^+ (Table 2.9). The ratio $k_{Na}+/k_K+$ indicates that the selectivity of transport for cationomycin is in favour of sodium as compared to potassium.

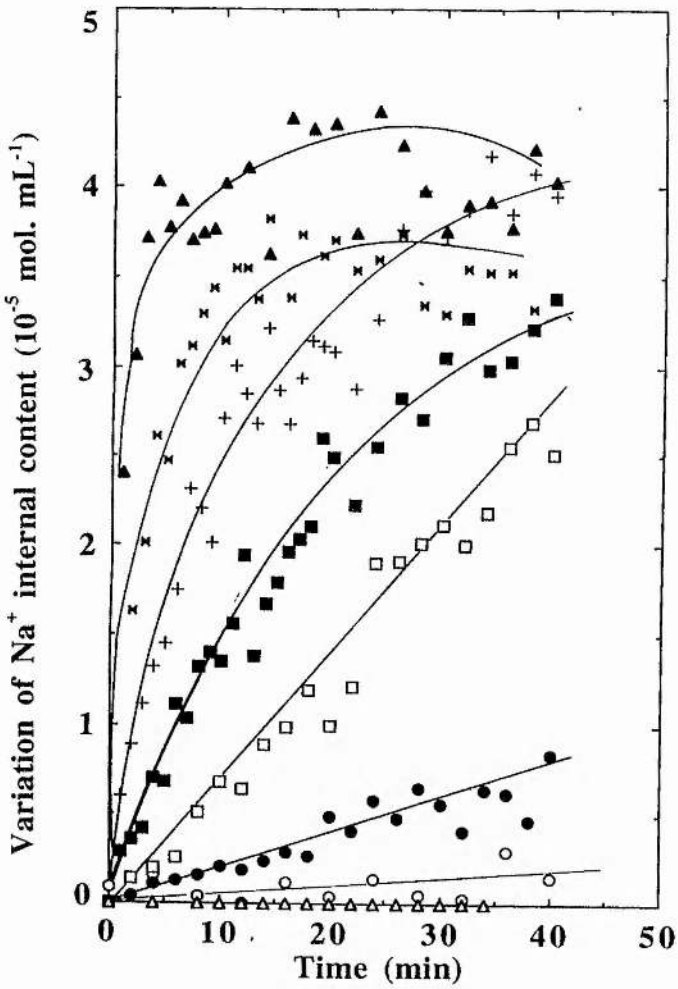

Figure 2.27 Effect of the increasing concentrations of cationomycin on the intraerythrocyte sodium content and ionophore-induced K^+ release. Time dependence of the variation of Na^+ internal concentration (ΔNa^+) determined from ^{23}Na NMR recorded every 1 or 2 min. at 79.39 MHz for 40 min. 2 ml of RBC (hematocrit 40%) were incubated at 310 K with increasing concentrations of cationomycin in the membrane ([HA]) in a buffer containing 98 $x10^{-3}$ M NaCl, 6 $x10^{-3}$ M $Na_7(P_3O_{10})_2$, 30 $x10^{-3}$ M sucrose, 5 $x10^{-3}$ M NaH_2PO_4, pH 7.4 $\Delta Na^+ = [Na^+]_{time\ t} - [Na^+]_{time\ 0}$.
(Δ) 2.6 $x10^{-4}$ M, (x) 1.3 x 10^{-4} , (+) 3.3 $x10^{-5}$M, (n) 1.6 $x10^{-5}$M
(r) 8.2 x 10^{-6}M, (O) 22.0x 10^{-6}M, (O) control sample, (D) deacylcationomycin 1.3 $x10^{-4}$M.

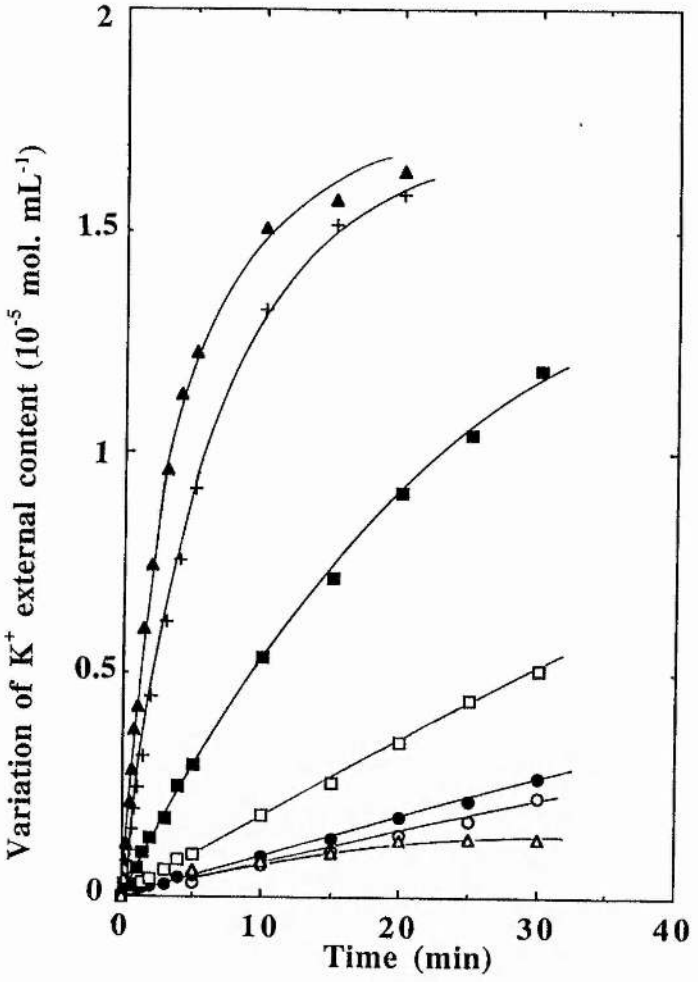

Figure 2.28 Effect of the increasing concentrations of cationomycin on the intraerythrocyte sodium content and ionophore-induced K^+ release. Time dependence of the variation of K^+ internal concentration (ΔK^+) in the supernatant measured by potentiometry every 5 min for 30 min. 5ml erythrocytes (hematocrit 20%) were incubated at 310 K in the presence of increasing concentrations of ionophores in the membrane ([^{m}HA]) in sodium buffer containing 140 x10^{-3}M NaCl, 30 x10^{-3} M sucrose, 5 x10^{-3} M NaH_2PO_4, pH 7.4 adjusted with choline hydroxide.

$\Delta K^+ = [K^+]_{time\ t} - [K^+]_{time\ 0}$.

(Δ) 1.3x10^{-4} M, (x) 6.6 x 10^{-5} (+) 1.6 x10^{-5}M, (n) 4.1 x10^{-5}M

(r) 2.0 x 10^{-6}M, (O) control sample, (D) deacylcationomycin 1.3 x10^{-4}M.

	Cationomycin min^{-1} l^{-1}	Monensin min^{-1} l^{-1}
$k_{Na}+$	43.5×10^{-3}	4.6×10^{-3}
k_K+	17.0×10^{-3}	1.0×10^{-3}
$k_{Na}+/k_K+$	2.5	4.6

Table 2.9 Kinetic constants of sodium $k_{Na}+$ and potassium k_K+ transport measured in human erythrocytes.

The ionic currents of transport for $Na^+(i_{Na}+)$ and $K^+(i_K+)$ were determined for monensin under the same experimental conditions in the membrane [^{m}HA] (Figure 2.28). The kinetic constants of transport (k) deduced from these results are reported in Table 2.9. The well-known selectivity of complexation and transport in favour of sodium, already observed for monensin, was confirmed here.[31,45-46,53-60]

These results clearly show that the efficiency of transport by cationomycin is much higher than that by monensin (about 10 fold for Na^+ and 17 fold for K^+). In addition, the selectivity of transport for Na^+ is lowered compared to that of monensin, however it is still substantial.

The following complementary experiments were performed:

- The time dependence of pH in the supernatant was measured with a glass electrode for cationomycin ([^{m}HA] $=1.3 \times 10^{-4}$ M). Under these conditions, no significant change was detected, which could result from an efficient buffering of the external medium, or also from the fact that Na^+/H^+ and K^+/H^+ exchanges take place in opposite directions, not necessarily with symmetrical effects. This was previously clearly shown for monensin.[46]

- The addition of 10^{-3} M ouabain, a well-established inhibitor of Na^+/K^+/ATPase, or the addition of 60 mM glucose, as an energy source, did not change the sodium currents induced by cationomycin or monensin ([^{m}HA] $=1.3 \times 10^{-4}$ M). These results clearly indicate that the ion transport induced by the ionophores, in the time range considered, do not seem to be efficiently compensated for by the erythrocyte ion transport systems and especially the Na^+/ K^+/ATPase. This is in good agreement with the pioneering work of

Pressman,[49] who reported that erythrocytes behave almost like inert model membranes even though they are energised.

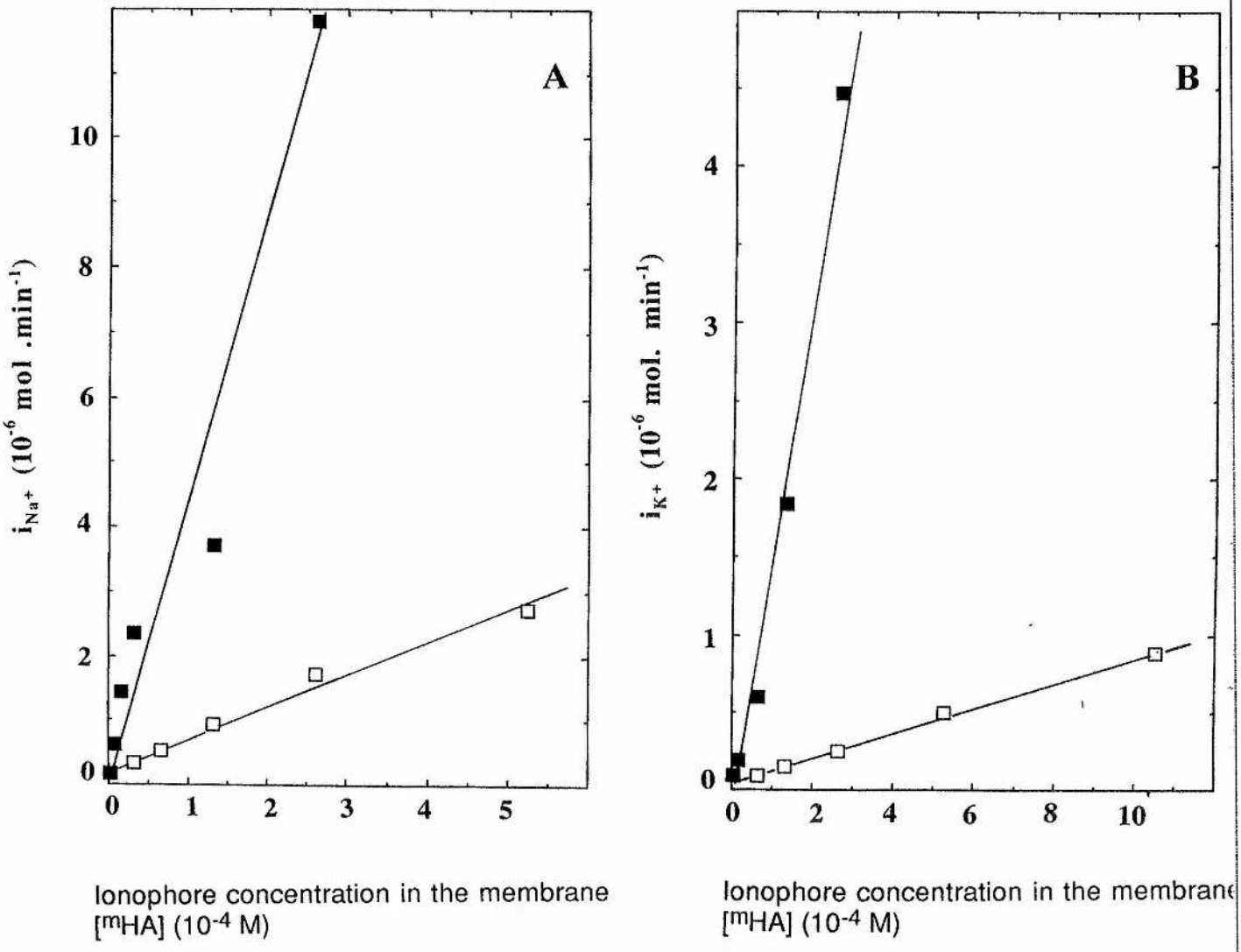

Figure 2.29 Correlation between sodium (A) and potassium (B) currents (i_{Na^+} and i_{K^+}) induced by cationomycin (n) and monensin (r) and the ionophore concentration in the membrane $i = k.[^mHA]$

- Deacylated cationomycin was also tested in our model ([^{m}HA]=1.3 x10^{-4}). No significant changes in sodium or potassium gradients were observed as shown in Figures 2.27 and 2.28. This result is in agreement with the slower transport of Na^+ measured by Ubukata[18,63] though in erythrocytes we observed an even lower transport efficiency.

2.5.2.3 Biological activities

The minimum inhibitory concentrations (MIC) determined on *Bacillus cereus* strain ATCC 14575 are much lower for cationomycin than for monensin. This result is in agreement with previous findings from the laboratory in Clermont-Ferrand (France); antibacterial activity increases with ionic selectivity in favour of potassium versus sodium.[29,58]
In Table 2.10 are reported some biological activities of cationomycin, deacylatedcationomycin and monensin.

Ionophore	IC_{50} *P. falciparum* ($ng.ml^{-1}$)	MIC *B. cereus* ($ng.ml^{-1}$)	*In vivo* toxicity on mice (nb of death)[47]
Monensin	1.5	1.56	2/10 (100mg /kg)
Cationomycin	35	0.05	0/10 (200 mg/ kg)
Deacylated-cationomycin	130	0.20	Not determined

Table 2.10 Comparison of biological activities of monensin, cationomycin and deacylatedcationomycin.

In contrast, cationomycin presents a lower antimalarial activity than monensin as evaluated by measuring the *in vitro* growth inhibition of *Plasmodium falciparum* IC_{50}.[64] This result is very surprising as the French group have shown that antimalarial activity was correlated with sodium and potassium transport efficiency.[46] As already shown by others, the toxicity of cationomycin in mice *in vivo* is very low.[14]
Deacylcationomycin presents poor biological activity. This result is in good agreement with the low antibacterial activity reported by Ubukata[18,63] and is

correlated with the loss of ionophoric properties of this compound. This reinforces the idea of the specific role of the aromatic side chain in the mode of action of cationomycin.

2.5.3 Conclusion

In this work we have studied the ionophoric properties of cationomycin, an unusual carboxylic polyether ionophore, in LUVs and human erythrocytes.
For transport by cationomycin in the model lipid membranes of the LUVs potassium is transported more rapidly and forms the more stable complex. The difference in transport rates arises because of a more rapid formation rate for the K^+ complex whilst the dissociation rates for the complexes of both metals are comparable. These results confirm the selectivity of complexation in favour of K^+ compared to Na^+ measured by Ubukata.[18,63]
In human erythrocytes, the efficiency of transport of cationomycin is much higher than that of monensin (10 x for Na^+ and 17 x for K^+) but the selectivity of transport in favor of K^+/Na^+ is decreased compared to monensin (x2).
The differences between the relative transport rates observed in vesicles and in erythrocytes could arise because of the more complex nature of the erythrocyte membrane containing a mixture of phospholipids and also a variety of proteins. We have, for example, previously shown that transport rates of ionophores for alkali metal ions are affected by the charge on the membrane surface.[61]
The study of deacylcationomycin confirms the crucial importance of the aromatic side chain.
Finally, comparison of monensin and cationomycin raises interesting question:
Why does such an efficient ionophore system as cationomycin in red blood cells present a rather poor antimalarial activity and an absence of toxicity *in vivo* while it is more active on bacteria? A detailed analysis of generally employed experimental conditions shows that serum proteins are present in both the growth medium of infected erythrocytes and the plasma of mice while they are absent in the growth medium of bacteria. In addition, previous experiments showed that increasing concentrations of serum induced an increase of IC_{50} for *P.falciparum*.[65] This recalls recent work that showed that serum proteins decreased the biological activities of monensin.[66,67]
Consequently, we suggest that cationomycin could also interact with serum proteins but to a much higher extent than monensin. As a consequence,

although cationomycin transports cations more efficiently than monensin in RBCs, its antimalarial and *in vivo* toxicity would be much lower. To check this hypothesis we have measured the partition coefficient of these two ionophores between the erythrocyte membrane and the protein phase.

References to chapter 2

1. J. Berger, A. I. Rachlin, W. E. Scott, L. H. Sternbach, M. W. Goldberg, *J. Am. Chem. Soc.*, 1951, **73**, 5295.
2. R. L. Harned, P. H. Hudy, C. J. Corum, K. L. Jones, *Antibiot. Chemother.*, 1951, **1**, 594.
3. A. Agtarap, J. W. Chamberlin, M. Pinkerton, L. Steinrauf, *J. Am. Chem. Soc.*, 1967, **89**, 5737.
4. A. A. Guffanti, L. E. Davidson, T. M. Mann, T. A. Krulwich, *J. Gen. Microbiol.*, 1979, **114**, 201.
5. Y. N. Antonenko, L. S. Yaguzhinsky, *Biochem. Biophys. Acta*, 1988, **938**, 193.
6. W. Duax, D. Smith, P. D. Strong, *J. Am. Chem. Soc.*, 1980, **102**, 6725.
7. D. Ward, K. T. Wei, T. G. Hoogerheide, A. J. Popov, *Acta Cryst.*, 1978, **B34**, 110.
8. W. K. Lutz, F. K. Winkler, J. D. Dunitz, *Helv. Chim. Acta*, 1971, **54**, 1103.
9. E. N. Duesler, I. C. Paul, in 'Polyether antibiotics' ed. J. W. Westley, Marcel Dekker, New-York (USA), 1983, Vol. 2, p. 172.
10. W. Paugborn, W. Duax, D. Langs, *J. Am. Chem. Soc.*, 1987, **109**, 2163.
11. S. N. Graven, S. Estrada-O, H. A. Lardy, *Proc. Natl. Acad. Sci.*, 1965, **654**, 56.
12. L. Steinrauf, M. Pinkerton, J. W. Chamberlin, *Biochem. Biophys. Res. Comm.*, 1968, **33**, 29.
13. T. Kubota, S. Matsutani, M. Shiro, H. Koyama, *J. Chem. Soc., Chem. Commun.*, 1968, 1541.
14. G. Nakamura, K. Kobayashi, T. Sakurait, K. Isono, *J. Antibiotics*, 1981, **34**, 1513.
15. M. Ubukata, J. Uzawa, K. Isono, *J. Am. Chem. Soc.*, 1984, **106**, 2214.
16. T. Sakurai, K. Kobayashi, G. Nakamura, K. Isono, *Acta Cryst.*, 1982, **B38**, 2471.

17. G. Dauphin, G. Jeminet, F. Vaufrey, *J. Chem. Soc., Perkin. Trans. 2*, 1993, 399.

18. M. Ubukata, Y. Hamazaki, K. Isono, *Agric. Biol. Chem.*, 1986, **50**, 1153.

19. D. H. Davies, E. W. Snape, P. J. Suter, *J. Chem. Soc, Chem. Commun.*, 1981, 1073.

20. I. L. Cameron, N. K. R. Smith, T. B. Pool, R. L. Sparks, *Cancer Res.*, 1980, **40**, 1493.

21. M. P. Blaustein, *Am. J. Physiol.*, 1977, **232**, C165.

22. R. D. Moore, J. W. Munford, T. J. Pillsworth, *J. Physiol. London*, 1983, **338**, 277.

23. D. G. Tosteson, *J. Gen. Physiol.*, 1955, **39**, 55.

24. O. Jardetsky, J. E. Wertz, *Arch. Biochem. Biophys.*, 1956, **65,** 569.

25. J. E. Wertz, O. Jardetsky, *J. Chem. Phys.*, 1956, **25**, 357.

26. R. R. Ernst, W. A. Anderson, *Rev. Sci. Instrum.*, 1966, **37**, 102.

27. C. S. Springer, *Ann. Rev. Biophysics. Biophysical. Chem.*, 1987, **16**, 375.

28. H. Degani, Z. Bar-On, *Period. Biol.*, 1981, **83**, 61.

29. C. C Bryden, C. N. Reilley, J. F. Desreux, *Anal. Chem.*, 1981, **53**, 1418.

30. M. M. Pike, C. S. Springer, *J. Magn. Reson.*, 1982, **46**, 348.

31. H. J. C. Berendsen, H. T. Edzes, *Ann. NY Acad. Sci.*, 1973, **204**, 459.

32. C. A. Rotunno, V. Kowalewski, M. Cereijido, *Biochim. Biophys. Acta*, 1967, **135**, 170.

33. G. Lindblom, H. Wennerstrom, B. Lindman, 1976, *ACS Symp. Ser.*, 1976, **34**, 372.

34. R. K. Gupta, P. Gupta, *J. Magn. Reson.*, 1982, **47**, 344.

35. B. C. Pressman, *Ann. Rev. Biochem.*, 1976, **45**, 501.

36. F. G. Riddell, S. Arumugam, P. J. Brophy, B. G. Cox, M. C. H. Payne, T. E. Southon, *J. Am. Chem. Soc.*, 1988, **110**, 734.

37. F. G. Riddell, S. Arumugam, B. G. Cox, *Biochem. Biophys. Acta.*, 1988, **944**, 279.

38. F. G. Riddell, S. J. Tompsett, *Biochem. Biophys. Acta*, 1990, **1024**, 193.

39. G. A. Morris, R. Freeman, *J. Magn. Reson.*, 1978, **29**, 433.

40. G. Bodenhausen, *Progr. NMR Spectr.*, 1981, **14**, 137.

41. C. Brevard, P. Granger in 'Handbook of high resolution multinuclear NMR', John Wiley &Sons, New York, 1981.

42. S.C. Chu, M. M. Pike, E. T. Fossel, T. W. Smith, J. A. Balschi, C. S. Springer, *J. Magn. Reson.*, 1984, **56**, 33.

43. L. T. Mimms, G. Zampighi, Y. Nozaki, C. Tanford, J. A. Reynolds, *Biochemistry,* 1981, **20**, 833.

44. G. R. Painter, B. C. Pressman, *Top. Curr. Chem.*, 1982, **101**, 83.

45. M. Rochdi, A. M. Delort, J. Guyot, M. Sancelme, G. Dauphin, G. Jeminet, *Bioelectrochem. Bioeng.*, 1994, **33**, 83.

46. M. Rochdi, A. M. Delort, J. Guyot, M. Sancelme, S. Gibot, J. G. Gourcy, G. Dauphin, C. Gumila, H. Vial, G. Jeminet, *J. Med. Chem.*, 1996, **39,** 588.

47. A. Nakamura, S. Nagai, T. Ueda, J. Sakakibara, Y. Hotta, K. Takeya, *Chem. Pharm. Bull.*, 1989, **39,** 2330.

48. A. Nakamura, S. Nagai, T. Takahashi, R. Malhan, N. Mukakami, T. Ueda, J. Sakakibara, M. Asano, *Chem. Pharm. Bull.*, 1992, **39,** 2331.

49. T. Ogino, G. I. Shulman, M. J. Avison, S. R. Gullans, J. A. Den Hollander, R. G. Shulman, *Proc. Nat. Acad. Sci.*, 1985, 1099.

50. E. Fernandez, J. Grandjean, P. Laszlo, *Eur. J. Biochem.*, 1987, **167**, 353.

51. R. S. Hotchkiss, S. K. Song, C. S. Ling, J. J. H. Ackerman, I. E. Karl, *Am. J. Physiol.*, 1990, R21.

52. J. P. Monti, M. Baz, R. Elsen, Y. F. Berland, A. D. Crevat, *Biochem. Biophys. Acta*, 1990, **1027**, 31.

53. F. G. Riddell, M. K. Hayer, *Biochem. Biophys. Acta*, 1985, **817**, 313.

54. R. Sandeaux, J. Sandeaux, C. Gavach, B. Brun, *Biochem. Biophys. Acta*, 1982, **68**, 127.

55. B. C. Pressman, *Fed. Proc.*, 1968, **27,** 1283.

56. B. G. Cox, N. Van Truong, J. Rzeszotarska, H. Schneider, *J. Am. Chem. Soc.*, 1984, **106**, 5965.

57. Y. N. Antonenko, L. S. Yaguzhinsky, *Biochem. Biophys. Acta*, 1988, **938**, 125.

58. C. Gaboyard, G. Dauphin, F. Vaufrey, G. Jeminet, *Agric. Biol. Chem.* , 1990, **54**, 1149.

59. D. C. Shungu, D. C. Buster, R. W. Briggs, *J. Magn. Reson.*, 1990, **89**, 102.

60. M. Hebrant, Y. Pointud, J. Juillard, *J. Phys. Chem.*, 1991, **95**, 3653.

61. F. G. Riddell, S. Arumugam, *Biochem. Biophys. Acta*, 1988, **945**, 65.

62. S. J. Tompsett, PhD. Thesis, University of St Andrews (UK), 1991.

63. M. Ubukata, Y. Hamazaki, K. Isono, *Agric. Biol. Chem.*,1988, **52**, 1637.

64. C. Gumila, M. L. Ancelin, G. Jeminet, A. M. Delort, G. Miguel, H. Vial, *Antimicrob. Agents Chemother.* , 1996, **3**, 602.

65. C. Gumila, M. L. Ancelin, G. Jeminet, A. M. Delort, G. Miguel, H. Vial, *Antimicrob. Agents Chemother.*, 1997, **41**, 523.
66. F. K. Jansen, A. Janse, J. M. Derocq, D. Carriere, P. Carayon, F. Veas, J. P. Jaffrezon, *J. Biol. Chem.*, 1992, **18**, 12577.
67. A. Franceschi, F. Dosio, C. Anselmi, R. Chignola, C. Candiani, M. Pasti, G. Tridente, M. Colombatti, *Eur. J. Biochem.*, 1994, **219**, 469.

Chapter 3
Spirotetrahydrofuran analogues as potential cation ionophores

3.1 Introduction

The aim of this collaboration with Prof. Leo Paquette and his team at the Ohio State University was to study spirotetrahydrofuran analogues as potential alkali cation carriers and especially Li^+. All syntheses, molecular modelling studies were carried out at the Ohio State University. The kinetic study using NMR techniques was conducted at the University of St Andrews. The result of these investigations was published in *Tetrahedron*, 1997, **53**, 7403.

As already described in the last chapter, the ionophoric antibiotics have widespread biological action.[1] They are effective against a wide range of microorganisms, including Gram-positive bacteria, anaerobic bacteria, and the malaria parasite. The biological action of ionophoric antibiotics arises from their ability to transport cations, notably Na^+ and K^+, through the membranes of cells. This disruption of the ionic balance leads inevitably to the death of the cell.
The natural ionophores display certain physiological characteristics that are vital for their action. Firstly, they must show rapid complexation/ decomplexation for the metal ion. Secondly, they must not bind the metal ion too strongly. The more strongly bound the metal ion, the less well it is released after transport through the membrane. A striking example of this is provided by lasalocid[2] (Figure 3.1) which displays a strong complexation with Ba^{2+} or Ca^{2+}, although it shows a very low transport efficiency.

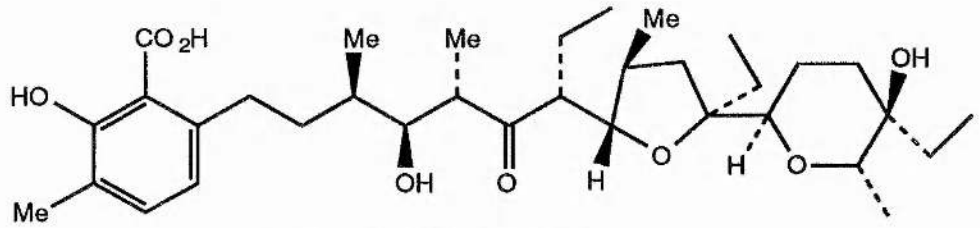

Figure 3.1 Structure of lasalocid.

This finding illustrates that tight metal ion binding by the ionophore ligand does not necessarily correlate with good carrier qualities. Rather, it is of importance that not too strong a binding occurs, which allows for a sufficiently rapid release of the metal ion after having passed through the artificial or biological membrane. However, with low complexation efficiency, the metal ion is never transported.

3.2 Spirotetrahydrofurans as potential alkali cation transporters

In Chapter 2 (section 2.3.5), we have already established the general architectural features of some ionophoric antibiotics. Having in mind these characteristics, the next steps were to design, synthesize, and study the kinetics of some analogues with NMR techniques. A set of new ionophoric materials designed to resemble to some degree the naturally occuring ionophoric antibiotics,[2-8] namely the carboxylic acids **1-6**, were targeted for investigation (Figure 3.2). The incorporation of stereochemically defined networks of vicinal spirocyclic tetrahydrofuran rings in proximity to the head group of a long-chain carboxylic acid was considered to offer several advantages. The distribution of oxygen centres, particularly in the diastereomeric trispiro polyether subset **3-6**, promised to be adequate for partial solubility in both aqueous and lipid environments. Knowledge of the interplay between structure and the several metal ion binding parameters referred to above was anticipated to provide insight into the important question of how the three-dimensional orientation of the oxygen atoms might be linked to the transportability of ions of different type. The octyl side chain was chosen to promote good lipid solubility whilst not inhibiting a small aqueous solubility.

On the basis of preliminary molecular mechanics calculations[9] on the simplified O-methyl analogues of **3-6**, the efficacy of binding and membrane transport as a function of systematic stereoinversion in these ladder-like arrays was expected to differ measurably. Although alkali metal ions have not been incorporated into the structures displayed in Figure 3.2, intramolecular coordination to the carboxylic acid group is seen to introduce differing conformational constraints on the remainder of the chain. This enforced adoption of different conformations could express itself quantitatively in conventional complexation scenarios as well as within the confines of a phospholipid bilayer.

3.2.1 Molecular modelling studies

The polyspirofuran analogues (Figure 3.2) differ in the stereochemical arrangement of the tetrahydrofuran rings. Each would be expected to bind metal ions and interact with aqueous solvent in a different manner.

Membrane transport is analysed in terms of three rates:[10] the first one is the rate at which metal-ionophore complexes are formed at the membrane surface k_f, the second one is the rate at which metal ions dissociate from the ionophore at the membrane surface, k_d and the last one is the rate at which ionophores diffuse between opposite surfaces of the membrane, k_{diff} as depicted in Figure 3.3.

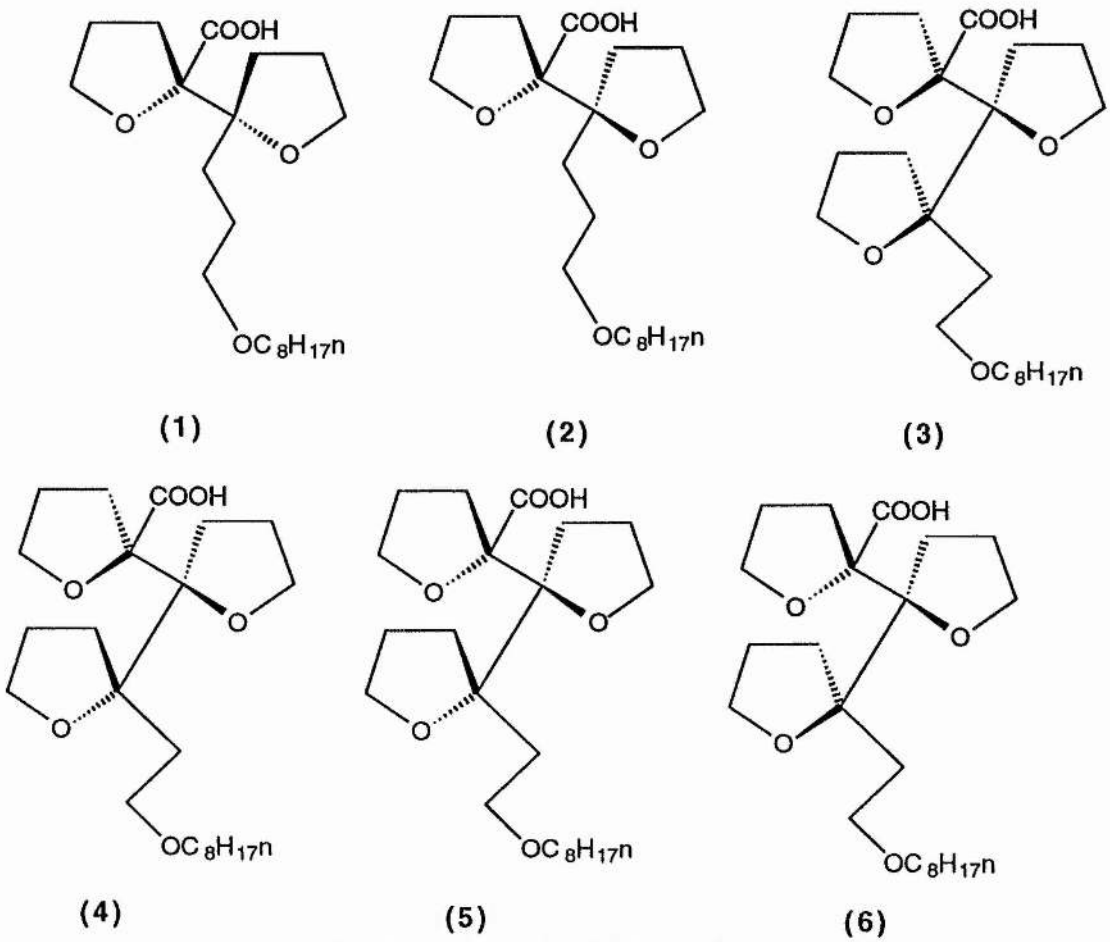

Figure 3.2 Structures of spirotetrahydrofuran analogues.

The thermodynamic stability of the metal-ionophore complex, which would be measured by the stability constant $K_s = k_f/k_d$, is not the rate-determining factor, since small k_d would inhibit ion transport by shutting down re-release of the metal ion. These rate constants can be obtained from NMR experiments[10] and compared with the results obtained by simulations.

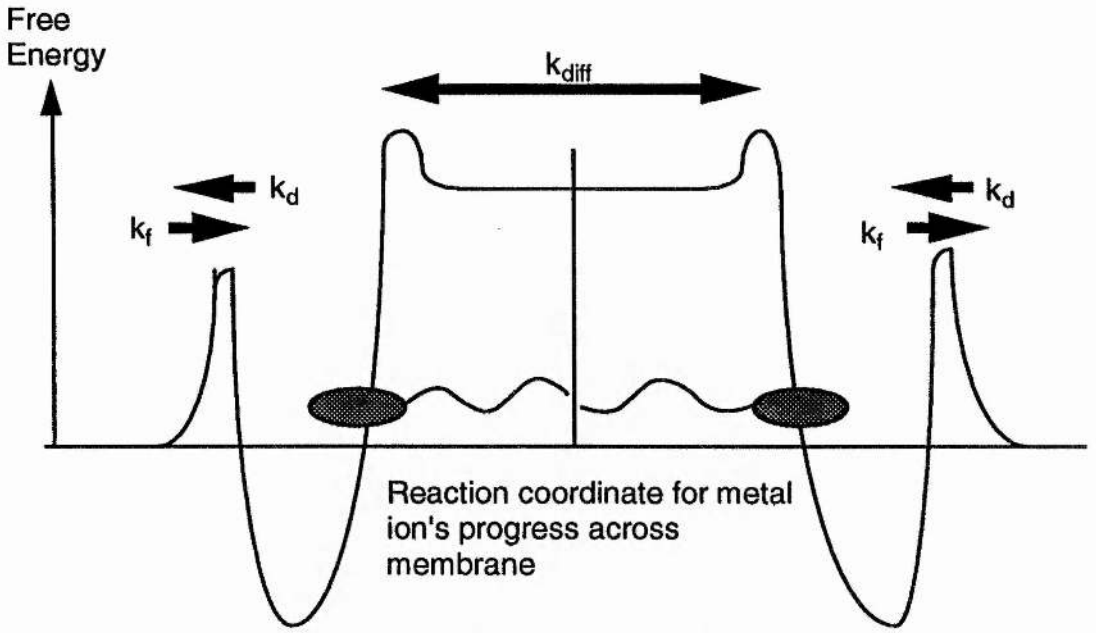

Figure 3.3 Schematic diagram showing energy barriers encountered by a cation during its movement across the membrane.

The results of the calculated binding energies indicate that isomer **3** with all three tetrahydrofuran oxygens on one side, most strongly binds a cation as shown in Table 3.1. However, in solution there will be a competition between binding of aqueous solvent and the ion, and the situation with respect to binding free energies might drastically change. Moreover, it is the rates, not thermochemical stability, that determine ion transport characteristics. The n-octyl substituent was replaced with a methyl group in order to remove conformational differences due only to this side chain. The total and relative energies of the lithium, sodium, and potassium carboxylates of acids **1-6** generated by this procedure are compiled in Table 3.1.

From the Table 3.1, the lowest energy conformation of **1** in the presence of each metal was calculated to be more stable than that of **2**, which is consistent with our experimental findings (Table 3.2). The lowest energy conformations determined for **3-6** are depicted in Figure 3.4. The calculations involving **5**-Li^+ and **5**-Na^+ are noteworthy. The stability associated with this pair of complexes originates from the capacity of four of the five oxygen atoms to enter into the coordination sphere of the metal ion (2.17-2.45 Å for Li^+; 2.20-2.49 Å for Na^+).

Acid	Li^+		Na^+		K^+	
	Total energy	Relative energy	Total energy	Relative energy	Total energy	Relative energy
1	-30.57	0	-28.03	0	-10.08	0
2	-29.30	1.27	-27.15	0.88	-9.49	0.59
3	-18.70	0.37	-16.54	0.06	1.29	0.12
4	-17.62	1.45	-15.47	1.13	2.07	-.90
5	-19.07	0	-16.59	0.01	3.46	2.29
6	-18.75	0.32	-16.60	0	1.17	0

Table 3.1 Energies of the alkali metal carboxylates of **1-6** as generated by the Monte-Carlo protocol in macromodel using the Amber Force Field[11] (All values are in kcal.mol^{-1}).

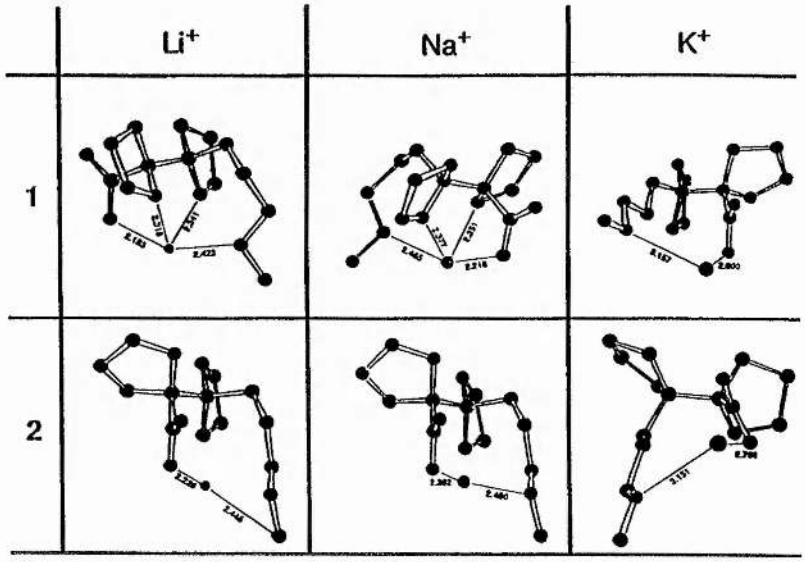

Figure 3.3 Lowest energy conformations of **1** and **2** with Li^+, Na^+, and K^+ as optimised by Amber force calculations.

$$[M^+]_{eq} + [Pic^-]_{eq} + [Host]_{org} \underset{}{\overset{K_a}{\rightleftharpoons}} [M^+ Pic^- Host]_{eq}$$

	K_a		
Host	Li^+	Na^+	K^+
1	$5.4x10^3$	$2.0x10^3$	$1.0x10^3$
2	$2.3x10^3$	$3.2x10^4$	$3.0x10^4$
3	$1.4x10^3$	$3.4x10^4$	$4.5x10^4$
4	$1.2x10^3$	$4.9x10^4$	$1.8x10^3$
5	$3.2x10^2$	$9.4x10^4$	$5.6x10^3$
6	$3.9x10^3$	$2.5x10^4$	$3.2x10^4$

Table 3.2 Association constants (K_a) determined by picrate extraction into chloroform at 293 K.[12]

Isomers	Li^+ (Å)	Na^+ (Å)	K^+ (Å)
1	2.18-2.42	2.20-2.47	2.16-2.80
2	2.23-2.45	2.26-2.49	2.77-3.15
3	2.23-2.44	2.27-2.49	2.77-3.04
4	2.24-2.45	2.27-2.49	2.78-3.10
5	2.17-2.44	2.20-2.49	2.76
6	2.23-2.44	2.28-2.48	2.76-3.04

Table 3.3 M^+-O Distances with different spirotetrahydrofuran analogues.[11]

3.3 NMR spectroscopy

As has been demonstrated in the last chapter, NMR methods provide an important tool for studying the transport rates of ionophoric antibiotics such as cationomycin for alkali metals. Because of the isochronicity phenomena (see Chapter 2 section 2.4.1.1), the NMR method involves the use of a contrast reagent between $^7Li^+$, $^{23}Na^+$, $^{39}K^+$ or $^{133}Cs^+$ inside and outside vesicles of phosphatidylcholine (PC). This effect may be achieved by chemical shift reagents such as paramagnetic lanthanides or by relaxation agents which relies on creating relaxation time differences between the intra- and extracellular ions. The ionophore is then added and the transport rate measured by one of a variety of NMR techniques. For the slowest exchange rates, metal/metal (*e.g* $^7Li/^{23}Na$

or $^{23}Na/^{39}K$) or isotope exchange (*e.g* $^{6}Li/^{7}Li$) can be employed . For exchange rates comparable with the nuclear relaxation rates, a magnetisation transfer experiment is used.

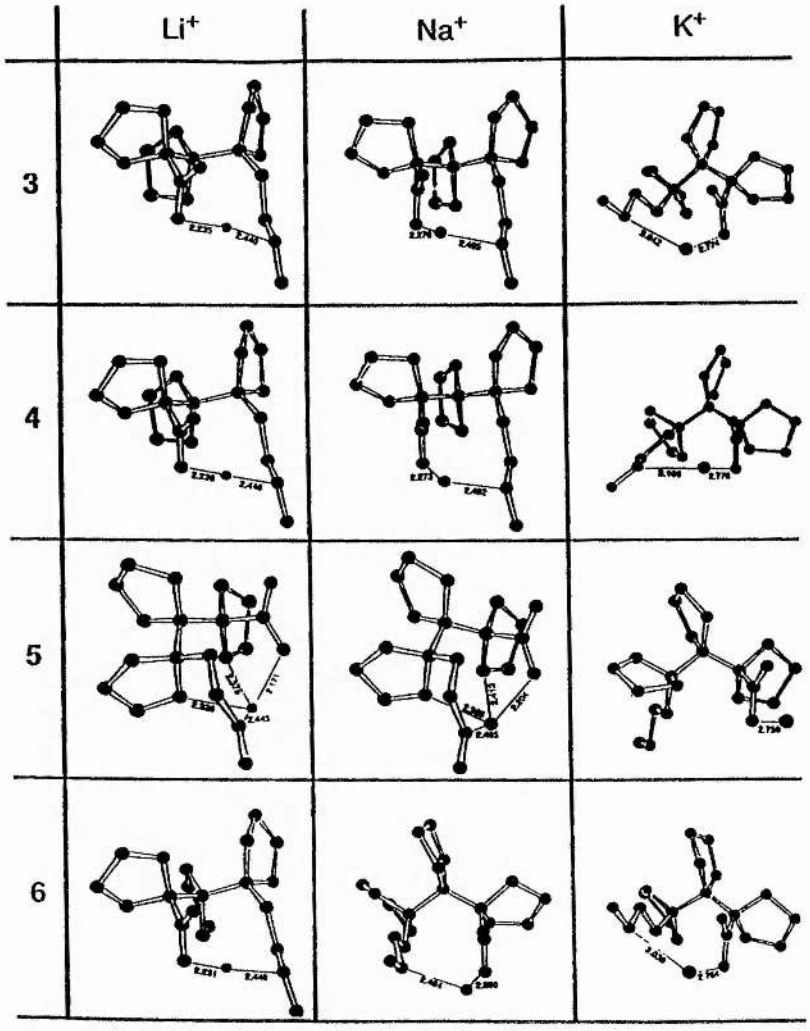

Figure 3.4 Lowest energy conformations of **3-6** with Li^+, Na^+, and K^+ as optimised by Amber force field calculations.

For the fastest exchange rates, dynamic line broadening is the technique of choice. It is generally possible to arrange the relative concentrations of lipid, metal and ionophore so that the exchange rates can be measured by one or other of these techniques.
We chose to look at Li^+/Na^+ exchange and follow the process by ^{23}Na NMR.

3.4 Results and discussion

All experimental details are reported in Chapter 6 (section 6.2).
Passive exchange rates of Na^+ with Li^+ varied from experiment to experiment and were in the range 10-50 $x10^{-5}$ s^{-1} and increased only slightly after addition of the synthesized material even when the ionophore/PC ratio was as high as 1/50.
We conclude that the six carboxylic acids synthesized in this work are poor mediators of the exchange of Li^+ and Na^+ in phosphatidylcholine membranes. By comparison with naturally occuring ionophoric antibiotics capable of transporting lithium the observed rates are around 10^4 times slower under similar conditions.

Structures	I/PC 10^{-3}	Passive diffusion k_1 (10^{-5} s^{-1})	Mediated diffusion k_2 (10^{-5} s^{-1})	Transport rate $k_3=k_2-k_1$ k_3 (10^{-5} s^{-1})
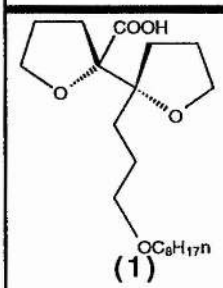 (1)	55.2	8.3	40.4	32.1
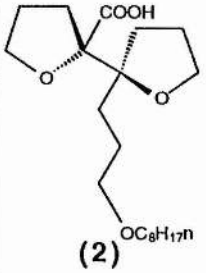 (2)	15.7	41.7	68.8	27.1

Table 3.4 The rate of diffusion for (**1**)-(**6**) at 100 mM [Li^+].

Structures	I/PC 10^{-3}	Passive diffusion k_1 (10^{-5} s^{-1})	Mediated diffusion k_2 (10^{-5} s^{-1})	Transport rate $k_3=k_2-k_1$ k_3 (10^{-5} s^{-1})
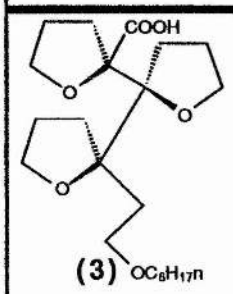 (3)	29.7	47.7	66.1	18.4
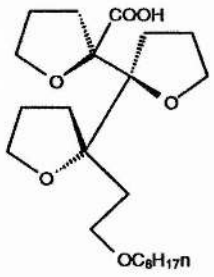 (4)	10.4	5.7	58.8	53.1
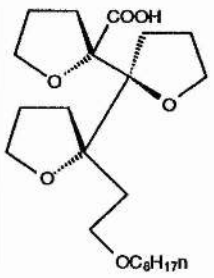 (5)	8.7	16.5	36.2	19.7

Table 3.4 (Continued)

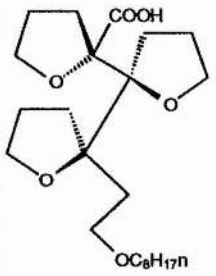

(6)

21.4	42.7	112.7	70.0

Table 3.4 The rate of diffusion for (**3**), (**4**), (**5**) and (**6**) at 100 mM [Li^+].

The very small differences observed between the passive exchange rates and the 'mediated' exchange rates reveals the current lower limit for measurement of ion transport kinetics using NMR spectroscopy. The experimental variation in the passive exchange rate becomes an important limiting factor. Ratio slower then say 5 $x10^{-4}$ s^{-1} cannot be measured with any precision.

3.5 Future perspective

From the literature, it is possible distinguish four categories[13] of synthetic compounds capable of transporting cations: crown-ethers, cryptands, open-chain poylethers and organometallic ligands. Shinar[14] and co-workers reported the transport of Li^+ and Na^+ ions through phosphatidylcholine bilayers mediated by the ionophore $[(C_5H_5)Co[P(O)(OEt)_2]_3]^-$ (**1**). This latter represents a new class of monoanionic tridentate ligands in which all three of the complexing donor atoms are oxygen and in which the metal ion is chelated to the organometallic complexes to the three P=O oxygens and depicts as 'half-sandwich' type.
A kinetic study of this organometallic compound with vesicles reveal a transport rate selectivity for Li^+ over Na^+ by a factor of between 20 and 40, but it was rather less effective at transporting lithium than the naturally occuring ionophore monensin.
All naturally occuring ionophoric antibiotics described in Chapter 2 section 2.2.5 assume a stable conformation which directs the polar ligating moieties into a central cavity suitable for enclosing the alkali cation. Furthermore, the

aliphatic chain must insulate the internal ligating cavity sufficiently to ensure the stability of the ion while crossing the apolar membrane interior.
The transport rate of these spirotetrahydrofuran analogues in comparison with polyether antibiotics are low due to the 'non' wrapping of alkali cations and the absence of strong bonding between alkali cations and oxygens atoms.
Despite the low rate of transport, we believe these spirotetrahydrofurans point the way towards the right ' design' for efficient and harmless carriers of alkali cations.

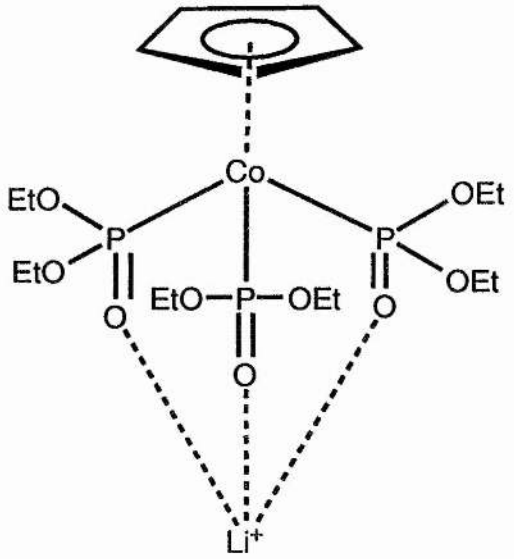

Figure 3.5 Structure of (cyclopentadienyl) tris diethylphosphite cobalt Li^+ salt (**1**).

References to chapter 3

1. F. G. Riddell, *Chem. Britain*, 1992, 533.
2. S. P. Young, B. D. Comperts, *Biochem. Biophys. Acta*, 1977, **469**, 281.
3. L. A. Paquette, M. Stepanian, U. V. Mallavadhani, T. D. Cutarelli, T. B. Lowinger, H. J. Klemeyer, *J. Org. Chem.*, 1996, **61**, 7492.
4. L. A. Paquette, M. Stepanian, B. M. Branan, S. D. Edmondson, C. R. Bauer, R. D. Rogers, *J. Am. Chem. Soc.*, 1996, **118**, 4504.

5. L. A. Paquette, B. M. Branan, M. Stepanian, *Tetrahedron Lett.*, 1996, **37**, 1721.

6. B. M. Branan, L. A. Paquette, *J. Am. Chem. Soc.*, 1994, **116**, 7658.

7. L. A. Paquette, B. M. Branan, D. Friedrich, S. D. Edmondson, R. D. Rogers, *J. Am. Chem. Soc.*, 1994, **116**, 506.

8. L. A. Paquette, J. T. Negri, R. D. Rogers, *J. Org. Chem.*, 1992, **57**, 3947 and relevant references cited therein.

9. L. A. Paquette, *personal communication.*

10. F. G. Riddell, S. Arumugam, P. J. Brophy, B. G. Cox, M. C. Payne, T. E. Southon, *J. Am. Chem. Soc.*, 1988, **110**, 734.

11. M. Stepanian, W. E. Trego, D. G. Bolin, L. A Paquette, S. Sareth, F. G. Riddell, *Tetrahedron* , 1997, **53**, 7403.

12. K.E. Koenig, G. M. Lein, P. Struckler, T. Kaneda, D. J. Cram, *J. Am. Chem. Soc.*, 1979, **101**, 3553.

13. R. Hilgenfield, W. Saenger, *Top. Curr. Chem.*, 1982, **101**, 1.

14. H. Shinar, G. Nivon, W. Klaui, *J. Am. Chem. Soc.*,1986, **108**, 5005.

Chapter 4
Transport by Anionophores

4.1 Introduction

The transport of anions, in particular chloride, is crucial for biological processes. It is believed that abnormalities in chloride transport are associated with several diseases including cystic fibrosis[1,2] and Duchenne muscular dystrophy.[3] In addition, the red cell membrane contains an anion channel as depicted in Figure 4.1 (also known as the Band 3 protein or the anion exchanger) that plays a key role in the transport of CO_2 by blood.

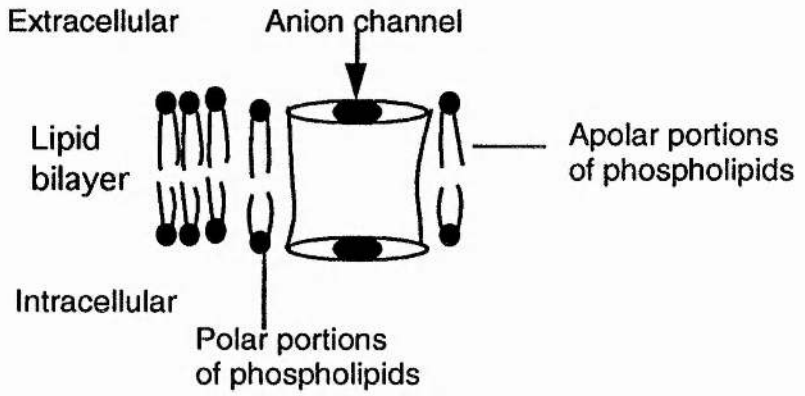

Figure 4.1 Schematic diagram of the anion channel of erythrocytes.[4]

Carbon dioxide inside the cell is converted into carbonic acid, H_2CO_3, by the action of carbonic anhydrase as depicted in Figure 4.2. Carbonic acid then dissociates into H^+ and HCO_3^-. The released proton is taken up by deoxyhemoglobin. Bicarbonate (HCO_3^-) leaves the red cell by means of band III protein in exchange for Cl^- as an antiport process. This one for one exchange means that the transport process is electrically neutral.

4.1.1 Anion transport

Anion coordination chemistry has received little attention compared to the numerous studies devoted to the coordination of cations, although anion complexation by organic ligands offers exciting and challenging development for organic, inorganic and biological systems. It is noteworthy to mention that at least two thirds of all enzymes act on negatively charged substrates. The main task is the design of organic receptors for efficient and selective binding of

inorganic anions and of negatively charged functional groups (carboxylate, phosphate, *etc.*) in organic and biological substrates. Anion inclusion complexes[5-8] have been described where the anion is bound inside a molecular cavity by ionic hydrogen bonds with ammonium sites leading to highly stable and selective cationic complexes.

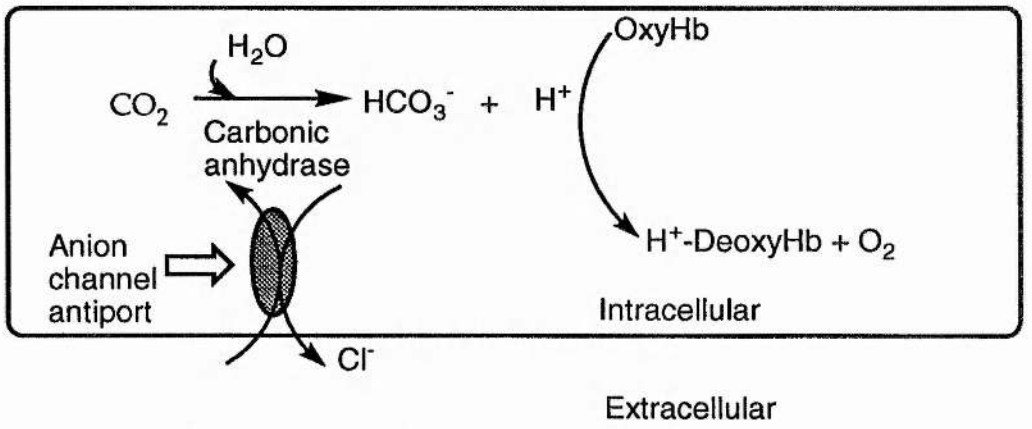

Figure 4.2 Anion channels in erythrocytes[4] play an important role in the transport of CO_2 by enabling HCO^{3-} to be exchanged for Cl^-.

Macrocyclic structures possess the architectural flexibility which should allow the designed arrangement in space of suitable anion binding sites.

4.1.2 NMR spectroscopy of halide anions

In previous chapters, we have demonstrated that NMR techniques have been powerful and successful tools for studying the transport of alkali metal ions through cell membranes or model phospholipid bilayers.
High resolution NMR techniques should also enable us to study the transport of halide ions, especially chloride and bromide, through artificial and biological membranes.

4.1.2.1 Isochronicity and invisibility phenomena

Table 4.1 illustrates that all halide ions are NMR active. Their sensitivities are all greater than that of ^{13}C but they display a quadrupolar effect. This latter leads to broader linewidths. In compensation, the shorter relaxation times allow data to

be acquired much more rapidly. NMR studies of halides encounter two similar problems to alkali metal studies (see Chapter 2 section 2.4.1) which are isochronicity and invisibility.

The isochronicity means the halide signals from the intra- and extracellular compartments occur at precisely the same chemical shift.

In Chapters 2 and 3, we have demonstrated that isochronicity can be overcome by using either a shift or a relaxation reagent for metal ions. The previous work[9,10] in this area showed that Mn^{2+} is a very efficient relaxation agent for $^{35}Cl^-$ ions and that it could be used in systems of large unilamellar vesicles to follow Cl^- transport mediated by anionophoric molecules. However, the major problem was that the vesicles prepared at 310 K were extremely susceptible to disruption by Mn^{2+} and to overcome this the work had to be conducted at acidic pH.

Nucleus	^{35}Cl	^{37}Cl	^{79}Br	^{81}Br
Spin number	3/2	3/2	3/2	3/2
Natural abundance(%)	75.53	24.47	50.54	49.46
Receptivity relative to $^{13}C=1$	20.2	3.8	226	277
Frequency relative to ^1H= 100 MHz	9.80	8.16	25.05	27.00
Quadrupole moment (10^{-28} m^2)	-8.0×10^{-2}	-6.32×10^{-2}	0.33	0.28

Table 4.1 Nuclear properties of halides.[11]

As reported by Shakar-Hill and Shulman,[12] Co^{2+} is both a moderate shift reagent and a relaxation agent for $^{35}Cl^-$. The use of Co^{2+} gives rise to a major problem: the relaxation appears to be paramagnetic in origin and so the linewidth (in Hz) varies with the square of the magnetic field whilst the shift difference (in Hz) varies linearly. Thus, at the high magnetic fields desirable for sensitivity, the shifted line is also considerably broadened. To resolve the intra- and extracellular signals requires higher concentrations of Co^{2+} as the magnetic field increases. However, as indicated above, for relaxation agents high magnetic fields are an advantage as they increase the rate of the paramagnetic relaxation process increasing the linewidth of the relaxed signal. This requires less of the reagent to achieve the desired line broadening. The advantage of using Co^{2+} as

a contrast reagent is that it allows the simultaneous observation of both intra- and extracompartmental signals.

The second problem is the invisibility of halide ions which arises from the quadrupolar nucleus. This gives rise to a more rapid overall nuclear relaxation with the outer transitions relaxing more rapidly than the inner transition. The outer transitions have 60% of the signal intensity and the inner transition 40%.
In principle, the intracellular resonance of any quadrupolar nucleus should be visible, although in practice this is not always possible owing to instruments being unable to cope with the very short relaxation times and consequently the short dead time delays required and the broad lines observed.

4.2 Kinetic studies of steroid-based cryptands for halide anions

Cryptands based on the cholic acid skeleton were kindly suplied by Prof. Antony Davis and his team at Trinity College Dublin (Ireland).

4.2.1.Introduction of steroid-based cryptands for halide anions

The transport of anions, especially chloride, plays a crucial role in biological systems. As already mentioned for cation carriers (polyether antibiotics and spirotetrahydrofuran analogues), anion carriers need to fulfil several criteria such as being electrically neutral and lipophilic.
Anion carriers which fulfil these criteria rely on the cooperative action of neutral hydrogen bond donor groups.[13] For strong and selective binding, these groups should be comparatively acidic, preorganised to complement the target anion and minimize intramolecular hydrogen bonding, and embedded in lipophilic structures which maintain solubility in nonpolar media. It has been reported that cholic acid chemically modified (Figure 4.3) though its architectural feature into a 'cryptand' type can bind halide anions using a well-dispersed but convergent 3D array H-bond donor functinality.[14-23]
In collaboration with the University of Dublin (Ireland) we have studied the kinetics of cholic acid derivatives which have a great affinity for chloride anion in a nonpolar organic solvent. The new anion carriers are based on podand-type architecture as depicted in Figure 4.4. Anion recognition is achieved through three NH-containing groups attached to the steroid through positions 3, 7 and12.

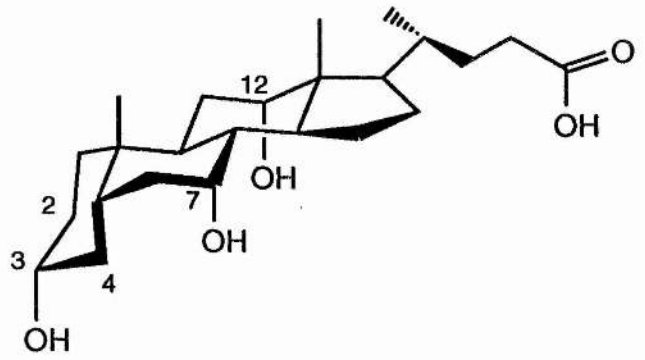

Figure 4.3 Structure of cholic acid.

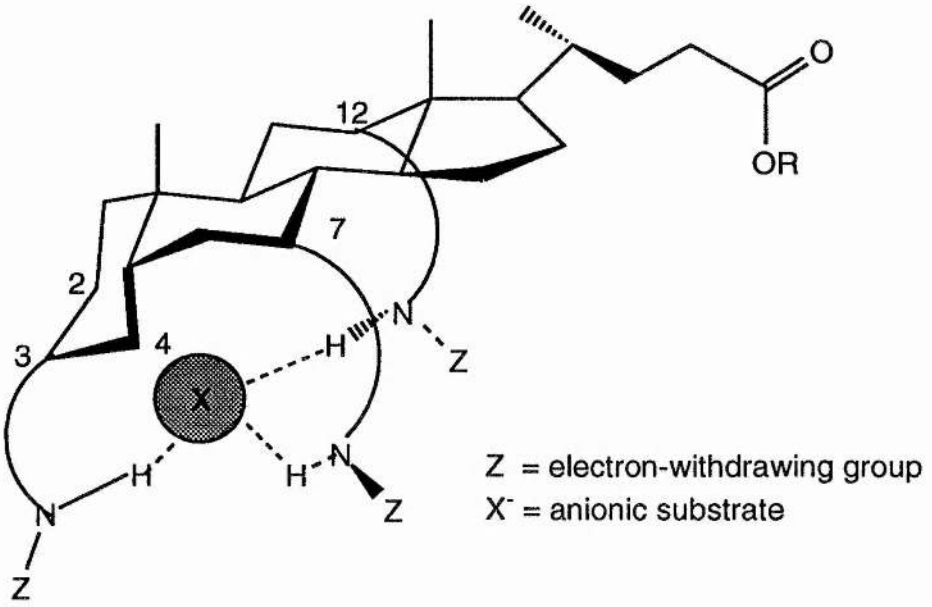

Figure 4.4 Schematic structure of anion binding.

Anionophore 1

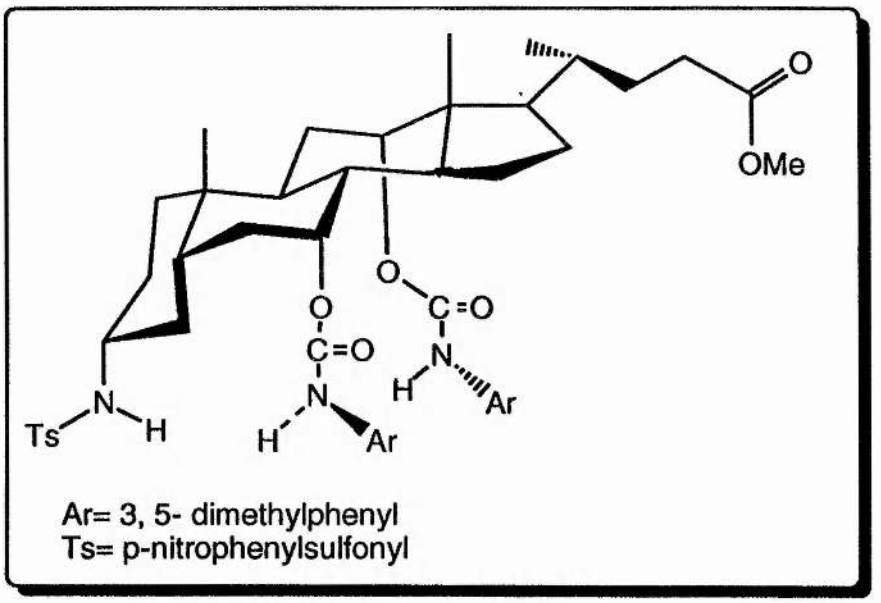

Figure 4.5 Structure of methyl-3α-(p-nitro phenyl sulfonyl amino)- 7α, 12α- (3, 5-dimethylphenyl) cholanoate.

Anionophore 2

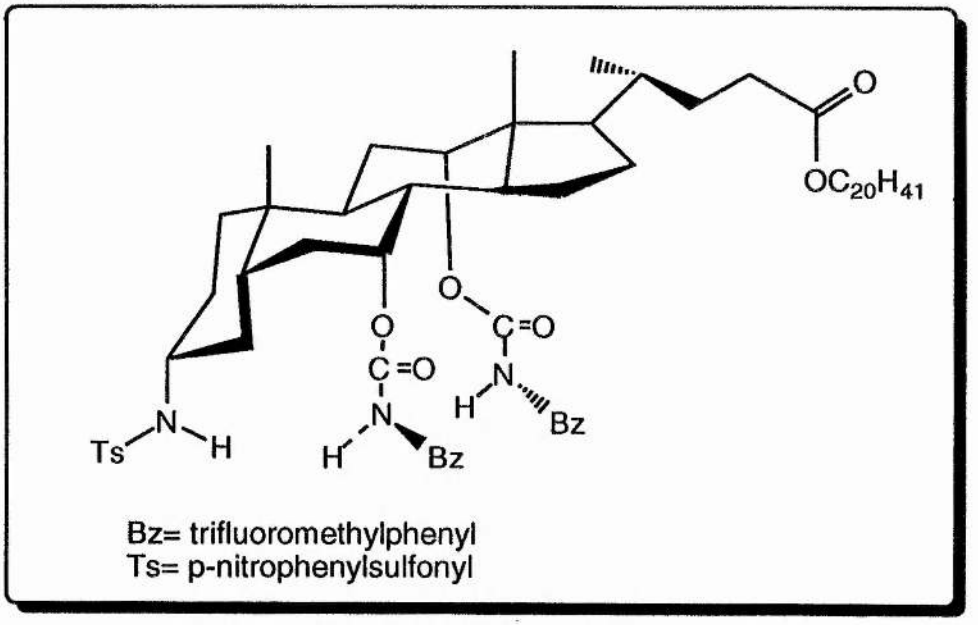

Figure 4.6 Structure of eicosyl-3α-(p-nitro phenyl sulfonyl amino)-7α,12α-trifluoro methyl phenyl amino carbonyloxy) cholanoate.

Anionophore 3

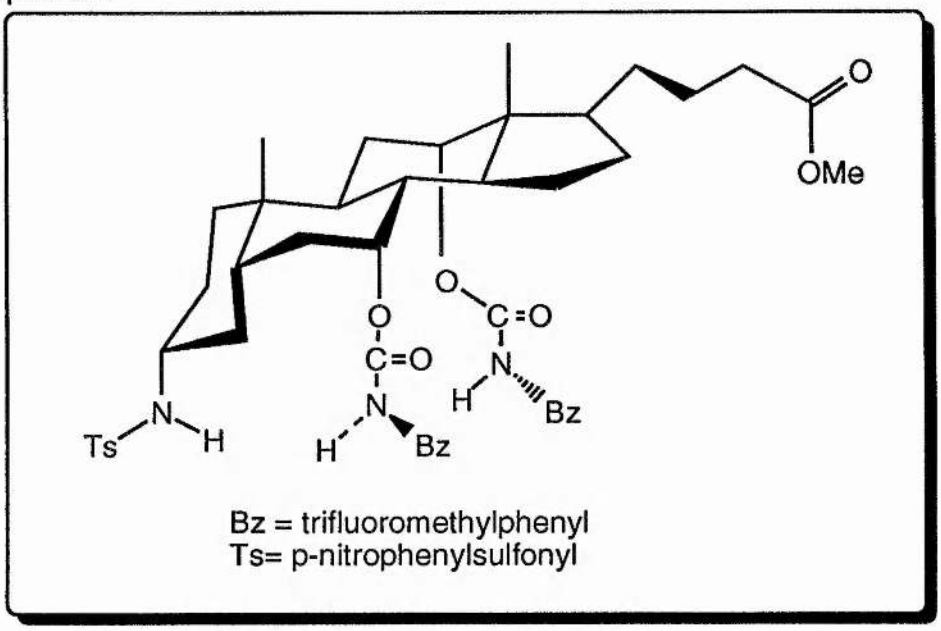

Figure 4.7 Structure of methyl-3α-(p-nitro phenyl sulfonyl amino)-7α,12α-trifluoro methyl phenyl amino carbonyloxy) cholanoate.

4.3 Results and discussion

All experimental details are reported in Chapter 6 (section 6.3).
In this chapter, are reported preliminary kinetic results of some anionophores depicted in Figures 4.5, 4.6, 4.7.

Anionophore 1 added (μl)	A1/PC (10^{-4})	Leakage (10^{-5} s^{-1})	Leakage and diffusion (10^{-5}s-1)	Diffusion (10^{-5}s-1)
0	0	0	0	0
10	38.9	3.7	6.4	2.7
20	77.8	3.7	8.7	5.0
30	116.7	3.7	8.5	4.8
40	155.6	3.7	8.4	4.7

Table 4.2 Exchange rates of anionophore 1.

The kinetic result for chloride/ bromide anions mediated by anionophore 1 (methyl-3α-(p-nitro phenyl sulfonyl amino)- cholanoate) is given in Figure 4.8 and Tables 4.2. By adding small aliquots of anionophore 1 to the vesicle, the

diffusion rate increases for Cl/Br exchange until reaching a saturation stage. Suggesting that all vesicles are used for the Cl/ Br exchange between the intra- and extracellular. The rate of transport is maximal which is depicted in form of 'plateau'.

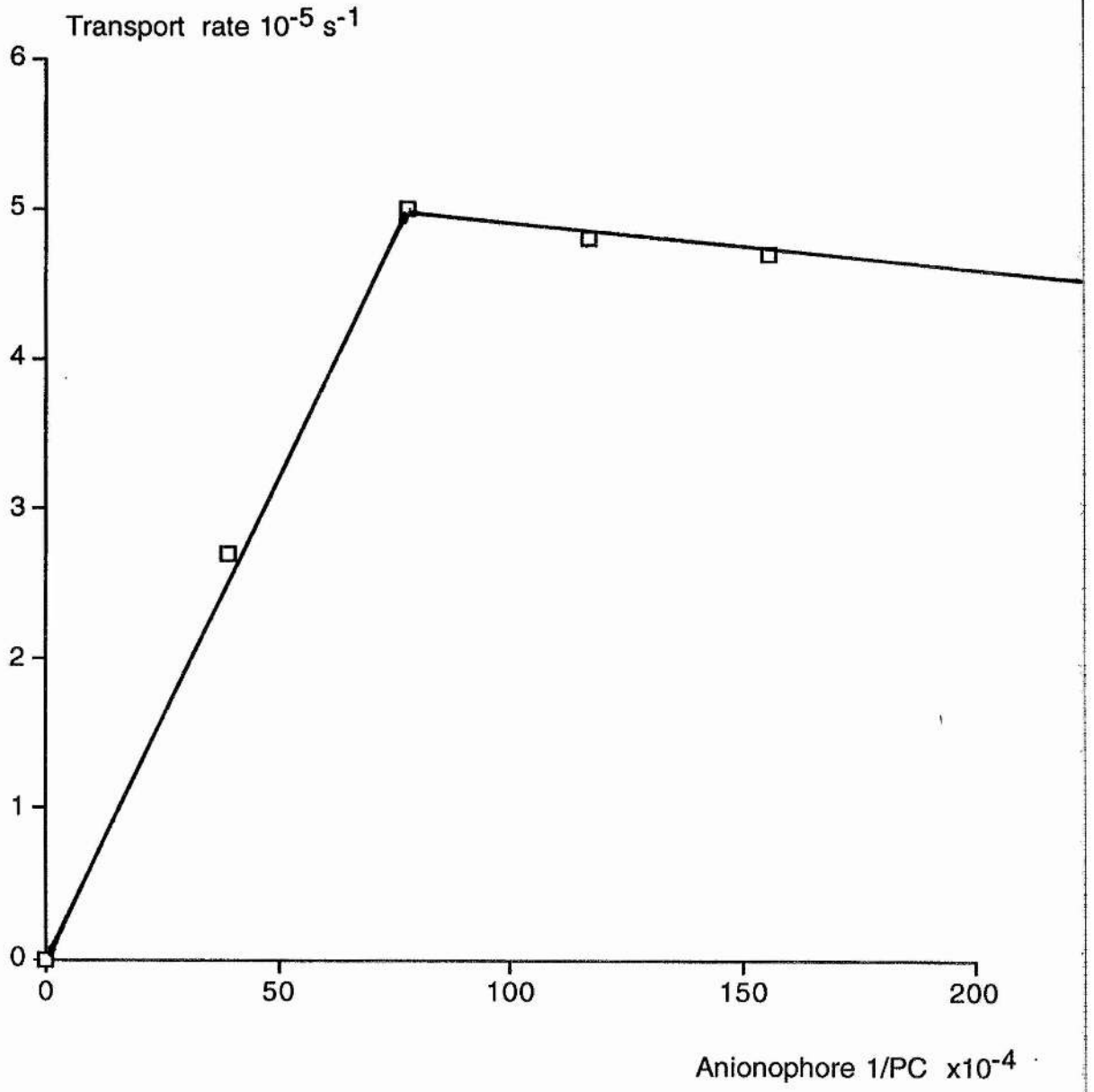

Figure 4.8 Rate of diffusion with anionophore 1.

Table 4.3 and 4.4 illustrate the Cl^-/Br^- exchange rate of anionophore 2 (eicosyl-3α-(p-nitro phenyl sulfonyl amino)-7α,12α-trifluoro methyl phenyl amino carbonyloxy) cholanoate and anionophore 3 (methyl-3α-(p-nitro phenyl sulfonyl amino)-7α,12α-trifluoro methyl phenyl amino carbonyloxy) cholanoate).

For every small aliquots of anionophore 2 (denoted as A2) or 3 (denoted as A3) studied, the transport rate in the direction 'in' to 'out' varies linearly with the A2/PC and A3/PC ratio, suggesting a first-order kinetic relationship between anionophores 2 and 3 and the transport rate. These early studies indicate transport by a 1:1 complex.

Anionophore 2 added (μl)	A2/PC (10^{-4})	Leakage (10^{-4} s^{-1})	Leakage and diffusion ($10^{-4}s$-1)	Diffusion ($10^{-4}s$-1)
0	0	0	0	0
10	45.4	2.3	2.7	0.4
20	90.8	2.3	3.3	1.0
30	136.2	2.3	3.9	1.6
40	181.6	1.1	3.0	1.9

Table 4.3 Exchange rate of anionophore 2.

Anionophore 3 added (μl)	A3/PC (10^{-4})	Leakage (10^{-4} s^{-1})	Leakage and diffusion ($10^{-4}s$-1)	Diffusion ($10^{-4}s$-1)
0	0	0	0	0
10	41.8	1.4	3.8	2.4
20	83.6	1.4	5.6	4.2
30	125.4	1.4	6.1	4.7

Table 4.4 Exchange rate of anionophore 3.

It is worth noting that the exchange rate constants such as the leakage and diffusion rates, for anionophores 2 and 3 are about 10 times higher than those for anionophore 1. All vesicles for these anionophores were prepared in the same condition and yet no logical explanations have been found for these differences.

In brief, it appears that the design of anionophore adopted by the group in Dublin is a sensible approach. Our results certainly show that anion transport is

occuring and strongly suggest that increasing the lipophilicity increases the transport rate.

The importance of this work is that uncharged carriers have been shown to transport halide ions.

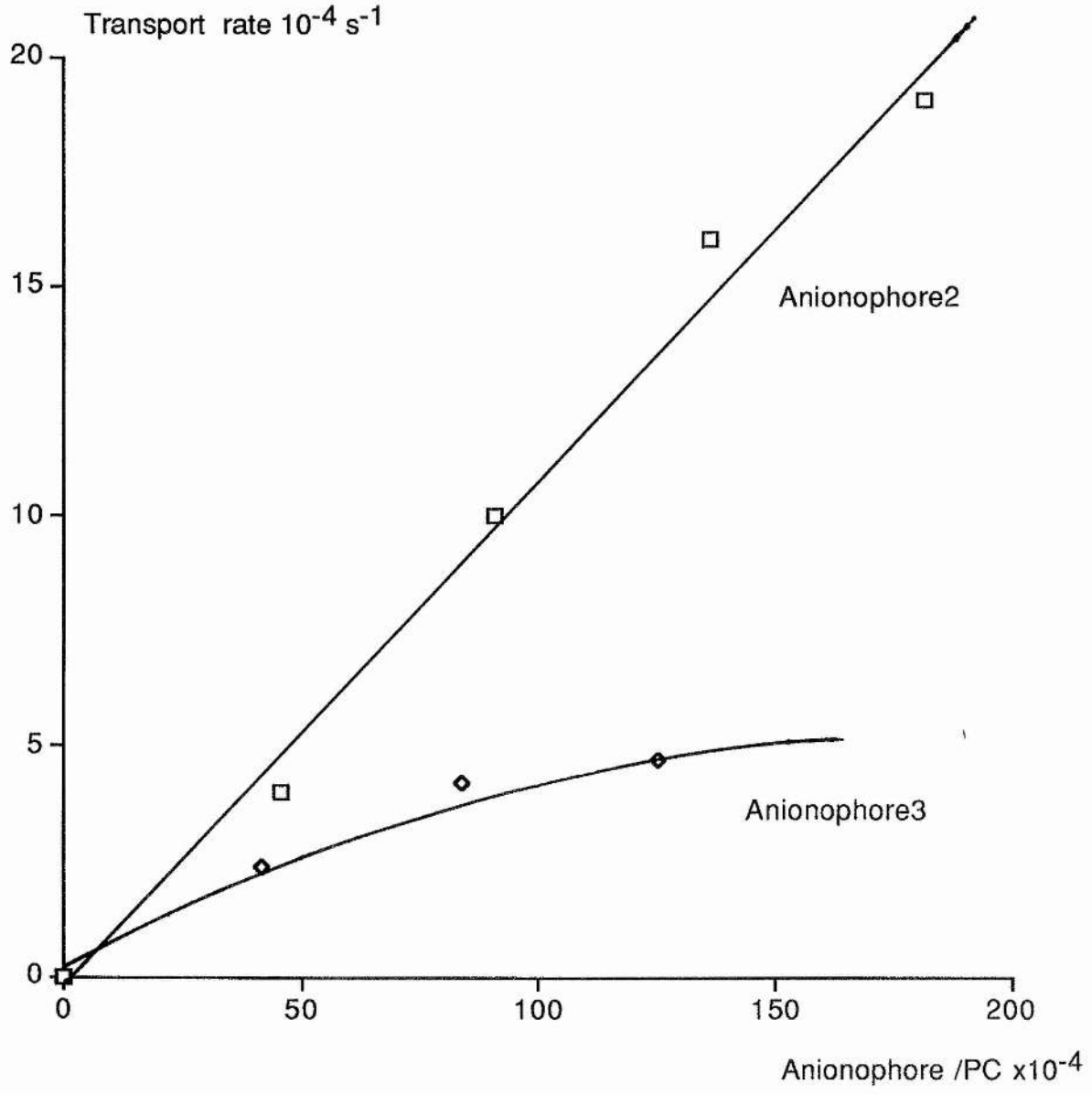

Figure 4.9 Rate of diffusion with anionophores 2 and 3.

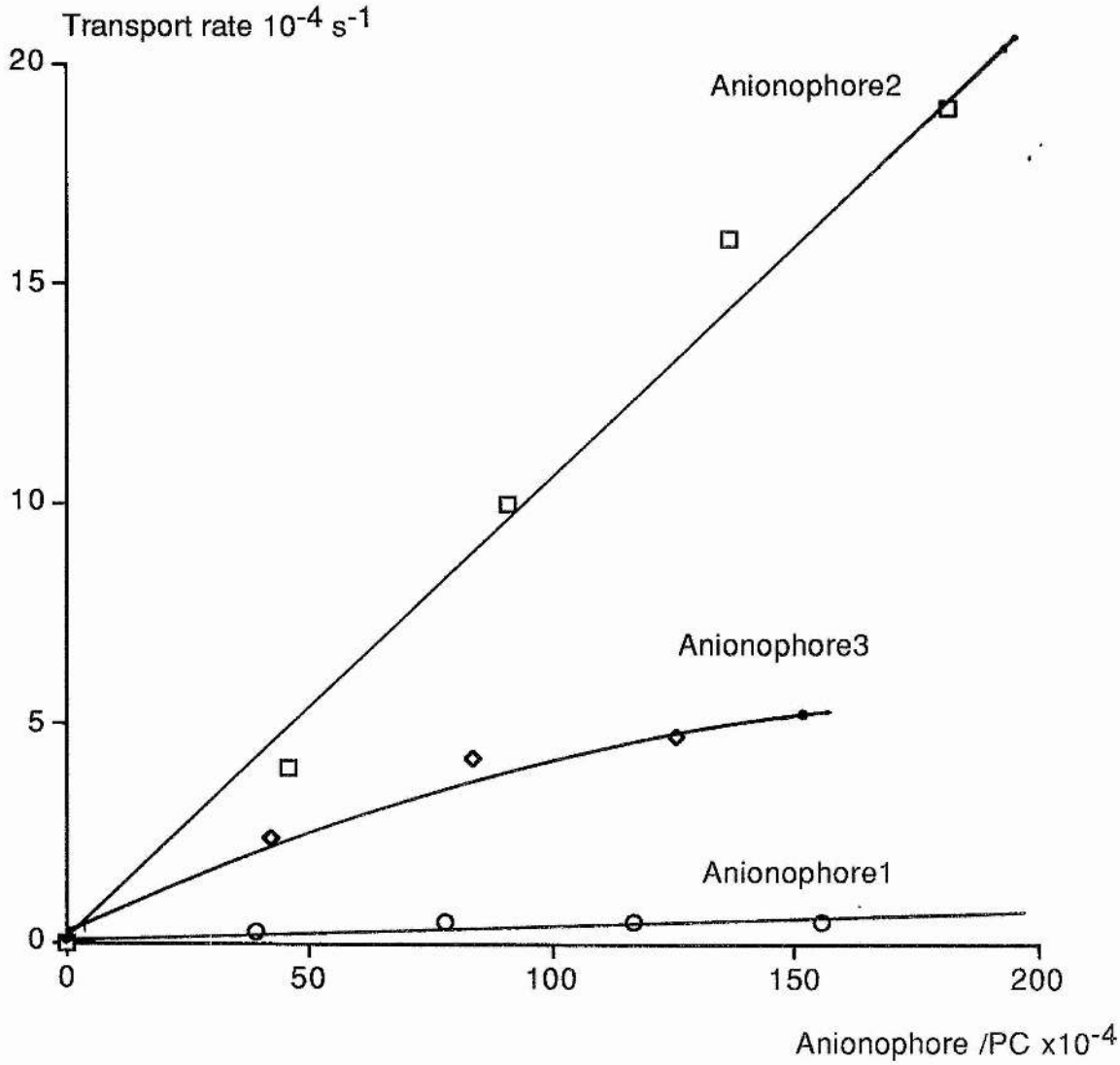

Figure 4.10 Rate of diffusion with anionophores 1, 2 and 3.

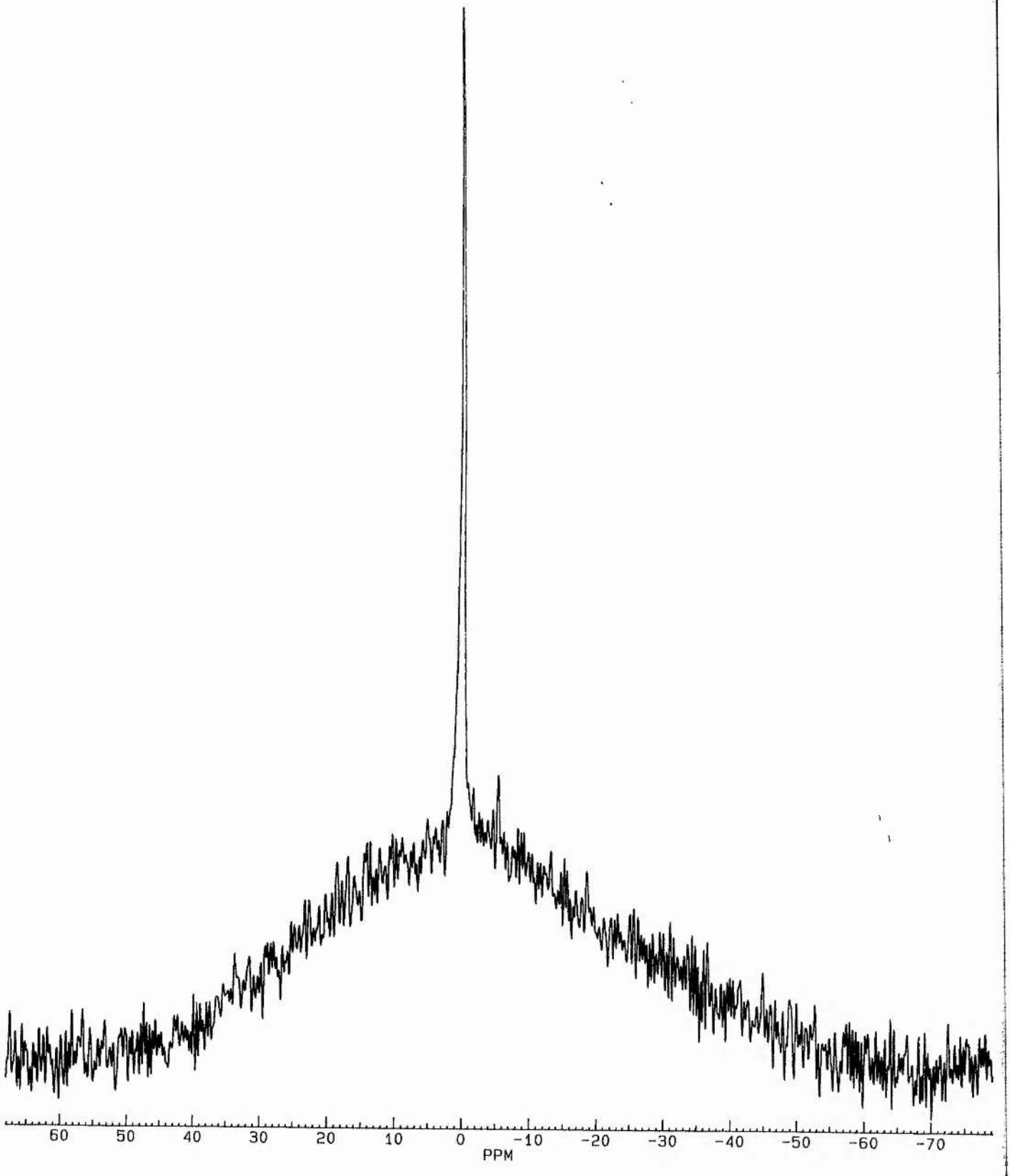

Figure 4.11 ^{35}Cl spectrum taken using a relaxation agent experiment with anionophore 1 at 200 mM [Cl^-]. The relatively sharp line is from the intravesicular $^{35}Cl^-$. The much broader line is from the relaxed extravesicular $^{35}Cl^-$.

References to chapter 4

1. P. M. Quinton, *Nature*, 1983, **301**, 421.
2. C. Higgins, *Nature*, 1989, **341**, 103.
3. C. N. Pato, M. H. Davis, M. J. Doughty, S. H. Bryant, E. Gruenstein, *Proc. Natl. Acad. Sci. USA*, 1983, **80**, 4732.
4. L. Stryer in 'Biochemistry', W. H. Freeman & Company, New York, 1988, p. 305.
5. C. H. Park, H. Simmons, *J. Am. Chem. Soc.*, 1968, **90**, 2431.
6. E. Graf, J. M Lehn, *J. Am. Chem. Soc.*, 1976, **98**, 6403.
7. F. P. Schmidtchen, *Angew. Chem.*, 1977, **89**, 751.
8. J. M. Lehn, E. Sonveaux, A. K. Willard, *J. Am. Chem. Soc.*, 1978, **100**, 4914.
9. F. G. Riddell, Z. Zhou, *J. Inorg. Biochem.*, 1994, **55**, 279.
10. F. G. Riddell, Z. Zhou, *Magn. Reson. Chem.*, 1995, **33**, 66.
11. C. Brevard, P. Granger in 'Handbook of high resolution multinuclear NMR', John Wiley &Sons, New York, 1981, p. 106, 140.
12. Y. Shakar-Hill, R. J. Shulman, *Biochemistry*, 1992, **31**, 6272.
13. F. G. Riddell, S. Arumugam, A. Patel, *J. C. S. Chem. Comm.*, 1990, 74.
14. A. P. Davis, J. J. Perry, R. P. Williams, *J. Am. Chem. Soc.*, 1997, **119**, 1793.
13. A. P. Davis, J. F. Gilmer, J. J. Perry, *Angew. Chem., Int. Ed. Engl.*, 1996, **35**, 1312.
14. A. P. Davis, *Chem. Soc. Rev.*, 1993, **22**, 243.
15. R. P. Bonar-Law, J. K. M. Sanders, *J. Am. Chem. Soc.*, 1995, **117**, 259.
16. H. P. Hsieh, J. G. Muller, C. J. Burrows, *J. Am. Chem. Soc.*, 1994, **116**, 12077.
17. Y. A. Cheng, T. Suenaga, W. C. Still, *J. Am. Chem. Soc.*, 1996, **118**, 1813.
18. V. Janout, M. Lanier, S. L. Regen, *J. Am. Chem. Soc.*, 1996, **118**, 1573.
19. U. Maitra, L. J. D'Souza, *J. Chem. Soc., Chem. Commun.*, 1994, 2793.
20. P. Venkatasan, Y. Cheng, D. Kahne, *J. Am. Chem. Soc.*, 1994, **116**, 6955.
21. A. P. Davis, J. J. Walsh, *J. Chem. Soc., Chem. Commun.*, 1996, 449.
22. A. P. Davis, S. Menzer, J. J. Walsh, D. J. Williams, *J. Chem. Soc., Chem. Commun.*, 1996, 453.

Chapter 5
Complete assignment of the NMR spectrum of tetronasin (M139603)

5.1 Basic concepts in NMR theory

In this chapter, we deal with some general concepts[1-3] of NMR theory which excludes the application of density matrix theory.

NMR (Nuclear Magnetic Resonance) studies the interactions of electromagnetic radiation with matter. In the case of NMR, the radiation is in the radio frequency of the electromagnetic spectrum, and the matter with which it interacts is the nucleus of the atom.

Certain nuclei possess a magnetic moment, generated by the spin property of the nucleus. This magnetic moment is able to interact with applied magnetic fields. This interaction gives rise to different energy levels, or nuclear spin states, depending on the spin number of the nucleus. For a nucleus with spin I, there are 2I+1 energy levels. Therefore for a nucleus with spin number 1/2, there will be two energy levels as depicted in Figure 5.1.

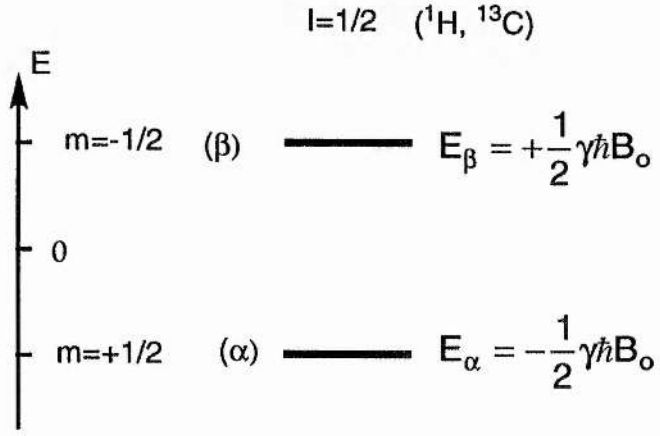

Figure 5.1 Energy level schemes[4] for I=1/2.

In this chapter, we restrict the study to nuclei with I=1/2 for which only two spin states exist, for example ^{1}H, ^{31}P, ^{15}N, ^{13}C.

Nuclei with I=0 will have only one spin state and will therefore be NMR-inactive.

A set of empirical rules summarises the relationship between the composition of a nucleus (the number of protons and neutrons, p and n respectively) and its spin number (I).

(i) if p and n are both even numbers I is zero (^{12}C, ^{16}O)

(ii) if (p+n) is an odd number I is half integer (^{1}H, ^{13}C, ^{15}N, ^{17}O)

(iii) if both p and n are odd numbers I is integer (^{2}H, ^{14}N)

One spin state (that aligned with the applied field (z-axis)) is of lower energy (α–state) than the one aligned against the applied field (β-state) (-z axis). At a given field strength, B_o, each nucleus absorbs at a particular frequency in the radio frequency range, dependent on the transition energy between the two spin states. Since this is small (in favour of the α-state), the net energy absorption in an NMR experiment is relatively small and the technique is relatively insensitive compared to other spectroscopic techniques. However, as the strength of B_o increases the population difference becomes more pronounced and sensitivity enhances as depicted in Figure 5.2.

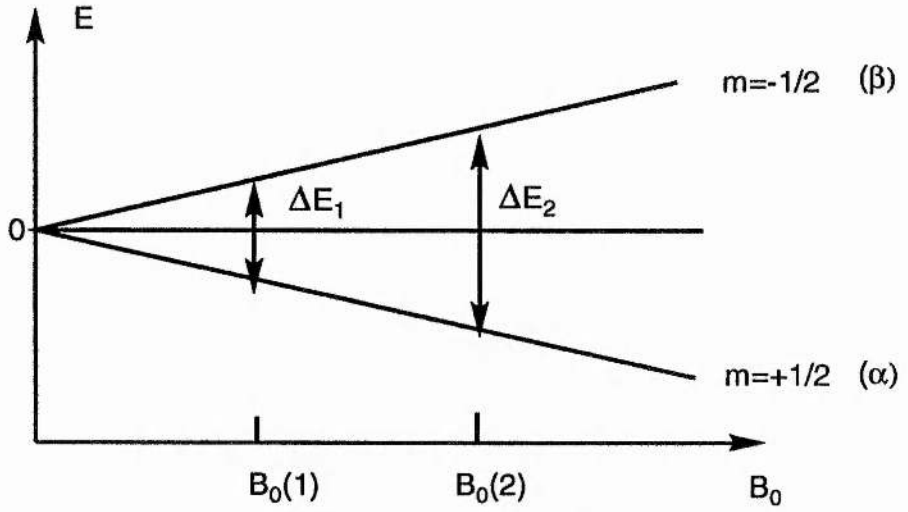

Figure 5.2 The energy difference[4] ΔE between two adjacent energy levels as a function of the magnetic flux density B_0.

In addition to the generation of different spin states, the interaction of a magnetic moment with the applied magnetic field also leads to the generation of an angular force, which results in the precession of the magnetic moment around B_o at the Larmor frequency[5] ω_0. This frequency is dependent on the gyromagnetic ratio of each species of nucleus and the applied field B_o.
The precession of nuclei around B_o gives rise to magnetisation along the +z-axis and in the xy-plane. However, the xy component is equal to zero because the distribution of the xy component in a population of nuclei is random; magnetisation of an individual nucleus in the population along the +y-axis is cancelled by that of a second nucleus with an xy component along the -y axis. Both nuclei have components along the +z-axis; therefore the net magnetisation

of a population of nuclei is along the +z-axis, aligned with the direction of the applied field, B_o.

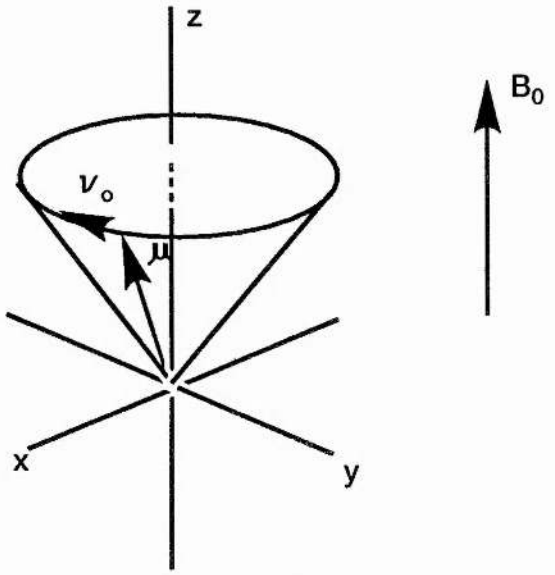

Figure 5.3 Nuclear precession[5]: nuclear charge and nuclear spin give rise to a magnetic moment of nuclei. The magnetic vector μ precesses in a static magnetic field with Larmor frequency υ_o about the direction of the magnetic flux density vector.

The signal observed during an NMR experiment is in the xy-plane, that is perpendicular to B_o. Since there is no net magnetisation in this plane at equilibrium, there is no NMR signal. A signal is induced by the application of a second field, B_1, in the xy-plane (perpendicular to B_o and the net magnetisation aligned along the +z-axis). A torque is induced by the interaction of the net magnetisation of the nuclei with B_1. If B_1 is applied for a certain time then the net magnetisation moves through 90° and precesses in the xy-plane (90° pulse) and a signal is now detected by the receiver coil (in the xy-plane).

When the B_1 field is switched off, the magnetisation precessing in the plane relaxes, over time, back to its equilibrium position, along the +z-axis. As it does so the amount of magnetisation detected in the xy-plane by the receiver coil decreases and the free induction decay (FID) is recorded. The FID is in the time domain. The recognisable NMR spectrum, in the frequency domain, is created by Fourier Transformation of the FID. The relaxation times T_1 and T_2 are used to describe the time for the net magnetisation to relax back to the equilibrium

position: T_1, the longitudinal time, for the relaxation of the z-component of the net magnetisation to return to +z-axis (aligned with B_0). T_2, the transverse relaxation time, for the xy components of the net magnetisation to relax back to equilibrium, that is, to zero. The length of the transverse relaxation time T_2 is important in determining the width of the NMR signal (line width).

If the B_1 field is on for longer than the time to flip the net magnetisation through 90°, into the xy-plane, then the observed signal will not be at a maximum (as it is at 90°); at 180° there will be no signal (magnetisation is aligned along the -z-axis), at 270° the signal will be a negative minimum (in the -xy-plane), and at 360° there is no signal (along the +z-axis).

The precise position of a signal from an individual nucleus in a spectrum is governed by two factors. The predominant factor is the strength of the applied field, B_0. However, in an NMR experiment, all nuclei are subject to the same B_o field. It is local effects, such as fields generated in the electron clouds surrounding a given nucleus and neighbouring nuclei, thereby changing the effective field experienced by that nucleus and its position in the spectrum. The spectrum is described in terms of chemical shift, δ, which is independent of the applied field, B_o

$$\delta = \frac{(B_{reference} - B_{sample})}{B_{reference}} x10^6 ppm \qquad \text{Equation 5.1}$$

where $B_{reference}$ is the magnetic field of the reference nuclei and B_{sample} the field at the sample nuclei.

The fundamental resonance condition for all NMR experiments states

$$\upsilon = \frac{\gamma B}{2\pi} \qquad \text{Equation 5.2}$$

From Equation 5.1, this can be written

$$\delta = \frac{(\upsilon_{sample} - \upsilon_{reference})}{oscillator.frequency(Hz)} x10^6 \qquad \text{Equation 5.3}$$

The chemical shift (in parts per million, ppm) of a nucleus is dependent on the covalent character of its environment and the effects of neighbouring atoms, either covalently attached or close through space, both of which affect the exact field experienced by an individual nucleus.

5.1.1.Relaxation times

In the NMR experiment the thermal equilibrium of the spin system is disturbed by irradiating at the resonance frequency. This alters the population ratios and causes transverse magnetic field components (M_x and M_y) to appear. When the perturbation ceases the system relaxes until it once again reaches equilibrium. There are two different relaxation processes:

- the relaxation in the applied field direction, which is characterised by the spin-lattice or longitudinal relaxation time T_1. Longitudinal magnetisation owes its existence entirely to the difference between the populations of the nuclear spin states α and β. It follows that longitudinal relaxation necessarily involves population changes, so that the processes that bring it about are those that induce transitions between the spin states.

- and the relaxation perpendicular to the field direction, which is characterised by the spin-spin or transverse relaxation time T_2. Transverse relaxation involves the loss and dephasing of individual contributions to the macroscopic transverse magnetisation M_{xy}, so that their resultant sum becomes zero. This too will be caused by transitions, but it will also be brought about by any process that perturbs the individual contributing Larmor frequencies. Since the spin-spin relaxation time T_2 is less important from a chemical point of view than T_1, the following paragraph will focus mainly on the longitudinal relaxation mechanism.

5.1.2 Spin lattice relaxation mechanisms

Spin lattice relaxation[6] is always associated with a change in the energy of the spin system, as the energy absorbed from the pulse must be given up. It is transferred to the surroundings, the lattice (neighbouring molecules), whose

thermal energy therefore increases. There are a number of mechanisms which contribute to spin lattice relaxation:

-dipole-dipole (DD) or simply dipolar relaxation
- quadrupolar relaxation (Q)
- spin-rotation (SR) relaxation
- chemical shift anisotropy relaxation (CSA)
- scalar relaxation (SC)

5.1.2.1 Dipolar relaxation

For spin number I=1/2, the main contribution to the spin-lattice relaxation of nuclei is the dipole-dipole coupling. It can be directly measured through the nuclear Overhauser effect (nOe). This interaction between the nuclear dipoles arises from the fact that each nucleus is surrounded by other magnetic nuclei, in the same or in adjacent molecules, which are in motion. Their motion causes fluctuating magnetic fields at the position of the nucleus being observed. The frequency band is comparatively broad, and is largely influenced by the viscosity of the solution. If these fluctuating fields have components of the appropriate frequency, they can induce nuclear spin transitions.

For low molecular weight molecules in mobile liquids, the correlation time τ_c is very small. Hence, $\omega\tau_c << 1$, which is referred to the extreme narrowing condition.[6]

$$\frac{1}{T_1^{DD}} = \frac{3}{2}\gamma^4\hbar^2\sum_i r_i^{-6}\tau_c \qquad \text{Equation 5.4}$$

γ = magnetogyric ratio
τ_c = correlation time
$\hbar$ = Planck constant divided by 2π
r = distance between the two protons

The rate of relaxation depends strongly upon the magnetogyric ratio and upon theinverse sixth power of the distance r between the interacting spins. Thus directly bound H has the greatest influence on T_1 for ^{13}C.

5.2 Basic concepts of two-dimensional NMR

5.2.1 Periods in two-dimensional NMR

Two dimensional NMR experiments are characterised by four time periods[7] labelled preparation, evolution, mixing, and detection.

5.2.1.1 Preparation

The nuclear spins are prepared for the experiment by establishing some well defined state. Since all 2D NMR experiments require multiple, separate NMR experiments, it is necessary to start all of them from the same state. This state can be thermal equilibrium where all spins have their 'natural' magnetisation governed by Bolzmann statistics. Alternatively, this state may be one in which all the spins for one type of nucleus are randomised in orientation (saturated) while another type of nucleus is in thermal equilibrium. A wide variety of experiments can be considered, in which this preparation period consists only of a delay sufficient to give equilibrium magnetisation for all nuclei. The final part of the preparation period usually involves one or more pulses that place magnetisation(s) at right angles to the direction of the magnetic field axis. This part allows discrimination between chemically different nuclei on the basis of their respective precession rates during the evolution period.

5.2.1.2 Evolution

Since nuclear moments precess around the direction of a magnetic field, differences in the nuclear precession rate allow one to probe each type of nucleus under well-defined conditions. We can construct these conditions out of RF fields, magnetic fields and nuclear spin interactions such as J-couplings or through- space dipolar magnetic interactions.
The magnetisations induced by the preparation period are permitted to evolve over a varied period of time under this well-defined magnetic and RF environment.

5.2.1.3 Mixing

At the end of the evolution time, it is possible to redistribute nuclear magnetisations among the spins. This distribution may involve the use of pulses and/ or time periods. The idea is to allow spin communication and therefore interactions of nuclei with J-coupling and dipolar couplings.

5.2.1.4 Detection

Finally, the NMR spectrum of these nuclei is monitored or recorded in the form of a normal chemical shift pattern. The appearance of the spectrum will usually differ in intensity or phase from the ordinary spectrum, but the features are still similar. These phase and/or intensity variations can be investigated by varying the evolution time from zero to some upper limit and by collecting spectra for each new value of the evolution time used in the experiment. These variations can reveal pertinent details about the chemical and magnetic environments of the nuclei present during the evolution time and can produce information that might otherwise be unobservable.

5.3 Types of interactions in two-dimensional NMR

After having established the four different periods in two dimensional NMR, two types of interactions need to be considered:

-The first one is scalar (J couplings) which gives rise to the observed multiplets in 1D NMR. It is effective only between spins which are separated by few bonds in the molecule. The magnitude of the scalar coupling is sensitive to the torsion angle between single and double bonds, and hence provides information about structure.

-The second one is the dipolar coupling of two spins, which operates through space. It is responsible for the dominating mechanism of relaxation. Dipolar coupling generates also the mutual relaxation between spatially neighbouring nuclei, the so-called cross relaxation. The intramolecular cross relaxation gives rise to the nuclear Overhauser enhancement (nOe) effect, *i.e* to a variation in the intensity of a signal as a result of a disturbance in the

populations of another nucleus. The nOe effect depends on the distance between the cross-relaxing nuclei, and hence allows the determination of intramolecular interatomic distances.
The nOe values allow the determination of three-dimensional structures.

A third mechanism for coherence transfer is provided by exchange processes, such as chemical reactions. This process is out of the scope of this chapter.

5.3.1 Two-dimensional NMR using scalar coupling

5.3.1.1 Standard COSY

The basis of the COSY[8-10] (COrrelation SpectroscopY) experiment is the process of coherence transfer in which magnetisation is transferred between coupled spins.
The COSY experiment consists of two 90° pulses separated as depicted in Figure 5.4 by a time period t_1 and the result of performing this experiment for the A nucleus of an AX spin system (A and X both protons) may be explained as follows.
Two different cases need to be considered for AX system, J(A,X)=0 and J(A,X)≠0. In both cases the effect of the initial $90°_x$ pulse is the same, the bulk magnetisation being flipped into the x'y' plane.
Following the initial $90°_x$ pulse, when J(A,X)=0 the magnetisation vectors fan out in a way which is dependent on the Larmor frequency of A alone. The second $90°_x$ pulse is called a mixing pulse and essentially mixes the components of the transverse magnetisation, *i.e* it causes coherence transfer between the coupled signals. When J(A,X)=0 this second pulse has no effect on the information contained in the transverse magnetisation, which is therefore invariant to any time delay before the second RF pulse. This means that in the 2D spectrum all that is observed is a contour with the coordinates (δ_A, δ_A); this is called a 'diagonal peak' and similarly for X, *i.e* (δ_X, δ_X).
When J(A,X)≠0 this second $90°_x$ pulse results in coupling information being transferred between the spins of the X and A nuclei. The A magnetisation vectors precessing at frequency υ_A are (partially) transferred to υ_X by this second pulse, and then precess at υ_X during t_2. In this way modulation of the transverse magnetisation is dependent on the Larmor frequencies of both A and X.

The 2D COSY spectrum of the spin-coupled AX system, therefore, consists of diagonal peaks (δ_A, δ_A), (δ_X, δ_X) and also of off-diagonal (or cross) peaks with coordinates (δ_A, δ_X), (δ_X, δ_A). These off-diagonal peaks indicate that A is indeed spin coupled to X as depicted in Figure 5.4.

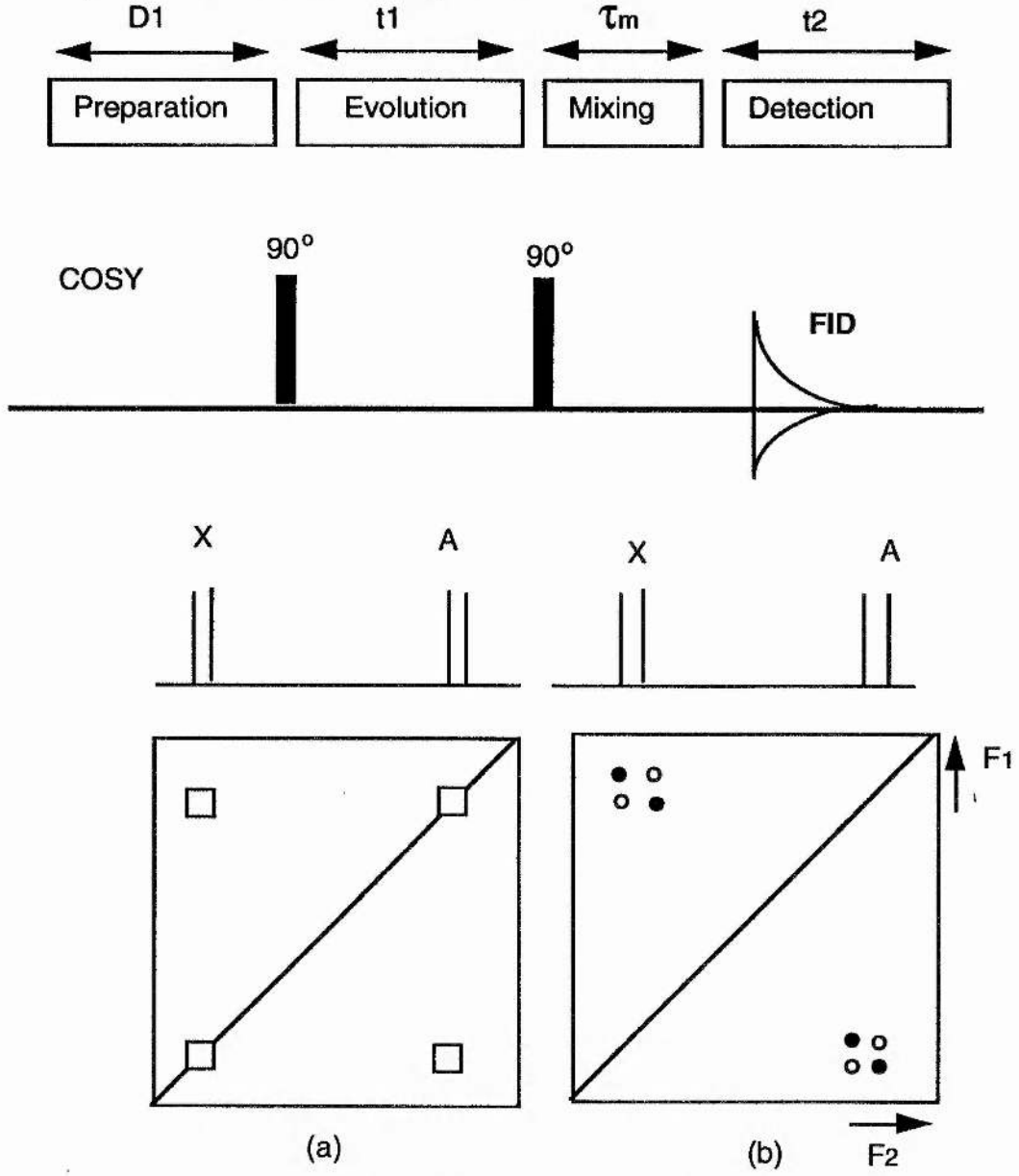

Figure 5.4 The correlation spectroscopy[10] (a) 2D absolute value mode contour for the AX case (b) Phase sensitive contour plot of the off-diagonal peaks for the AX case (positive signals shown as solid circles, negative signals as open circles). Diagonal peaks are omitted for clarity.

5.3.1.2 Relayed COSY

Several other COSY variants may be encountered in practice, the most important of which is relayed-COSY.[11,12] This uses an additional coherence transfer step to give extra connectivity information.
A three-spin system A-B-C which has no coupling between A and C would only give A-B and B-C cross peaks in a normal COSY spectrum, whereas with relayed-COSY a cross peak would also be detected between A and C. This could be crucial in proving that all three spins were part of the same coupling network, particularly if B appears in a crowded region of the spectrum. It is possible to run a double relayed COSY which gives an extra connectivity in the molecular backbone. However, this technique is usually substituted by TOCSY (TOtal Correlation SpectroscopY). This latter technique will be described in the next section (Chapter 5.3.1.5).

5.3.1.3 COSY 45

COSY 45[13] is composed of two pulses of 90° and 45°: this technique has an advantage over basic COSY. Reducing the intensity of transfer between parallel transitions simplifies the appearance of the spectrum around the diagonal, by reducing cross peaks within multiplets. In a complex spectrum this can make it possible to identify correlations that would otherwise be hidden in the clutter of peaks close to the diagonal.

5.3.1.4 DQF-COSY

DQF-COSY[14,15], Double Quantum Filtered Correlation SpectroscopY, is composed of three 90° pulses. The advantage of DQF-COSY over COSY is that crosspeaks near the diagonal are not masked, because by passing the coherence through a double quantum filter, we can obtain diagonal peaks and crosspeaks that are both in the absorption mode. Thus, crosspeaks which lie close to the diagonal are not obscured by antiphase dispersion mode diagonal peaks. However, DQF-COSY is much more sensitive to errors than the COSY experiment which is forgiving of incorrect 90° pulse angles. Therefore, it is crucial to determine with accuracy the 90° pulse for the DQF-COSY. Another problem that can arise is the presence of artifacts due to pulsing too rapidly.

5.3.1.5 TOCSY

The idea underlying the TOCSY[16] (TOtal Correlation SpectroscopY) experiment, also known as HOHAHA, is that coupled spins can be made to exchange magnetisation by applying a pulse train which eliminates the effects of the chemical shift but retains the scalar coupling. This phenomenon is known as isotropic mixing and the advantage of it is that to a good approximation all the multiplet components in the resulting crosspeaks have the same phase; as a consequence, the crosspeaks do not suffer self-cancellation if the multiplet is poorly resolved. A second advantage is that the crosspeaks and diagonal peaks all have aborption mode lineshapes, again to a good approximation. These two factors make the experiment considerably more sensitive than COSY, despite the fact that there is some signal loss as a result of relaxation during the isotropic mixing sequence. The key to the TOCSY experiment is the way in which the isotropic mixing is achieved. A number of suitable sequences are available, most of which involve applying continuous but phase-modulated irradiation to the spins. The RF field strength required to give good mixing across the full proton bandwidth depends on the mixing sequence but values in the range from 6 to 10 kHz are usually used.

5.3.2 Two-dimensional NMR using dipolar coupling

The origin of the nOe lies in population changes[16] caused by a particular form of longitudinal relaxation as mentioned above, namely dipole-dipole cross relaxation. In the case of dipole-dipole relaxation, this 'local field' originates from the magnetic dipoles of other neighbouring spins. Because in this case the field itself originates from a spin, this opens the possibility for a cooperative relaxation mechanism in which both spins simultaneously flip, while the lattice accepts or provides energy corresponding to the net change.

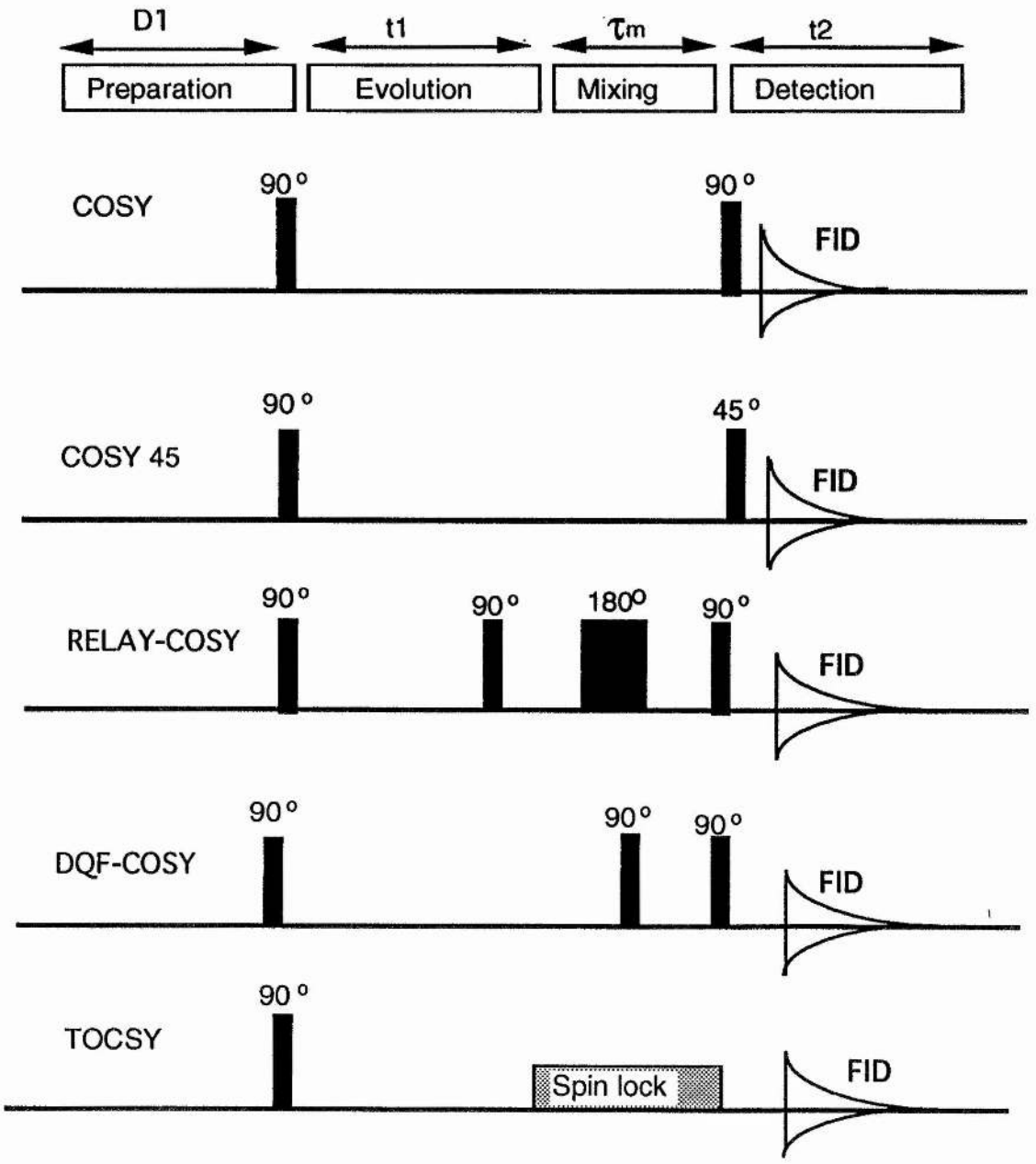

Figure 5.5 Pulse sequences using scalar couplings.

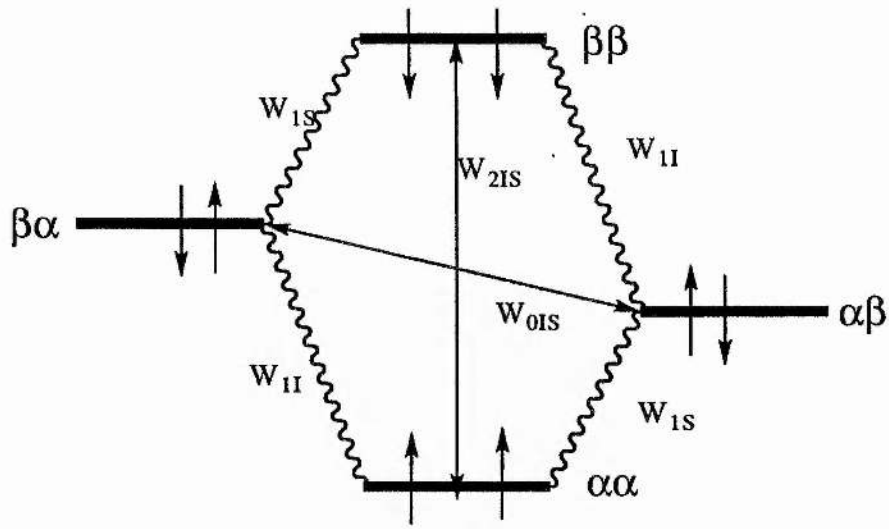

Figure 5.6 Energy level for two-spin system, showing the transitions probabilities (W_0, W_1, W_2) and spin states ($\alpha\alpha$, $\alpha\beta$, $\beta\alpha$, $\beta\beta$).

Two types of cross relaxation need to be considered:

- The first one is characterised by the double quantum transition probability W_{2IS} where both spins flip in the same sense, and the energy change accommodated by the lattice corresponds to the sum of the energies of the individual spin transitions. For these W_{2IS} transitions to occur, the local field resulting from the lattice motions must contain fluctuations at the sum frequency $(\omega_I+\omega_S)$.

- The second one is characterised by the zero quantum transition probability W_{0IS}, in which the spins flip in opposite senses. This implies that a very much smaller energy change is accommodated by the lattice, corresponding to the difference between the energies of the individual transitions. For W_{0IS} transitions, the local field must contain fluctuations at the difference frequency $(\omega_I-\omega_S)$.

Suppose that spin S is saturated, thereby equalising the populations of states $\alpha\alpha$ and $\alpha\beta$ and (separately) equalising the populations of the states $\beta\alpha$ and $\beta\beta$. For all of the relaxation transitions involving S there will now be an excess of downward transitions (i.e high -> low energy), since there are more spins in the

high energy state than would be the case at equilibrium. The excess of downward single spin flips of S (W_1 transitions) has no effect on the intensity of I.

However, if spin S flips downwards during a W_2 transition, spin I also flips downwards, thereby increasing the population difference across the I spin transitions. When W_2 transitions predominate over W_0 transitions, saturation of S causes the intensity of I to increase, which corresponds to a positive nOe enhancement.

Conversely, for a W_0 transition, if the spin S flips downwards the spin I must flip upwards, thereby decreasing the population difference across the I spin transitions. Therefore if W_0 transitions predominate over W_2 transitions, saturation of S causes the intensity of I to decrease, implying a negative nOe enhancement.
If there are equal rates for W_2 and W_0 transitions, the opposing effects cancel and there is no nOe at all.

These points may be expressed more formally using the Solomon equations[17] which form the basis for the theory of the nOe.

For a system of two isolated spins 1/2, the time dependence for the longitudinal component of I spin magnetisation is given by.[17,18]

$$\frac{dI_Z}{dt} = -(I_Z - I_Z^0)(W_{0IS} + 2W_{1I} + W_{2IS}) - (S_Z - S_Z^0)(W_{2IS} - W_{0IS})$$

Equation 5.2

If S is saturated until steady state is reached, then dI_z/dt and S_z may both be set to zero, whereupon rearrangement and substituting $I_Z^0 = (\gamma_I / \gamma_S) S_Z^0$ gives

$$f_I\{S\} = \frac{I_Z - I_Z^0}{I_Z} = \frac{\gamma_S}{\gamma_I} \frac{W_{2IS} - W_{0IS}}{W_{0IS} + 2W_{1I} + W_{2IS}}$$

Equation 5.3

where $f_I\{S\}$ is the fractional steady state nOe enhancement measured at I upon completely saturating S.
The values of the various transition probabilities can be shown to be

$$W_{0IS} = \frac{1}{20}K^2 J(\omega_I - \omega_S)$$

$$W_{1I} = \frac{3}{40}K^2 J(\omega_I) \qquad \text{Equation 5.4}$$

$$W_{2IS} = \frac{3}{10}K^2 J(\omega_I + \omega_S)$$

where

$$K = (\mu_0 / 4\pi)\hbar\gamma_I\gamma_S r_{IS}^{-3} \qquad \text{Equation 5.5}$$

Given that K always appears as its square, this shows that all of these intramolecular dipole-dipole transition probabilities depend linearly on the inverse sixth power of the internuclear distance r_{IS}.

The various spectral density functions $J(\omega_X)$ each describe the power available at the corresponding frequency ω_X from molecular motions to stimulate relaxation.

These spectral density functions provide the vital link between transition probabilities and molecular tumbling properties.

If it is assumed that molecular tumbling is isotropic, and that it can be described by a correlation function that is a simple exponential decay with a rate constant τ_c then the spectral density functions are given by

$$J(\omega_X) = \frac{2\tau_C}{(1+\omega_X^2\tau_C^2)} \qquad \text{Equation 5.6}$$

There are three regions that we can distinguish according to molecular tumbling and molecular weights.

For small molecules molecular tumbling is very rapid, τ_c is very short and $\omega_X\tau_c << 1$. This is called the extreme narrowing condition (Figure 5.10).

$$f_I\{S\} = \frac{\gamma_S}{2\gamma_I} \qquad \text{Equation 5.7}$$

which in the homonuclear case is just +50%.

As molecular weight increases and tumbling becomes slower, the spectrum of rates of molecular motions becomes more and more concentrated at low frequencies. The spectral densities $J(\omega_I+\omega_S)$ and $J(\omega_I)$ become progressively smaller until they cease to make any significant contribution to relaxation. In other words, the local field produced by motions of neighbouring dipoles in large molecules has no frequency component high enough to stimulate W_2 and W_1 transitions.

For homonuclear systems in still larger molecules where $\omega\chi\tau_c >> 1$, all the spectral densities other than $J(\omega_I-\omega_S)$ become insignificant, dipolar relaxation is completely dominated by W_0 transitions and nOes are all negative. This limit is known as the spin diffusion limit as depicted in Figure 5.8.

Where $\omega\chi\tau_c \approx 1$ the numbers of W_2 and W_0 transitions are nearly equal, resulting in small or zero nOe enhancements irrespective of the internuclear distances involved.

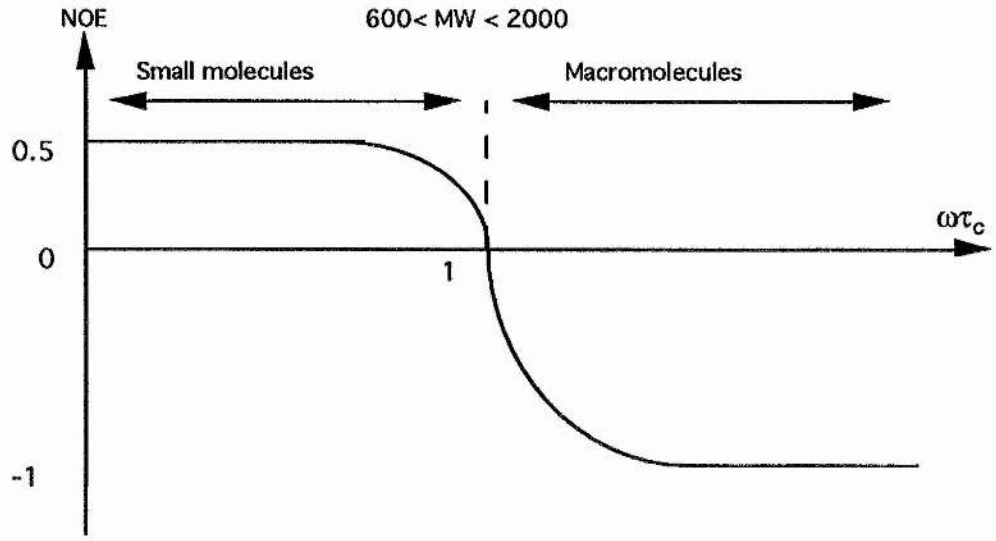

Figure 5.7 Maximum theoretical homonuclear[19] nOe enhancement for two-spin system relaxing exclusively *via* dipolar interactions, as a function of $\omega\tau_c$.

For small rapidly tumbling molecules where $\omega\tau_c << 1$, the maximum nOe enhancement is +50%, while for large, slowly tumbling molecules where $\omega\tau_c >> 1$, the maximum enhancement is -100%.

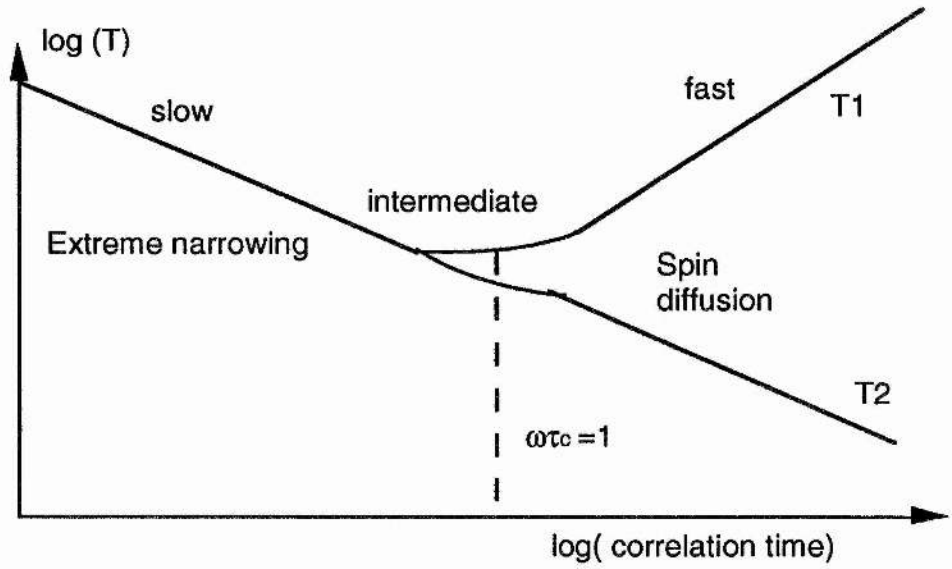

Figure 5.8 Plots of T_1 and T_2 vs correlation time[20] τ_c.

5.3.2.1 NOESY

The NOESY[21,22] (Nuclear Overhauser Effect SpectroscopY) experiment is usually used to identify pairs of protons that are undergoing cross-relaxation, *i.e* protons that would show an nOe in a 1D experiment. The characteristic feature of the NOESY pulse sequence is the mixing time τ_{mix}. The cross-peaks are generated by magnetisation transfer that takes place during the mixing time so the length of this delay must be chosen according to the rate of the transfer process. The cross-relaxation arises as a consequence of dipole-dipole coupling between the different nuclear spins. The nOe is distance dependent (nOe intensity is related to distance between the two nuclei r as r^{-6}) and the way in which the nOe evolves is also dependent on the motion of molecules in solution, since dipole-dipole coupling is modulated by Brownian motion. The nOe intensities may be positive or negative, depending on the molecular mobility, and thus the signal may go to zero. This situation can occur at certain measuring frequencies for slowly tumbling molecules (proteins, macromolecules).

For nuclei with I=1/2 the predominant relaxation pathway is via dipolar interactions with other spins.

A complicating factor is that the NOESY pulse sequence cannot distinguish between magnetisation transfer caused by cross-relaxation and magnetisation

transfer caused by chemical exchange. Both give cross-peaks of the same sign as the diagonal.

5.3.2.2 ROESY

The ROESY[23,24] (Rotating frame Overhauser Effect SpectroscopY) experiment may be thought of as the rotating-frame analogue of NOESY. ROESY aims to determine the transverse cross-relaxation rates which are always positive. By contrast, the NOESY experiment yields longitudinal cross-relaxation rates and the nOe intensities may be positive, zero or negative depending on molecular mobility. There are a number of differences between the ROESY and NOESY experiments. The most important with macromolecules is that crosspeaks arising from spin diffusion are weaker and easier to identify in the ROESY experiment. For smaller molecules a second advantage arises from the fact that rotating frame cross relaxation rate has the same sign for all correlation times. This means that the ROESY experiment can be applied to all molecules irrespective of correlation time, in contrast to NOESY.
The rOe peaks are always positive which allows us to distinguish peaks arising from ROESY transfers and from chemical exchange effects which are always negative.

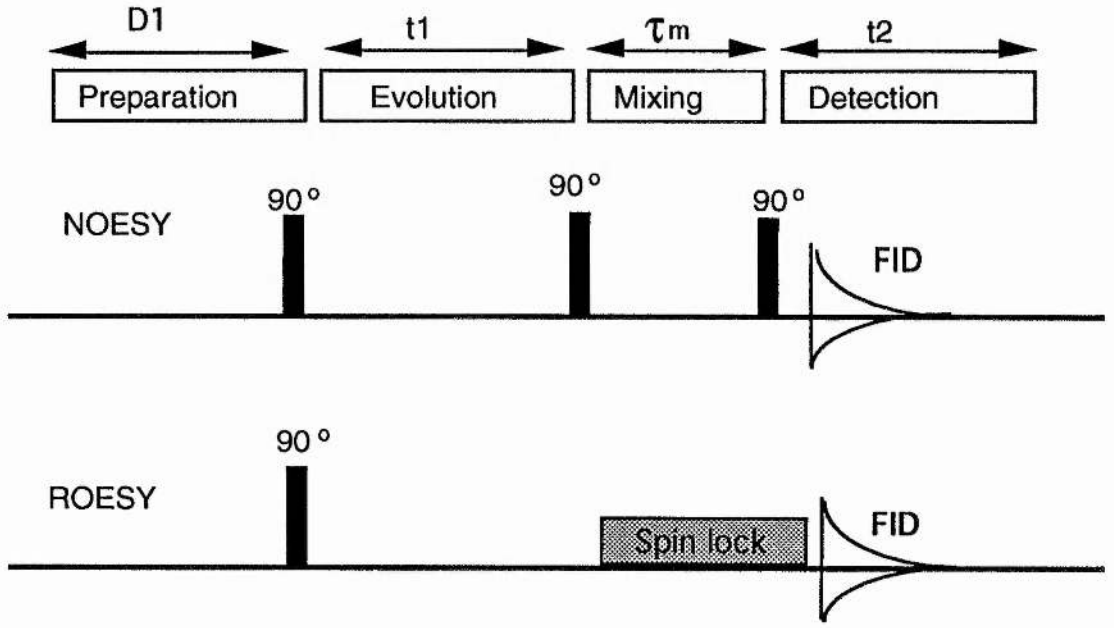

Figure 5.9 Pulses of NOESY and ROESY.

5.3.2.1 Problem with spin diffusion associated with large molecules

For homonuclear experiments with large molecules direct and indirect enhancements are all negative, and the predominance of W_0 transitions over all others means that indirect enhancements can be transmitted efficiently down a chain of spins.

In the limit of slow tumbling, [25,26] saturation of any spin in a homonuclear multispin system will, at steady state, cause a -100% enhancement of every other spin (Figure 5.7); in other words, the entire spectrum will become saturated and disappear: This process is known as spin diffusion.

This process renders steady state homonuclear experiments on large molecules completely useless in terms of determining structures. Even limited spin diffusion poses a severe problem for interpretation, since direct and indirect enhancements cannot be distinguished *a priori*, being all negative making it impossible to equate a given strength of enhancement with a given distance approximation.

5.3.2.2 Problem of spin diffusion associated with intermediate molecules

The ionophoric antibiotics have a molecular weight about 850 which corresponds to the region $\omega\tau_c \approx 1$. Consequently their nOe intensities are very small or zero which consistutes a very severe problem.[25,26]

However, this problem can be avoided by carrying out a different type of nOe experiment, in which nOe enhancements evolve not between elements of longitudinal magnetisation as in the conventional experiment, but rather between elements of transverse magnetisation during a period of spin locking.

Spin locking[27] is achieved by preparing the spin system with a 90° pulse, and then immediately applying a strong, continuous RF field (the spin locking field) along a transverse axis perpendicular to that of the 90° pulse. Thus a 90_x pulse would be followed by a spin locking field along the y' (or -y') axis. Viewed in the rotating frame, the equilibrium magnetisation **M°** is first tipped into the transverse plane by the pulse, and is then 'caught' by the spin locking field applied parallel to the new axis along which **M** now lies.

Spin locking suppresses the relative precession of chemically shifted resonances within the spectrum; in other words, while the spin locking field is switched on, all

the transverse magnetisation components from the different signals in the spectrum precess together, with a constant relative phase.

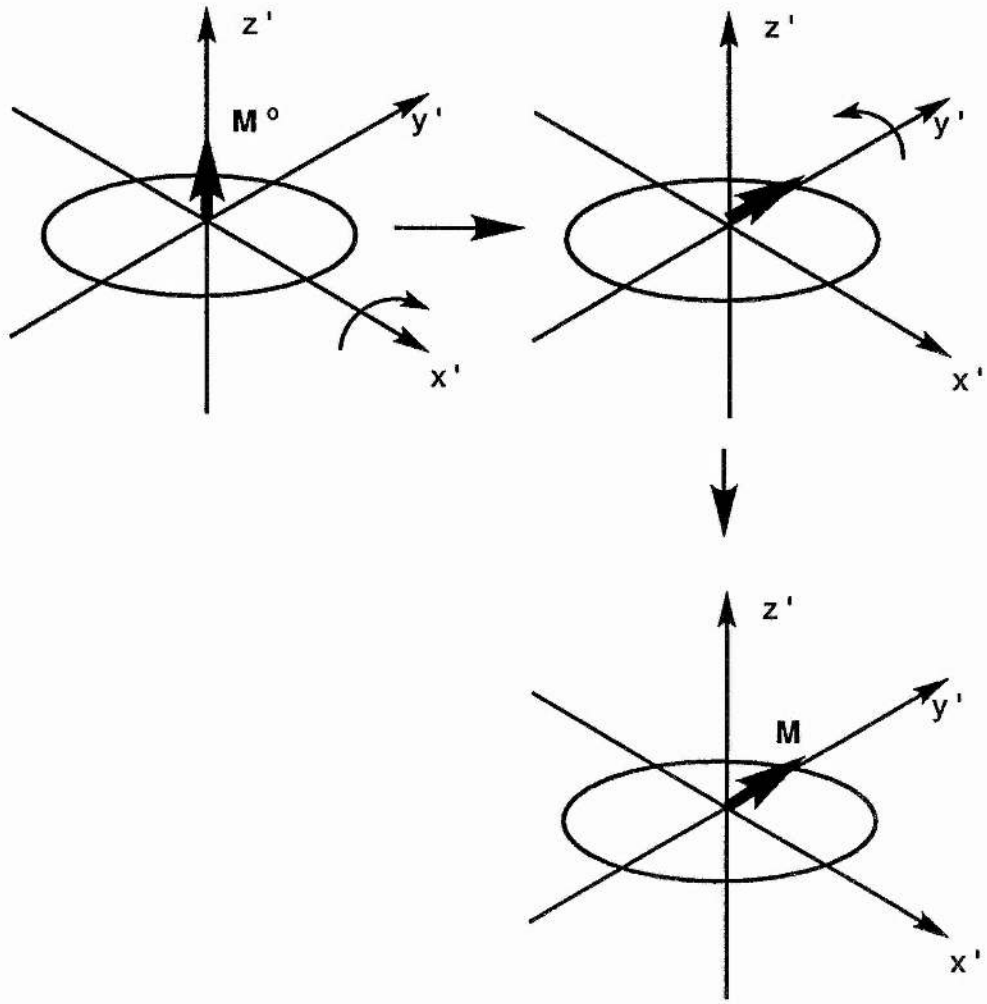

Figure 5.10 Schematic representation[27] of spin locking.

The reason why (rotating Overhauser effect) experiments differ fundamentally from longitudinal ones is that the transition probabilities for spin locked dipolar relaxation are based on different spectral densities.
The transverse cross relaxation rate σ_2 and transverse dipolar relaxation rate ρ_2 are given by.[16]

$$\sigma_2 = \frac{1}{40}K^2[\frac{9}{2}J(2\omega_1) - \frac{1}{2}J(0) + 6J(\omega_0)] \qquad \text{Equation 5.8}$$

$$\rho_2 = \frac{1}{40}K^2[\frac{9}{2}J(2\omega_1) + \frac{1}{2}J(0) + 9J(\omega_0) + 6J(2\omega_0)]$$ Equation 5.9

where ω_0 is the Larmor frequency and ω_1 is the frequency of precession about the B_1 field.

For comparison, the equivalent expressions for their longitudinal counterparts are

$$\sigma_1 = \frac{1}{20}K^2[-J(\omega_1 - \omega_S) + 6J(\omega_0)]$$ Equation 5.10

$$\rho_1 = \frac{1}{20}K^2[J(\omega_1 - \omega_S) + 3J(\omega_0) + 6J(2\omega_0)]$$ Equation 5.11

The key difference between these expressions is that, unlike σ_1, σ_2 cannot become negative. Typical spin locking field strengths in rOe experiments are between ω_1= 2kHz and 10 kHz. Since molecular motions in liquid samples will never be significantly slower than this, direct rOe enhancements are always positive. The positive rOe enables us to distinguish them from signals through chemical exchange which are always negative.

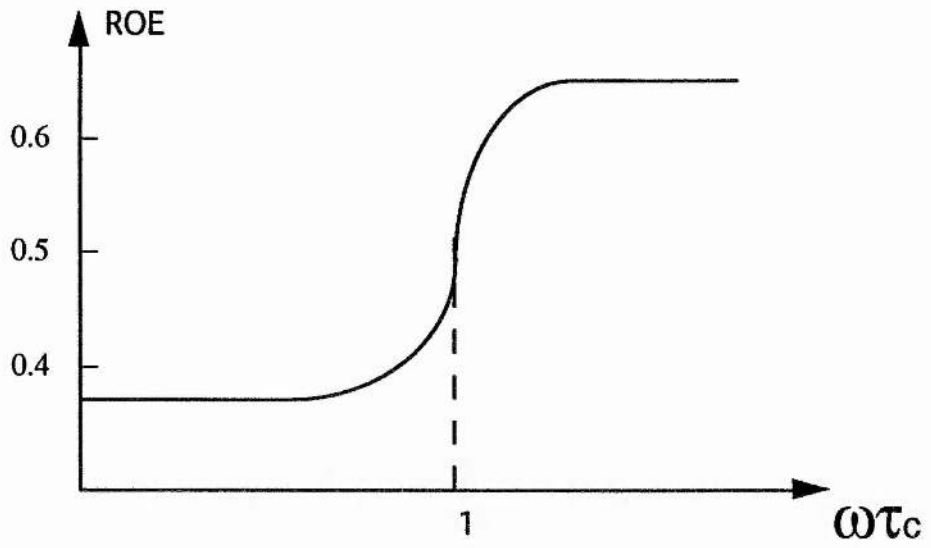

Figure 5.11 Maximum obtainable rOe enhancement[28] rOe_{max} in the isolated two-spin pair approximation, assuming that the spins are relaxed exclusively by homonuclear dipolar interactions.

NOESY is done *via* main magnetic field, therefore it is destroyed by molecular motion in MHz region. ROESY uses a spin lock field for the same purpose. It

has a precessional frequency for nuclei in the kHz region, hence for molecules tumbling in MHz region ROESY is not affected.

5.4 Heteronuclear correlation spectroscopy

Two dimensional spectra are in principle possible for heteronuclei by either dipolar or scalar interactions. However, the magnetic moments of heteronuclei are too small in comparison with protons, and since cross relaxation depends on the square of the magnetic moments it appears to be a serious limitation for the generation of NOESY and ROESY cross peaks.
Heteronuclear chemical shift correlation involves either direct or indirect detection of the heteronucleus. In the indirect mode,[29,30] dramatic enhancements of sensitivity can be achieved owing to the large sensitivity of protons with respect to heteronuclei. The overall sensitivity of a 2D NMR is dependent on the gyromagnetic ratio as depicted in Table 5.1

Type of transfer	Relative sensitivity	S=^{13}C
S (Direct)	$(\gamma_s)^{5/2}$	1
I -> S	$\gamma_I(\gamma_s)^{3/2}$	4
S-> I	$\gamma_s(\gamma_I)^{3/2}$	8
I -> S -> I	$(\gamma_I)^{5/2}$	32

Table 5.1 Relationship type of transfer and relative sensitivity.[29]

5.4.1 Heteronuclear Single Quatum Correlation experiment

Heteronuclear Single Quatum Correlation[31] (HSQC) experiment also known as the Overbodenhausen experiment in the NMR jargon. The first part of the sequence the first INEPT[32] (Insensitive Nuclei Enhanced by Polarisation Transfer) fragment transfers I-spin polarisation to the S-spin, which then precesses freely during the evolution period. After polarisation transfer back to the I spins, (reverse INEPT) a period is allowed for refocusing, so that broadband S-spin decoupling can be used without cancelling the I-spin signal.

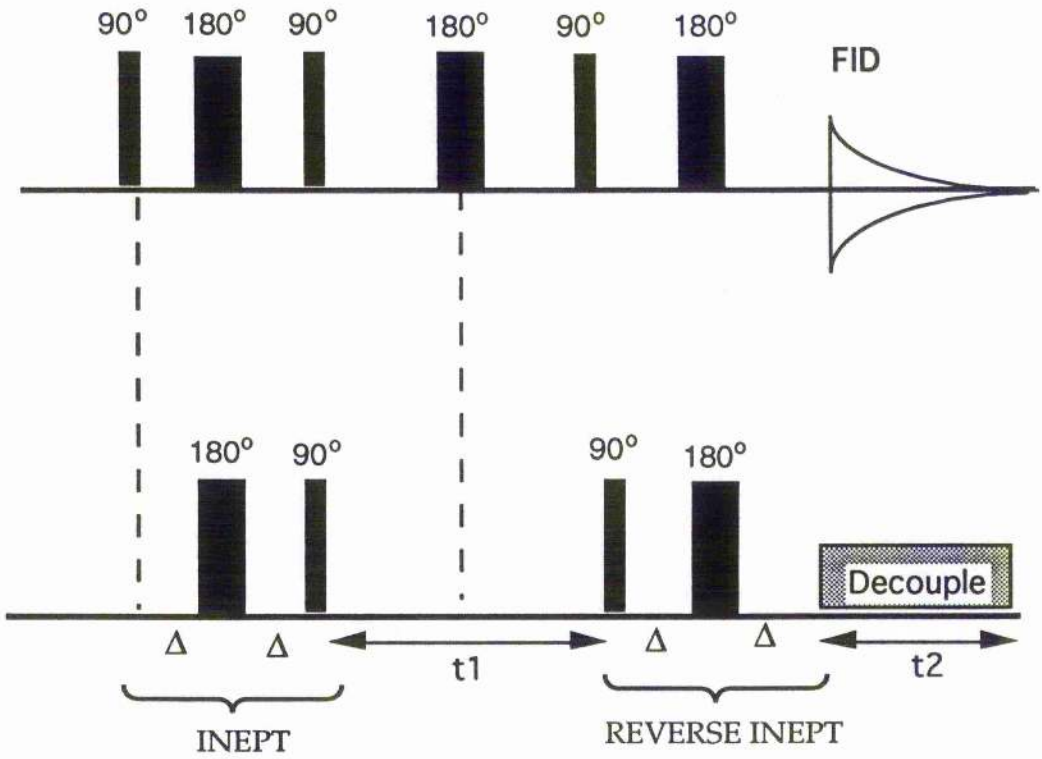

Figure 5.12 Heteronuclear single quantum coherence pulse sequence.[31]

5.4.2 Distortionless enhancement polarisation transfer

The Distortionless Enhancement Polarisation Transfer[33] (DEPT) sequence appears to be the method of choice for editing subspectra relating to CH, CH_2 and CH_3 groups through three different experiments. The DEPT sequence as depected in Figure 5.13 consists two 180° pulses (on the proton and carbon channels) to refocus the chemical shifts effects.
At least, three experiments are performed for different values of the flip angle θ° (generally 45°, 90°, 135°) yielding by appropriate linear combinations the subspectra associated with the three multiplicities CH, CH_2 and CH_3.

5.5 Strategy for spectral assignment of tetronasin

NMR spectroscopy offers the possibility of studying the conformational behaviour of molecules in solution and dynamic aspects. However, the structures established by NMR methods do not differ greatly from X-ray diffraction

structures. In this section, we describe the general strategy leading to the total assignment of tetronasin by using NMR techniques.

Even with high field spectrometers, some regions of ^{1}H NMR spectra of medium and large size molecules remain unresolved. Two dimensional NMR methods have been shown to be of great help to resolve the overlapping peaks allowing the total assignment for some molecules.

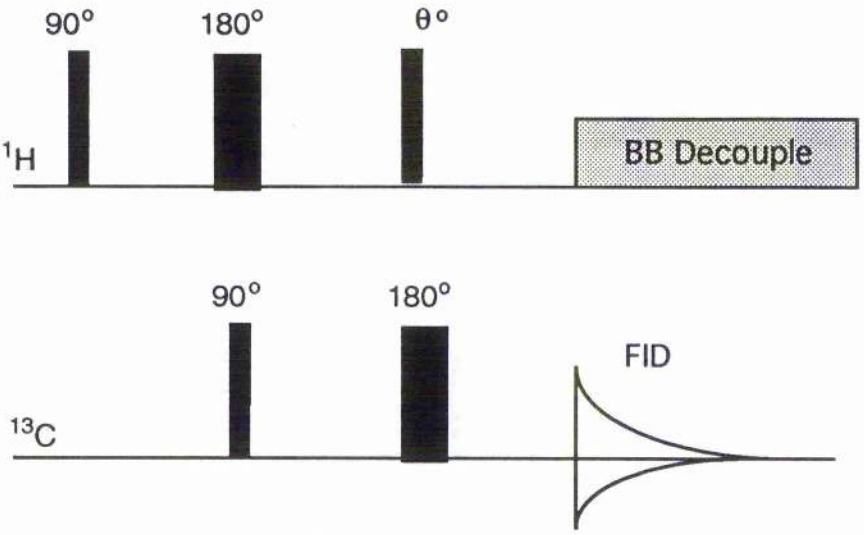

Figure 5.13 DEPT pulse sequence.[33]

COSY and COSY variant methods using ^{1}H correlations allow the elucidation of most parts of ^{1}H NMR spectra but do not, necessarily, lead to total assignments. On the other hand, δ-δ ^{13}C correlation INADEQUATE[34] (leads to complete assignment of ^{13}C NMR spectra, but this method is not very sensitive, requiring at least 1-2 mmol and is, therefore, often unsuitable for routine NMR assignments. In fact, it is possible to deduce, in most cases, total ^{1}H and ^{13}C assignments by an intercorrelation of ^{1}H and ^{13}C NMR spectral informations. The two dimensional heteronuclear chemical shift correlation gives this relationship. The ^{1}H-^{1}H 'COSY' chemical shift correlation provides a ^{1}H scalar coupling relationship. Then the ^{1}H-^{13}C chemical shift correlation, which is the backbone of the method, allows us to deduce ^{13}C assignments from ^{1}H ones. Since carbon connectivity is obtained through ^{1}H relations, the method fails when a quaternary carbon is encountered. Assignment of carbons of CH_2 groups bearing nonequivalent protons leads to the assignment of both protons. After a

number of steps back and forth between ^{1}H and ^{13}C assignments, the ^{1}H and ^{13}C spectra may finally be fully assigned as depicted in Figure 5.14.

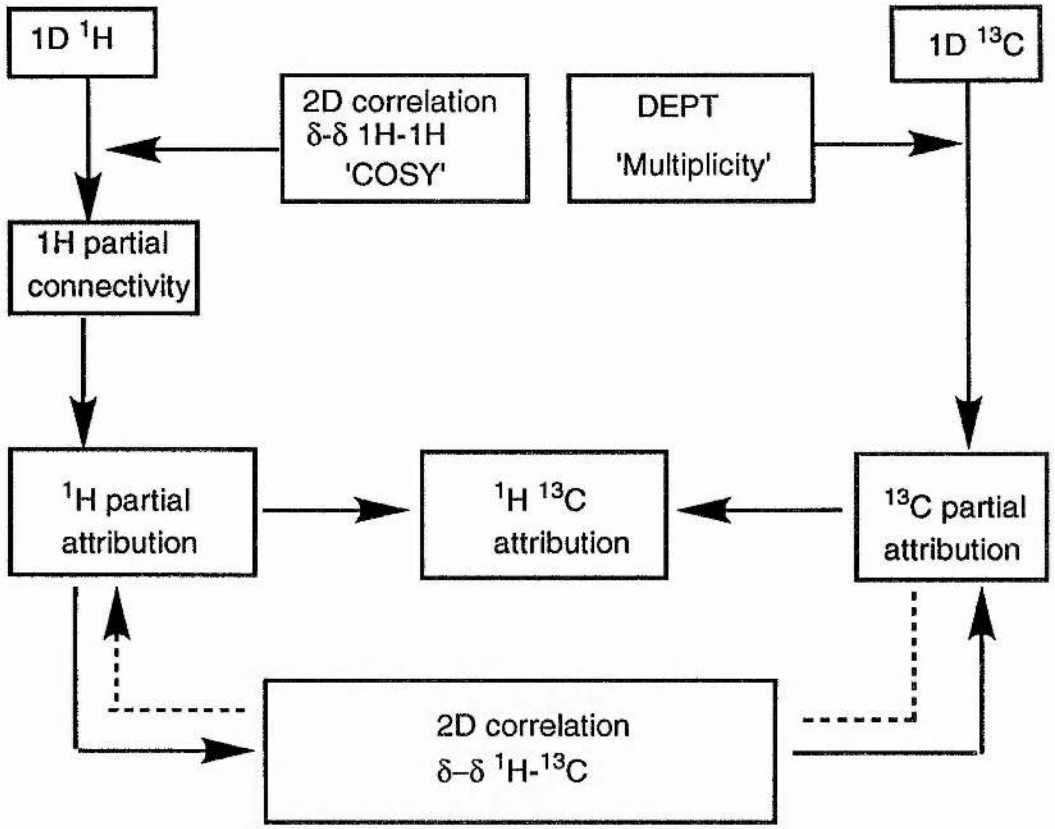

Figure 5.14 Operational strategy of NMR assignment.[35]

5.6 NMR of tetronasin

All experimental details are reported in Chapter 6 (section 6.4).

In this chapter, we propose to assign the NMR spectrum of tetronasin (Figure 5.15) by two-dimensional NMR techniques as a prelude to determining its 3D structure in solution.

Tetronasin or M139603 was isolated[36] from the aerobic fermentation of *Streptomyces longisporoflavus* (see Chapter 2 section 2.3.4) and its structure is different from other polyether antibiotics in that it possesses a biosynthetically rare group in the form of an acyltetronic acid moiety.

5.6.1 ^{1}H and ^{13}C NMR assignments of tetronasin

On looking at the structure of tetronasin-Na^{+}, then can be distinguished four aliphatic rings (A, B, C, D). The aim of NMR assignment consists of identifying proton(s) with characteristic chemical shift, splitting patterns and then utilising the homonuclear scalar experiments such as COSY, Relay COSY, COSY 45 and DQF-COSY as described in Chapter 5 section 5.3.1 to step along the chains of connectivities. Some of them are obvious to assign, for example the methoxy group CH_3O (C-35) appearing as a singlet at δ 3.31 ppm.

The crucial assignment of tetronasin relies on three methine groups at C19 (δ 5.51 ppm), C20 (δ 6.02 ppm), and C12 (δ 5.14 ppm). The C12 is adjacent to tertiary carbon C11 (δ 2.49 ppm) and appears as a doublet. From C11, it is possible to assign completely the aliphatic ring B. Some difficulties are encountered for the assignment of C8 and C9. These peaks are overlapped in the diagonal region (δ 1.14- 1.60 ppm) using standard COSY (Figure 5.18). Fortunately, these problems are overcome by using COSY 45 and DQF COSY (Figures 5.16 and 5.17) which give a clear and neat peaks in these regions.

At first glance, we may think that C19 hydrogen may have much lower field due the electronegativity of oxygen attached to C18 than its counterpart C20 hydrogen. However, this option is ruled out due to the COSY 45 and DQF COSY spectra connectivities. The C20 methene group is adjacent to tertiary carbon C21 (δ 2.18 ppm) bonded to a methyl group C33 (δ 0.91 ppm). This latter shows a doublet in ^{1}H NMR spectrum.

On other hand, the olefinic group C19 is adjacent to tertiary carbon C18 (δ 3.84 ppm) attached to oxygen atom in the ring C. From these crucial assignments, it is possible to establish the chemical shift of protons the ring C and D by stepping along the protons chains connectivities. The aliphatic ring A has two protons at chemical shifts of 4.27 and 4.35 ppm.

After having established the ^{1}H NMR assignment (see Chapter 5 Table 5.2), the next and obvious step was to determine the ^{13}C assignment by using two well-established NMR techniques DEPT and HSQC experiments. This was relatively simple and straightforward for the carbons with bonded protons, just by reading off the ^{13}C resonance using the proton signals for identification. By using HSQC and DEPT experiments, carbonyl groups that were attached to carbon (C2, C4, C28) can not be distinguished.

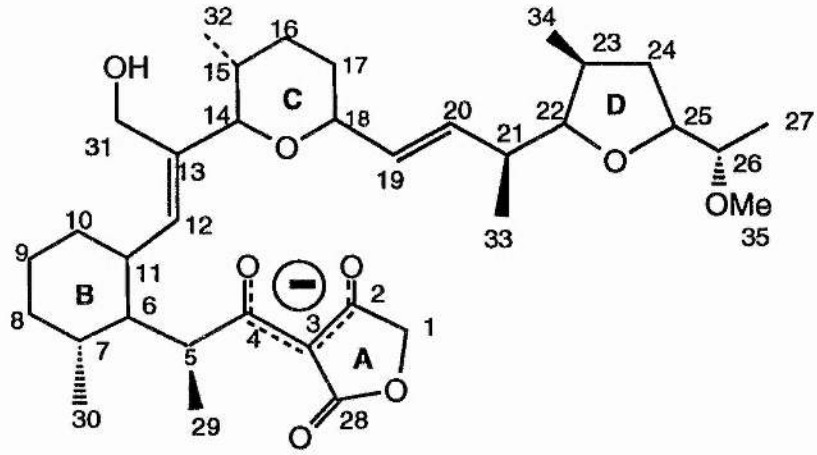

Figure 5.14 Structure of tetronasin.

^1H	Chemical shift (ppm)	^1H	Chemical shift (ppm)
1A	4.35	17B	1.60
1B	4.27	18	3.84
2	-	19	5.51
3	-	20	6.02
4	-	21	2.18
5	3.93	22	3.70
6	1.81	23	2.34
7	1.37	24A	1.76
8A	1.60	24B	1.63
8B	1.13	25	4.31
9A	1.25	26	3.25
9B	1.59	27	0.92
10A	1.35	28	-
10B	1.00	29	0.97
11	2.49	30	1.01
12	5.14	31A	4.28
13	-	31B	3.81
14	3.25	32	0.52
15	1.32	33	0.91
16A	1.20	34	0.94
16B	1.79	35	3.31
17A	1.44		

Table 5.2 ^1H NMR Assignment of tetronasin.

^{13}C	Chemical shift (ppm)	^{13}C	Chemical shift (ppm)
1	56.32	19	141.78
2	-	20	140.91
3	79.07	21	39.47
4	-	22	85.88
5	47.62	23	34.03
6	35.57	24	35.24
7	34.34	25	70.29
8	32.72	26	78.82
9	43.12	27	8.83
10	35.83	28	-
11	36.13	29	13.80
12	130.60	30	25.76
13	130.83	31	56.18
14	91.00	32	18.22
15	32.30	33	16.26
16	32.12	34	10.73
17	32.71	35	57.76
18	85.50		

Table 5.3 ^{13}C NMR Assignment of tetronasin.

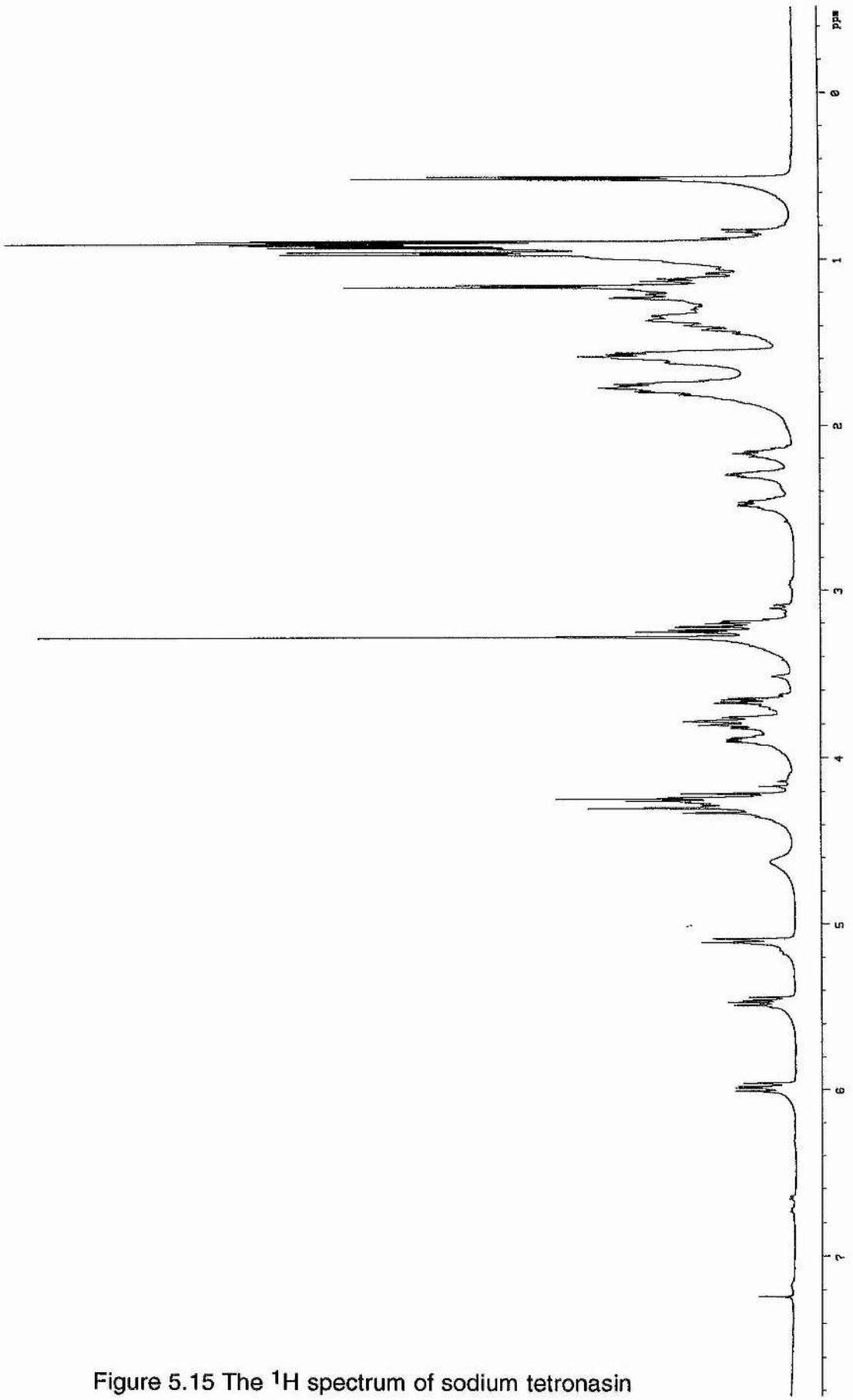

Figure 5.15 The ^{1}H spectrum of sodium tetronasin

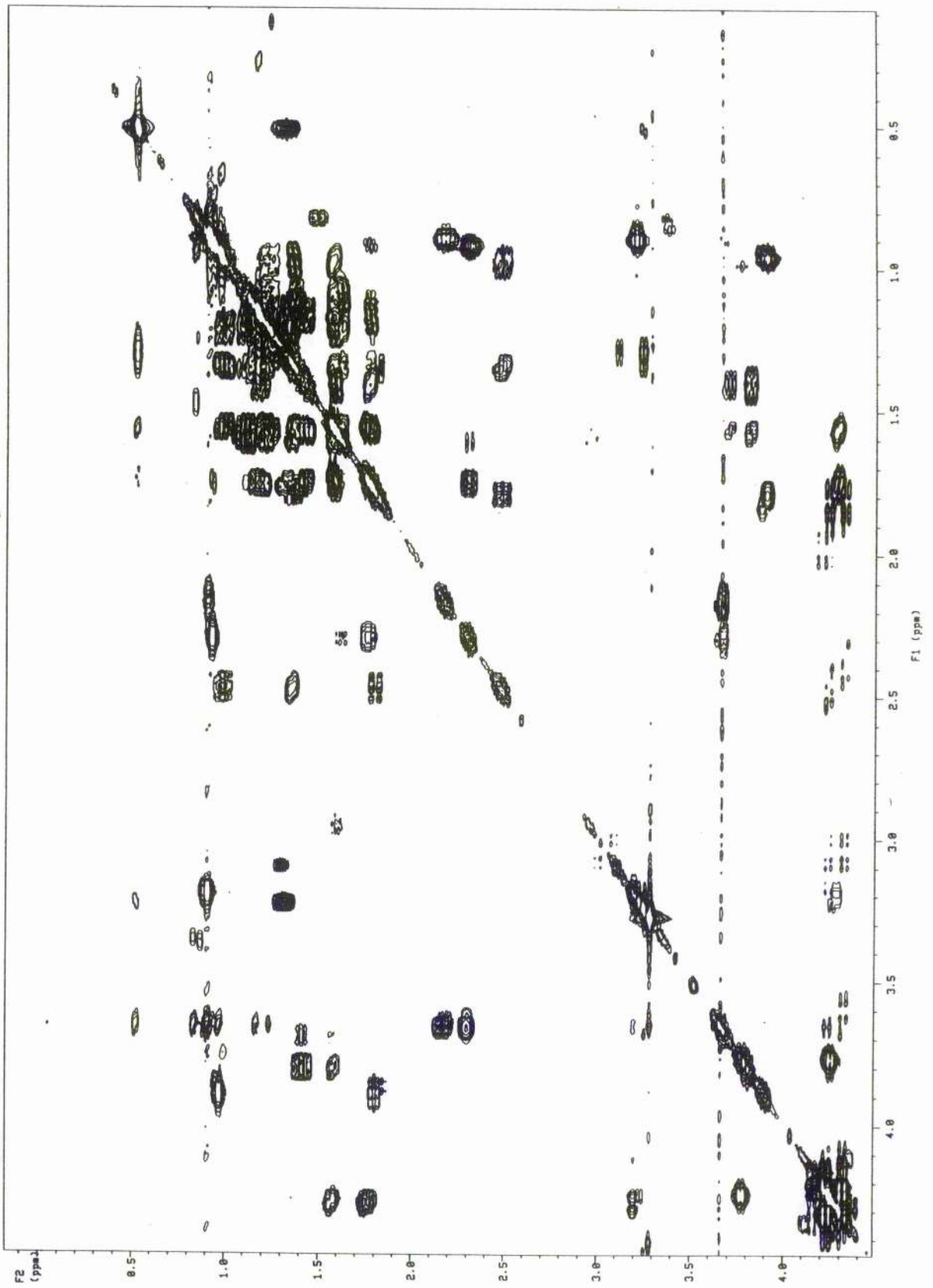

Figure 5.16 An expanded region of the COSY 45 spectrum of sodium tetronasin

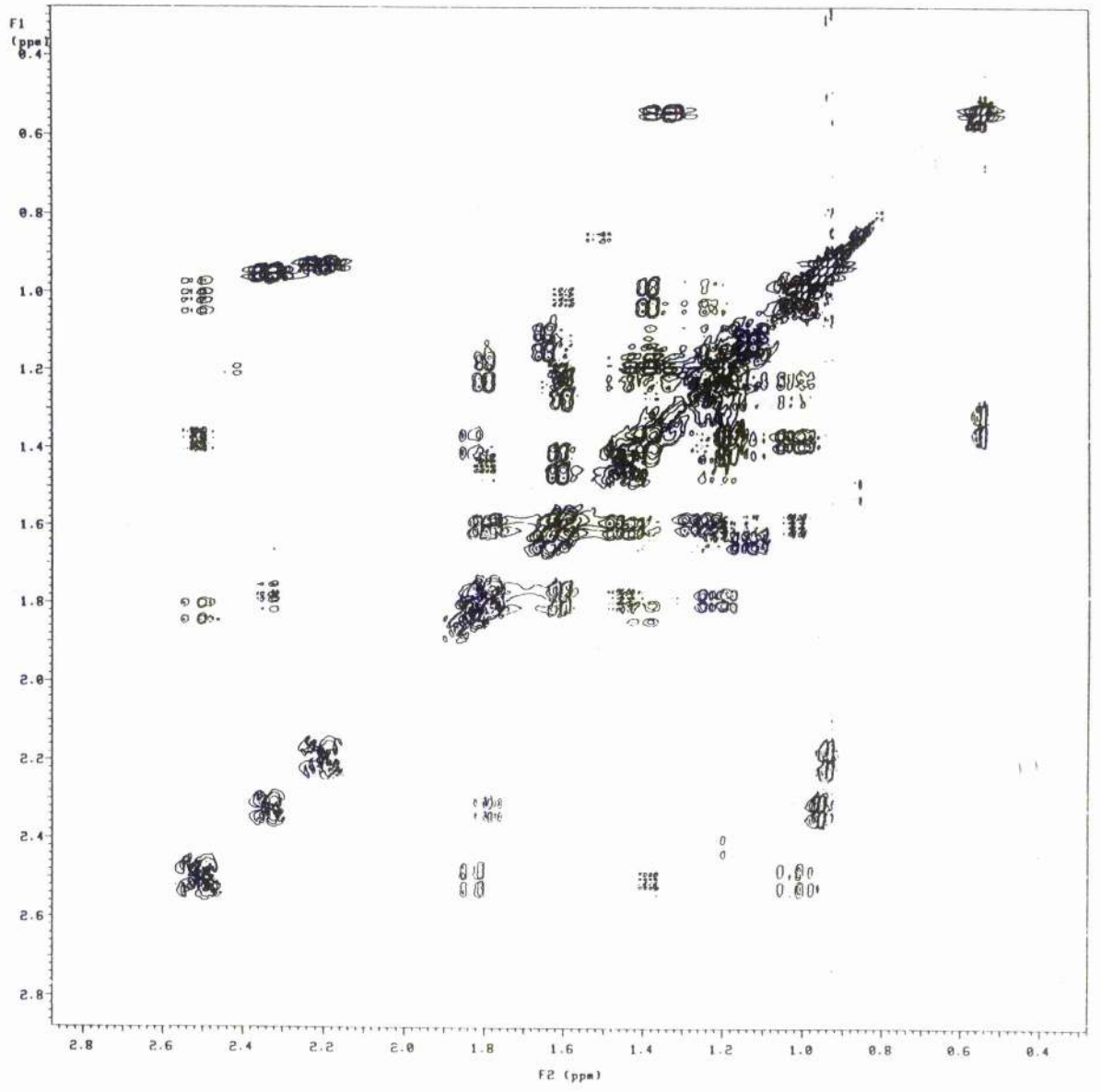

Figure 5.17 An expanded region of the DQF-COSY spectrum of sodium tetronasin

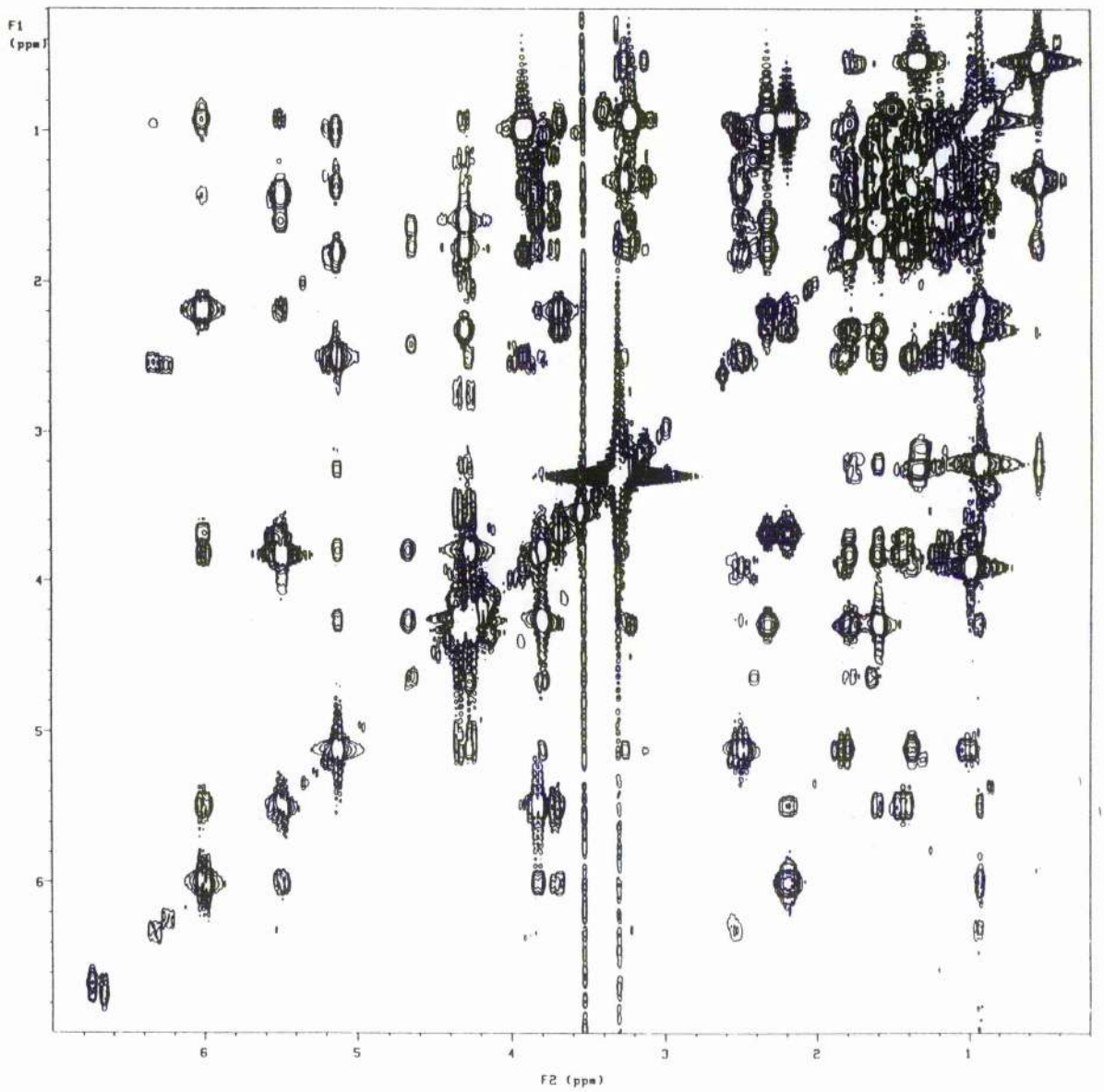

Figure 5.18 An expanded region of the standard COSY spectrum of sodium tetronasin

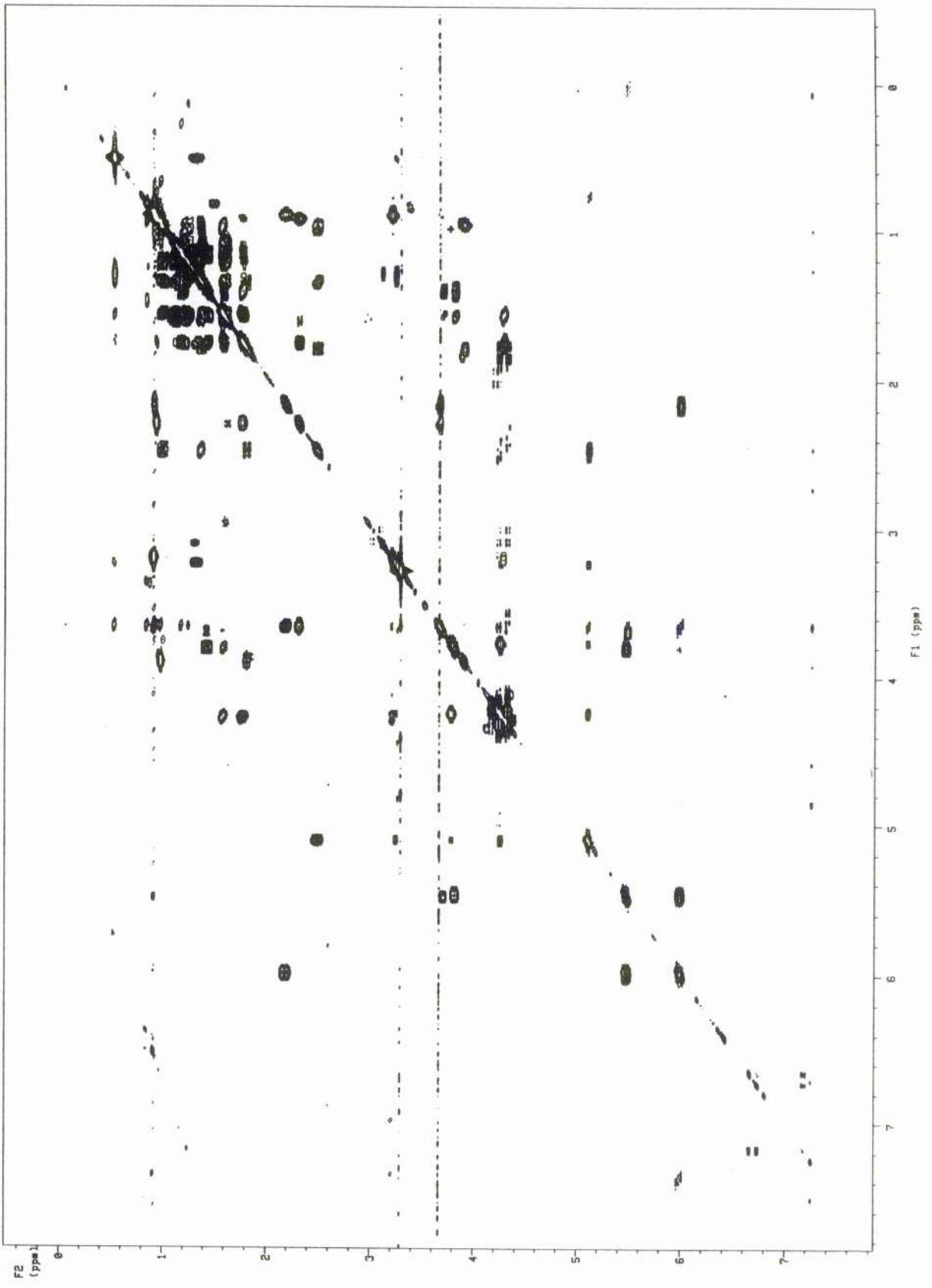

Figure 5.19 The COSY 45 spectrum of sodium tetronasin

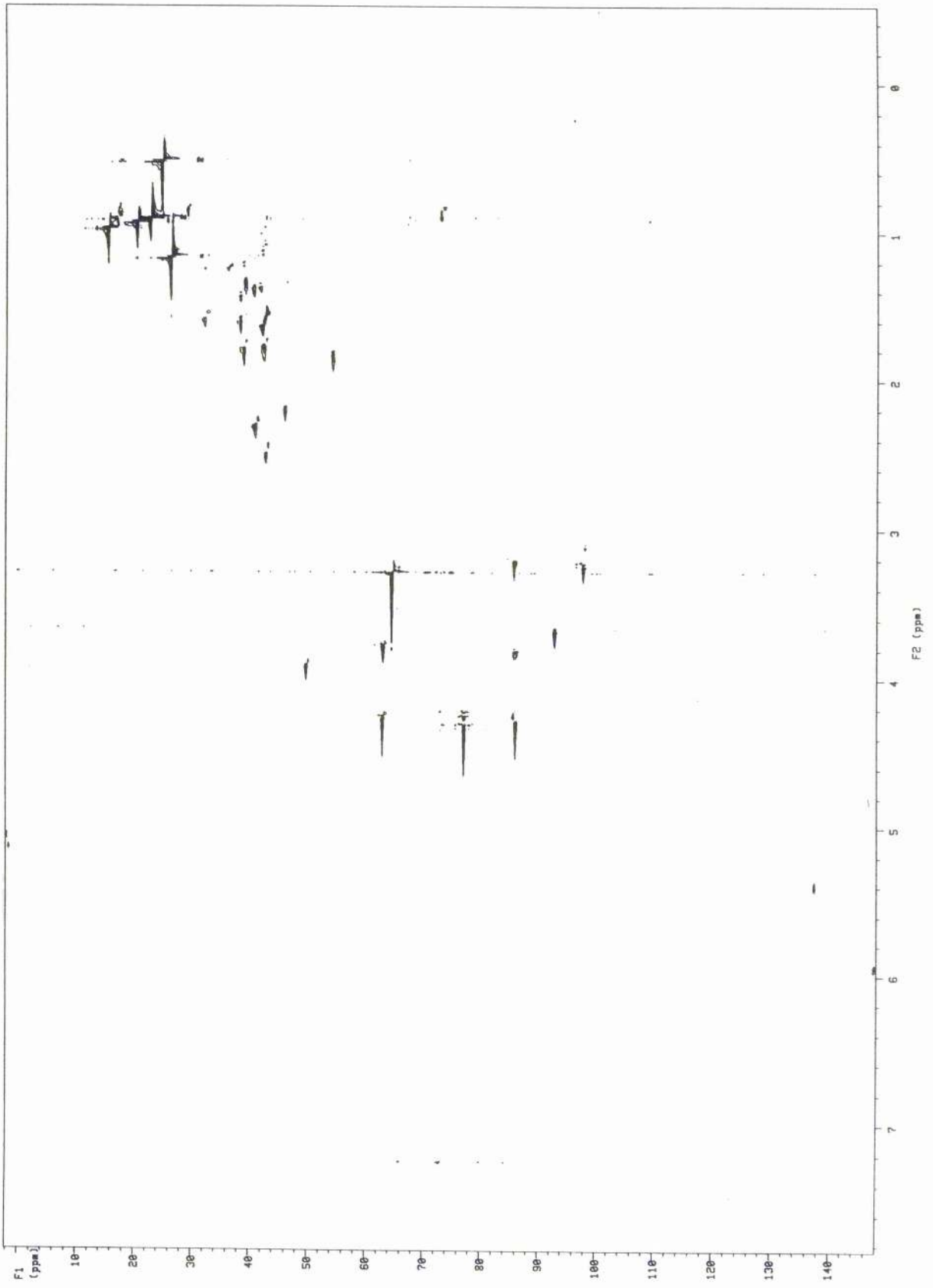

Figure 5.20 The HSQC (^{13}C-^{1}H)spectrum of sodium tetronasin

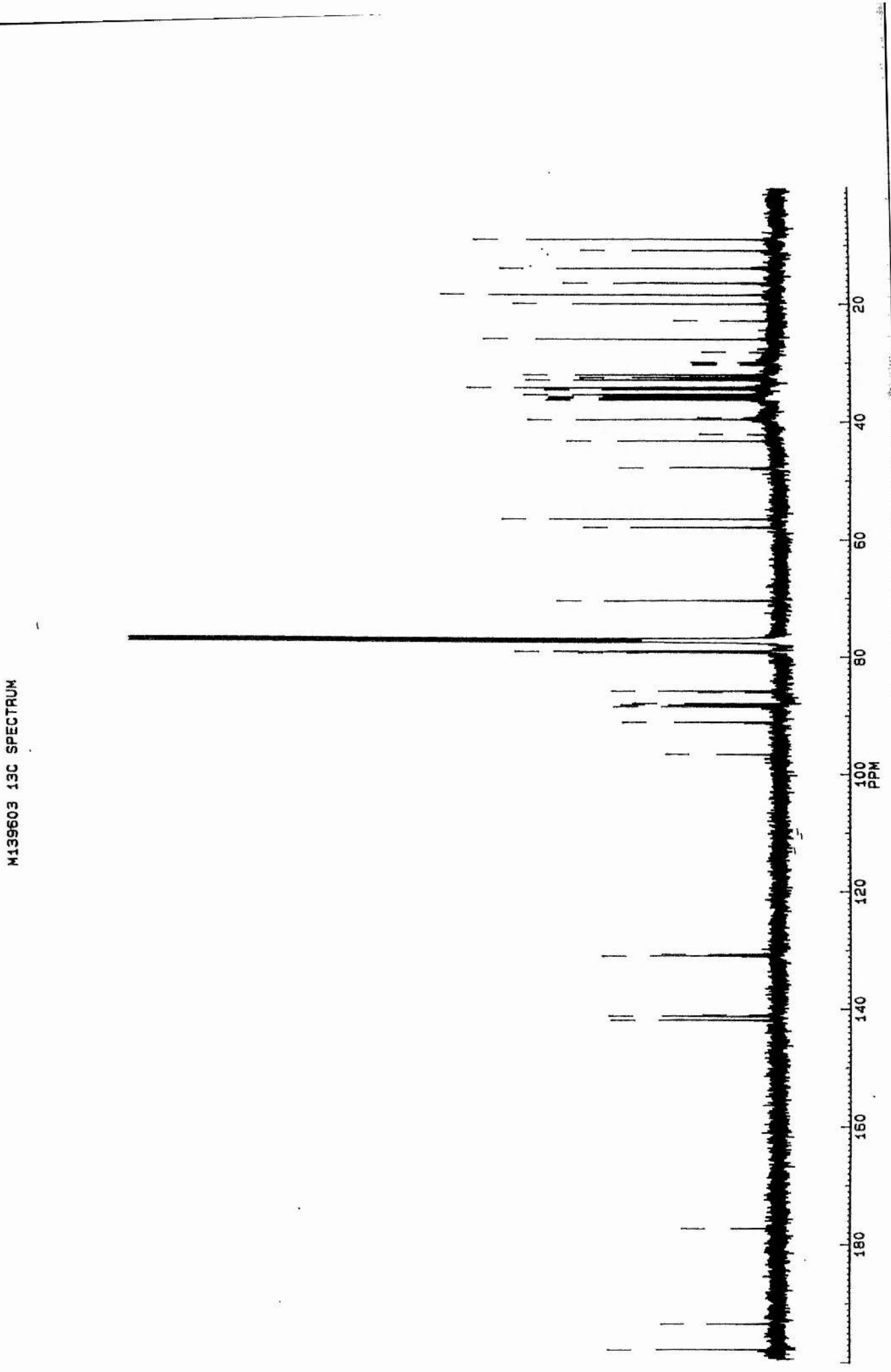

Figure 5.21 The ^{13}C spectrum of sodium tetronasin

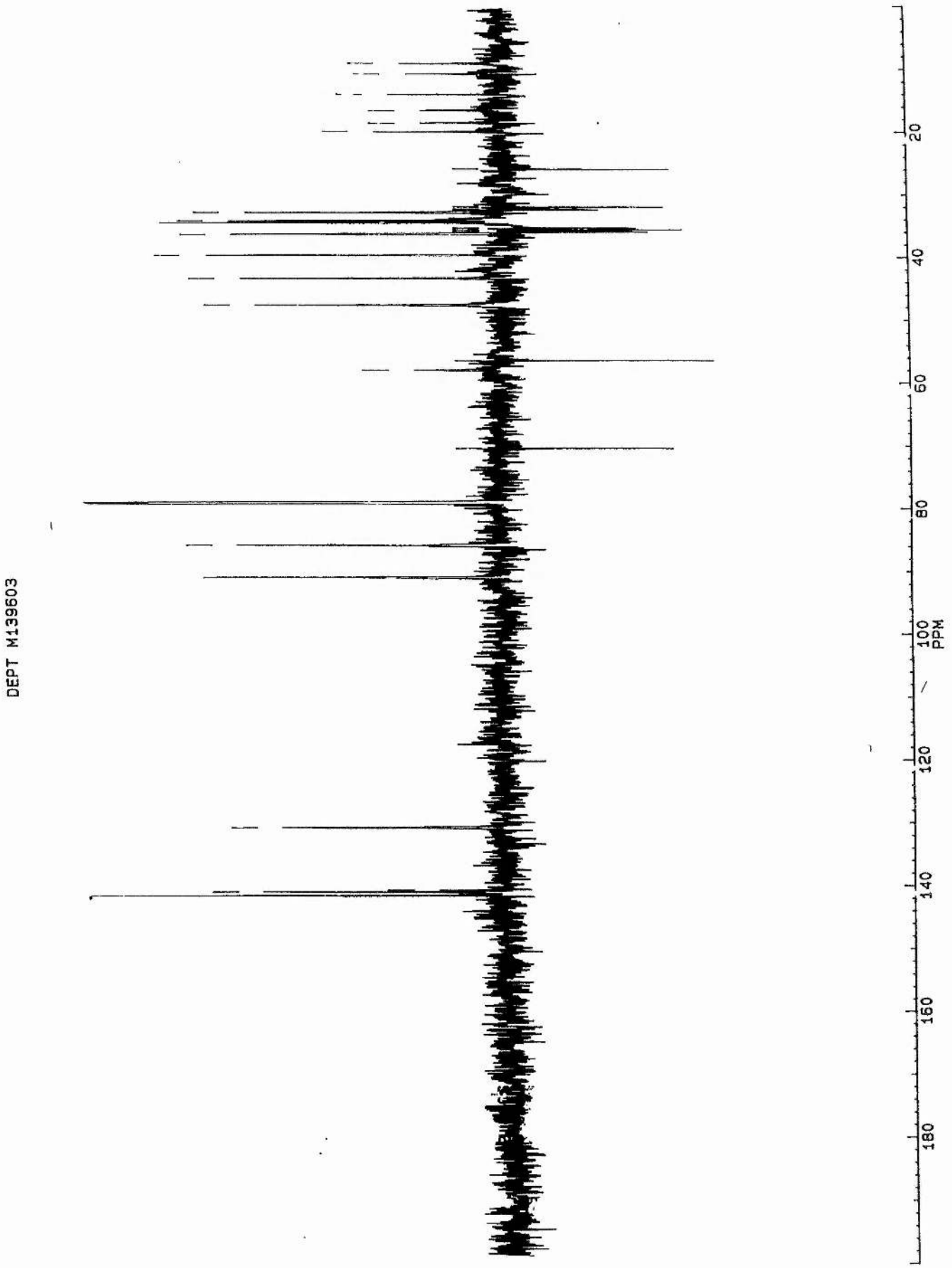

Figure 5.22 The DEPT spectrum of sodium tetronasin (θ=135°)

References to chapter 5

1. R. K. Harris, in 'Nuclear magnetic resonance spectroscopy' Pitman, London (UK), 1983.
2. H. Friebolin, in 'Basic one- and two-dimensional NMR spectroscopy', VCH, Weinheim (Germany), 1993.
3. W. Kemp, in 'NMR in chemistry: A multinuclear introduction', MacMillan Education Ltd, London (UK), 1986.
4. H. Friebolin, in 'Basic one- and two-dimensional NMR spectroscopy', VCH, Weinheim (Germany), 1993, p.5.
5. R. K. Harris, in 'Nuclear magnetic resonance spectroscopy', Pitman, London (UK), 1983, p.8.
6. R. J. Abraham, J. Fisher, P. Loftus in ' Introduction NMR spectroscopy', John Wiley & Sons, Chichester (UK), 1988, p.116.
7. G. A. Gray in 'Two-dimensional NMR spectroscopy: Applications for chemists and biochemists', ed. W. R. Croasmun, R. M. Carlson, VCH, Weinheim (Germany), 1987, p.11.
8. W. P. Aue, E. Bartholdi, R. R. Ernst, *J. Chem. Phys.*, 1976, **64**, 2229.
9. K. Nagayama, A. Kumar, K. Wuthrich, R. R. Ernst, *J. Magn. Reson.*, 1980, **40**, 321.
10. R. J. Abraham, J. Fisher, P. Loftus in ' Introduction NMR spectroscopy' John Wiley & Sons, Chichester (UK), 1988, p.161.
11. G. Eich, G. Bodenhausen, R. R. Ernst, *J. Am. Chem. Soc.*, 1982, **104**, 3731.
12. G. Wagner, *J. Magn. Reson.*, 1983, **55**, 151.
13. A. E. Derome, in 'Modern NMR techniques for chemistry research', Pergamon Press, Oxford (UK), 1987, p. 227.
14. U. Piantini, O. W. Sorensen, R. R. Ernst, *J. Am. Chem. Soc.*, 1982, **104**, 6800.
15. N. Muller, R. R. Ernst, K. Wuthrich, *J. Am. Chem. Soc.*, 1986, **108**, 6482.
16. D. Neuhaus, M. P. Williamson, in 'The nuclear Overhauser effect in structural and conformational analysis', VCH, Cambridge (UK), 1989, p.23.
17. I. Solomon, *Phys. Rev.*, 1955, **99**, 559.
18. D. Neuhaus, M. P. Williamson, in 'The nuclear Overhauser effect in structural and conformational analysis', VCH, Cambridge (UK), 1989, p.25.
19. F. Vaufrey-Mary, PhD. Thesis, University of Clermont-Ferrand (France), 1990.

20. S. W. Homans, 'A dictionary of concepts in NMR', Clarendon Press, Oxford (UK), 1989, p. 118.
21. J. Jeener, B. H. Meier, P. Bachmann, R. R. Ernst, *J. Chem. Phys.*, 1979, **71**, 4546.
22. A. Kumar, R. R. Ernst, K. Wuthrich, *Biochem. Biophys. Res. Commun.*, 1980, **95**, 1.
23. A. A. Bothner-By, R. L. Stephens, J-M. Lee, *J. Am. Chem. Soc.*, 1984, **106**, 811.
24. D. G. Davis, A. Bax, *J. Magn. Reson.*, 1985, **63**, 207.
25. D. Neuhaus, M. P. Williamson, in 'The nuclear Overhauser effect in structural and conformational analysis', VCH, Cambridge (UK), 1989, p.253.
26. D. Canet, in 'Nuclear magnetic resonance: Concepts and methods', John Wiley & Sons, Chichester (UK), 1991, p.156.
27. S. W. Homans, 'A dictionary of concepts in NMR', Clarendon Press, Oxford (UK), 1989, p. 307.
28. D. Neuhaus, M. P. Williamson, in 'The nuclear Overhauser effect in structural and conformational analysis', VCH, Cambridge (UK), 1989, p.312.
29. R. Freeman, in ' Spin choreography: Basic steps in high resolution NMR', Macmillan Press, Houndmills (UK), 1997, p.264.
30. F. J. M. Van de Ven, in ' Multidimensional NMR in liquids: Basic principles and experimental methods', VCH, Cambridge (UK), 1995, p.255.
31. G. Bodenhausen, D. J. Ruben, *Chem. Phys. Lett.*, 1980, **65**, 185.
32. G. A. Morris, R. Freeman, *J. Am. Chem. Soc.*, 1979, **101**, 760.
33. D. M. Doddrell, D. T. Pegg, M. R. Bendall, *J. Magn. Reson.*, 1982, **48**, 272.
34. A. Bax, in ' Two-dimensional nuclear magnetic resonance in liquids', Delft University Press, Dordrecht (Holland), 1982, p.155.
35. J. C. Beloeil, M. A. Delsuc, J. Y. Lallemand, G. Dauphin, G, Jeminet, *J. Org. Chem.*, 1984, **49**, 1797.
36. D. H. Davies, E. W. Snape, P. J. Suter, *J. Chem. Soc., Chem. Commun.*, 1981, 1073.

Chapter 6
Experimental

6.1 Experimental of chapter 2

6.1.1 Materials and methods

All the studies of cationomycin concerning the (Minimum Inhibitory Concentration) MIC determinations, antimalarial activity, erythrocytes experiments, and potentiometry (sodium, potassium and hydrogen) measurements were carried out at the University of Clermont- Ferrand (France). The kinetic studies of cationomycin involving the LUVs were investigated at the University of St Andrews (UK) and are presented as part of the original work in this thesis.

6.1.1.1 Origin of ionophores

Pure monensin A was produced by the University of Clermond-Ferrand (France) from *Streptomyces cinnamonensis* strain ATCC 15413. Cationomycin was obtained from Kaken Pharmaceutical (Japan) through a joint venture with Sanofi and the University of Clermond-Ferrand (France). Deacylcationomycin was prepared as previously described.[1]

6.1.1.2 MIC determinations

Minimum Inhibitory Concentration (MIC) of monensin, cationomycin, and deacylcationomycin derivatives were determined classically on *Bacillus cereus* ATCC 14579 in Mueller-Hinton broth, pH 7.4 (DIFCO) after 24 h incubation at 300 K. Ionophores dissolved in DMSO were added to 18 tubes; the concentration range was from 100 mg/ml to 1.56 ng/ml.

6.1.1.3 *In vitro* antimalarial activity against *P. falciparum*

Drug effects on the Nigerian strain of *Plasmodium falciparum* growth were measured *in vitro* in microlitre plates according to Desjardins.[2] Growth inhibition in the presence of the various compounds was expressed as percent of control parasitemia observed without drug. IC_{50} values, which represent the drug concentration required to inhibit parasite growth by 50%, were evaluated from the plot of log dose *versus* parasite growth expressed as a percent of the control and

are the means of at least two independent experiments, each in triplicate, using different stock drug solutions in DMSO. The IC_{50} values for monensin and cationomycin were previously published by the French team.[3] The value for deacylcationomycin was obtained under the same experimental conditions.

6.1.2 Experiments with LUVs

Large unilamellar vesicles were prepared from egg-yolk PC (Phosphatidylcholine) by a modification of the dialytic detergent removal technique introduced by Reynolds[4] and coworkers and described in previous papers from our group.[5-7] A typical preparation would have approximately 30 mmol of lipid in 1.5 ml of salt solution. Three dialyses (2 litres each, > 12 hours each) at 313 K against the chloride of the appropriate metal produced large, detergent-free, unilamellar vesicles with the same concentration of metal ion inside and outside. A final dialysis introduced tripolyphosphate into the external medium as described previously. Sufficient $DyCl_3$ (Na^+) or $TbNO_3$ (K^+), typically a few microliters of a 1M solution, was then added to generate a chemical shift difference of approximately 4 ppm for Na^+ and of 7 ppm for K^+.

Metal ion transport was studied by dynamic line broadening on either a Bruker AM 300 or Varian Unity 500 for (Na^+) at 308 K, or a Bruker MSL 500 (K^+) at 303 K. In all cases the spectrometer was field/ frequency locked on the deuterium resonance of D_2O in a capillary tube. Spectra were line broadened by typically 1Hz (Na^+) and 5Hz (K^+) to improve the signal to noise ratio. Approximately 90° pulse widths were employed with recycle delays of at least 3 times T_1 in all cases.
Addition of small aliquots (microlitre amounts of a standard solution of cationomycin in methanol) gave rise to dynamic line broadening effects which were then analysed as previously described to extract the rate constants. All lipids were purchased from Lipid Products.

6.1.3 Experiments with Red Blood Cells

All the experiments with Red Blood cells were conducted at the University of Clermont-Ferrand (France).

6.1.3.1 RBC preparation

Blood samples were collected from healthy adults in 50ml heparinised tubes and were immediately centrifuged to remove plasma and buffy coat (377 K, 300 g, 15 min.). Cells were washed three times with a sodium buffer containing 140 mM NaCl, 30 mM sucrose, 5mM NaH_2PO_4, pH 7.4 adjusted with sodium hydroxide. For ^{23}Na NMR experiments, the third wash was performed with a choline buffer containing 80 mM NaCl, 60 mM $Na_7Dy(PPP_i)_2$. Packed cells (hematocrit ~ 80%) were kept at 273 K and diluted just before use in the buffer. All the experiments were carried out at 310 K (a preincubation of about 15 min. was necessary for temperature equilibration).
The hematocrit was adjusted to approx. 40 % for ^{23}Na NMR experiments. These are typical values for human whole blood hematocrit. For K^+ and H^+ potentiometry experiments, the final hematocrit was ~ 20 %.
Cell viability was confirmed by ^{31}P NMR analysis, ATP was clearly detectable in the spectra.[8] Neither [ATP] nor the pH had changed after 45 min. kinetic run or even after 12 hours. Another indication of cell viability was the maintenance of Na^+ and K^+ gradients in the absence of an ionophore.

6.1.3.2 Sodium NMR experiments

^{23}Na NMR experiments were performed on a Bruker MSL 300 spectrometer at 79.39 MHz and 310 K. 2 ml of the cell suspension was transferred to 10 mm diameter tubes; a coaxial capillary (1 mm diameter) containing 7 $x10^{-3}$ M $[Na_7Dy(PPP_i)_2]$ in D_2O was used as an external intensity reference, and its calibration gave an equivalence for 16.7 mM sodium. Shimming and field frequency locking were carried out with D_2O.
The presence of $[Dy(PPP_i)_2.^{7-}]$ in the cell suspension allowed the distinction of Na^+_{in} from the Na^+_{out} signal; it was shown to be non-toxic for erythrocytes by Ogino and coworkers.[9] It was prepared from $Na_5(PPP_i)$ and $DyCl_3.H_2O$ (molar ratio 2:1). ^{23}Na NMR spectra were accumulated in 1 or 2 min. blocks over 40 min. (90° pulse 16.5 µs, repetition time 0.4 s, 150 or 300 scans, 2 K data points). No line feed correction was applied, and direct measurements of the sodium areas were achieved by computer integration of the NMR signals. For the various kinetic runs recorded in the presence of ionophores, the sum of the NMR integrations of Na^+_{in} and Na^+_{out} signals remained constant. This clearly

indicates that Na^+_{in} was 100% visible, in agreement with other work.[8-13] [Na^+] is given for an hematocrit of 40%; internal sodium content [Na^+_{in}] was calculated as follows:

$$[Na^+_{in}] = 47.4 \frac{A_{in}}{A_{ref}}$$

A_{in} and A_{ref} are the integrals of internal sodium and sodium in the capillary determined from ^{23}Na NMR spectra. The variation of the internal content of sodium is expressed as

$$\Delta Na^+ = Na^+_{\text{time t}} - Na^+_{\text{time 0}}$$

Each experiment was repeated 3 to 5 times, and the mean values were plotted (the relative error did not exceed 10%).

6.1.3.3 Potassium potentiometry

The experiments were performed in a thermostatically controlled cell with magnetic stirring and the K^+ concentrations were measured with a selective electrode (Ingold type 15 221 3000) previously calibrated.
Typically, 1.66 ml of the packed cells and 5 ml of buffer were incubated at 310 K for 15 min., 20 ml of a solution of ionophore in DMSO were added and data were recorded for 45 min. Each experiment was repeated 3 to 5 times, and the mean values were plotted (the relative error did not exceed 10 %).

6.1.3.4 Hydrogen potentiometry

The external pH was measured with a glass electrode (Ingold, U-402-2S7) previously calibrated as previously described.[13]

6.1.3.5 Ionic current (i) of sodium and potassium

$i=k.[^mHA]$
i= current of Na^+ or K^+ expressed in mmol. min^{-1} with respect to 1 ml of erythrocyte suspension.

k: kinetic constant of transport
$[^{m}HA]$: ionophore concentration in the membrane. $[^{m}HA] = [^{t}HA] \times (^{t}V/^{m}V)$
$[^{t}HA]$ analytical ionophore concentration in the whole suspension.
^{m}V is the volume of the membrane. It was evaluated as follows: the number of cells per ml was calculated from the normal mean cell volume of 87 mm^3 and found to be 2.3 $x10^9$ $cells.ml^{-1}$ for potentiometry experiments (20% hematocrit) and 4.6 $x10^9$ $cells.ml^{-1}$ for NMR experiments (40% hematocrit). The thickness of the erythrocyte membrane was taken to be about 35 Å, the volume of the membrane in 1 ml of erythrocytes suspension was thus 7.6 $x10^{20}$ $Å^3$ and 15.3 $x10^{20}$ $Å^3$ for potentiometry and for NMR experiments respectively. As an illustration, a concentration of 2 $x10^{-7}$ M in the whole suspension ($[^{t}HA]$) corresponds to a concentration in the membrane ($[^{m}HA]$ of 1.3 $x10^{-4}$ M for NMR experiments and 2.6 $x10^{-4}$ M for potentiometry.

The currents of Na^+ influx into the cells were determined graphically (initial rates) from ^{23}Na NMR experiments. The currents of K^+ efflux were determined graphically (initial rates) from potentiometry measurements.

6.2 Experimental of chapter 3

Large unilamellar vesicles were prepared from egg-yolk phosphatidylcholine by a modification of the dialytic detergent removal technique introduced by Reynolds and coworkers[4] and described in our previous papers.[5-7] A typical preparation would have a total of ca 50- 60 mmol of lipid in 3 ml of aqueous lithium chloride solution (100 mM). Three 12 h dialyses (>2 liters each) at 313 K produced large detergent-free unilamellar vesicles (LUV). The vesicle suspension was split into three measured portions of about 1 ml each and to each portion was added an equal volume of a solution containing sodium tripolyphosphate (10 mM), sodium chloride (50 mM), and choline chloride (20 mM). A small amount (1-2 ml) of a solution of dysprosium chloride (1 M) was then added to generate a chemical shift difference of *ca* 4.5 ppm between the 'in' and 'out' ^{23}Na signals.
^{23}Na NMR spectra were recorded on a Bruker MSL 500 spectrometer operating in high resolution mode using 10 mm o.d. tubes. In all cases, the spectrometer was field-frequency locked on the ^{2}H signal from $^{2}H_2O$ in the inner compartment of a coaxial tube. All spectra were obtained at ambient laboratory temperature

(293 K). Passive exchange of the Li^+ inside the vesicles (initially 100% of the alkali metal ions in) with the Na^+ outside the vesicles (initially 50% of the alkali metal ions out) was followed by measuring the intensity of the 'in' signal for *ca* 20 min., at which point an aliquot of ionophore in methanol solution (a few µl) was added rapidly and the rate of passive plus mediated exchange was measured. The amount of ionophore added was sufficient to generate an ionophore/PC ratio of between 1/1000 and 1/200. The infinity value for the 'in' signal was found either by allowing the system itself to reach equilibrium or by adding a small amount of an efficient naturally occuring ionophore such as salinomycin. The difference between the rates gave the mediated rate of exchange.
The egg yolk phosphatidylcholine was purchased from Lipid Products.

6.3 Experimental of chapter 4

6.3.1 Experiments with LUVs

Vesicle suspensions were prepared at 277 K as described previously[5-7] from egg yolk phosphatidylcholine using the dialytic detergent removal technique introduced by Reynolds.[4] Egg yolk phosphatidylcholine was supplied by Lipid Products. NMR spectra were run on a Bruker MSL 500 spectrometer using 10 mm o.d. tubes with a coaxial capillary tube containing D_2O as field /frequency lock. Operating frequencies were ^{35}Cl at 49.00 MHz ; ^{81}Br at 135.07 MHz. Ninety degree pulses were used with interpulse delays of 250 ms (at least five times T_1).
In a typical preparation, 61.6 mmol of PC together with 15 equivalents of n-octyl glucopyranoside (Sigma) were dissolved in 3 ml 200 mM NaCl solution. This solution was then dialysed against 2 litres of 200 mM NaCl solution in a cold room (approx. 277 K). The external solution was changed four times at 10-12 hour intervals. The vesicle suspension was split into three measured portions of about 1 ml each portion and to each portion was added 1ml of NaBr (200 mM). A volume 15 µl of Mn^{2+} (1M) was added to generate a relaxation time difference between the 'in' and 'out' $^{35}Cl^-$ signals, broadening the external signal until it was no longer visible.

6.4 Experimental of chapter 5

Tetronasin[14] Na^+ salt (*ca.* 10 mg) was dissolved 1 ml $CDCl_3$ and was stirred under 1 M NaCl for 30 minutes and the organic layer containing $CDCl_3$ was taken and was filtered through a Pasteur pipette with a small plug of glass wool and small amount of anhydrous Na_2CO_3. In order to avoid any paramagnetic effects due to the presence oxygen in the $CDCl_3$, the 5 mm NMR tube was degassed three times and sealed.

All NMR spectra were recorded on a Varian Unity 500 at 303 K. All 2D spectra were recorded and processed in the phase sensitive mode with quadrature detection in both dimensions. Prior to two-dimensional Fourier Transformation, data were apodised by the application of a sine-bell shift function in order to improve the effective resolution.

(1) 1D 1H NMR spectrum (500 MHz): size 8 K; sweep width 5656 Hz, 16 scans.

(2) COSY 45 spectra: D1-90°-t_1-45°-t_2; relaxation delay 1.6 s, 90° pulse 7.8 μs.

(3) DQF-COSY spectra: D1-90°-90°-t_1-90°-t_2; relaxation delay 1.5 s, 90° pulse 7.9 μs.

(4) Relay-COSY: D1-90°-t_1-90°-Δ-180°-Δ–t_2: relaxation delay 2.0 s, 90° pulse 7.9 μs, Δ= 32.2 ms.

(5) TOCSY spectra (500 MHz): pulse sequence D1-90°-t_1- MLEV17-t_2; relaxation delay D1=1.6 s; 8 scans for each of 512 t_1 increments; size in acquisition domain 4 K; duration spin lock period 80 ms.

(6) NOESY spectra: pulse sequence D1-90°-t_1-90°-t_{mix}-90°-t_2; relaxation delay 1.3 s, 90° pulse 7.6 μs

(7) ROESY spectrum: D1-90°-t_1-spin lock-t_2; relaxation delay1.5 s, 90° pulse7.6 μs.

(8) HSQC spectrum: D1-90°-Δ-180°-Δ–90°-180°-Δ–90°-180°
with GARP decoupling, Δ= 16 ms, 90° pulse7.6 μs.

(9) DEPT spectra: D1-90°-180°-θ° relaxation delay 2.8 s, θ°=45°, 90°, 135°, 90° pulse11.2 μs for ^1H , 90° pulse10 μs for ^{13}C.

References to chapter 6

1. M. Ubukata, Y. Hamazaki, K. Isono, *Agric. Biol. Chem.*,1986, **50**, 1153.
2. R. E. Desjardins, C. J. Canfield, J. D. Haynes, J. D. Chulay, *Antimicrob. Agents Chemother.*, 1979, **16**, 710.
3. C. Gumila, M. L. Ancelin, G. Jeminet, A. M. Delort, G. Miguel, H. Vial, *Antimicrob. Agents Chemother.* , 1996, **3**, 602.
4. L. T. Mimms, G. Zampighi, Y. Nozaki, C. Tanford, J. A. Reynolds, *Biochemistry*, 1981, **20**, 833.
5. F. G. Riddell, S. Arumugam, P. J. Brophy, B. G. Cox, M. C. H. Payne, T. E. Southon, *J. Am. Chem. Soc.*, 1988, **110**, 734.
6. F. G. Riddell, S. Arumugam, B. G. Cox, *Biochem. Biophys. Acta.*, 1988, **944**, 279.
7. F. G. Riddell, S. J. Tompsett, *Biochem. Biophys. Acta*, 1990, **1024**, 193.
8. M. Rochdi, A. M. Delort, J. Guyot, M. Sancelme, G. Dauphin, G. Jeminet, *Bioelectrochem. Bioeng.*, 1994, **33**, 83.
9. T. Ogino, G. I. Shulman, M. J. Avison, S. R. Gullans, J. A. Den Hollander, R. G. Shulman, *Proc. Nat. Acad. Sci.*, 1985, 1099.
10. E. Fernandez, J. Grandjean, P. Laszlo, *Eur. J. Biochem.*, 1987, **167**, 353.
11. R. S. Hotchkiss, S. K. Song, C. S. Ling, J. J. H. Ackerman, I. E. Karl, *Am. J. Physiol.*, 1990, R21.
12. J. P. Monti, M. Baz, R. Elsen, Y. F. Berland, A. D. Crevat, *Biochem. Biophys. Acta*, 1990, **1027**, 31.
13. M. Rochdi, A. M. Delort, J. Guyot, M. Sancelme, S. Gibot, J. G. Gourcy, G. Dauphin, C. Gumila, H. Vial, G. Jeminet, *J. Med. Chem.*, 1996, **39**, 588.
14. D. H. Davies, E. W. Snape, P. J. Suter, *J. Chem. Soc., Chem. Commun.*, 1981, 1073.

Chapter 7
Conclusions and future work

7.1 Conclusions with ionophoric antibiotics

The aim of this section was to study the exchange rate of alkali cations mediated by polyether antibiotics such as cationomycin. These kinetic studies have established a linear relationship in accord with previous investigations and involved a 1:1 complex between sodium or potassium and the cationomycin during the transport process. These kinetic investigations enable us to calculate the rate constants of formation (k_f) and dissociation (k_d) in the membrane. The gradients of both graphs show very similar dissociation rates and the main difference is in the intercepts which show that the K^+ complex has a more rapid formation rate. The ratio of gradient to intercept gives the stability constant of the metal/ ionophore complexes in the membrane surface and it is the K^+ complex that is the more stable. The values for K^+ are lower than those for Na^+ showing more rapid transport of K^+ at all concentrations studied. Cationomycin both transports K^+ more rapidly than Na^+ and forms a more stable complex with K^+. In biological systems cationomycin will be almost exclusively involved in K^+ transport.

7.2 Conclusions with spirotetrahydrofuran analogues

The aim of this section was to study the kinetics of spirotetrahydrofuran analogues provided by Prof. Leo Paquette (The Ohio State University). The structures of these analogues were calculated and optimised by modelling programs. However, the exchange rates obtained showed poor alkali metal ion transport in comparison with polyether antibiotics. It is worth noting that all these analogues possess a spirotetrahydrofuran group which is present in polyether antibiotics. No logical and definitive answer has yet been found to explain these mediocre rates. The 'non' wrapping alkali cations and the absence of strong binding between alkali cations and oxygens atoms lead to unstable complexes. In the membrane interface, this 'chelation' is destroyed and therefore no alkali cation exchange is observed.

7.3 Conclusion and future work with steroid-based cryptands for halide anions

It is not possible from the preliminary studies to draw any definitive conclusions and further work needs to be carried out in order to understand fully the kinetics of these steroid-based cryptands.

The kinetic result for chloride /bromide anions mediated with anionophore 1 (methyl-3α-(p-nitro phenyl sulfonyl amino)- cholanoate) reveals that the transport rate increases as Cl/Br increases until reaching a saturation point. At this stage, all vesicles are used in the transport of Cl/Br exchange.

On the other hand, the exchange rate of anionophore 2 (eicosyl-3α-(p-nitro phenyl sulfonyl amino)-7α,12α-trifluoro methyl phenyl amino carbonyloxy) cholanoate and anionophore 3 (methyl-3α-(p-nitro phenyl sulfonyl amino)-7α,12α-trifluoro methyl phenyl amino carbonyloxy) cholanoate) displays a linear relationship suggesting a first-order kinetic process.

7.4 Conclusion and future work with tetronasin

A complete assignment of tetronasin has been established with the use of two dimensional techniques. The next step will be the structural determination of tetronasin. The main source of geometrical information employed in determining 3D structures of macromolecules by NMR spectroscopy is derived from nuclear Overhauser enhancement (nOe) measurements. This enables us to deduce to the proximity of protons in space and the geometry.

APPENDIX1

The transport data for cationomycin with sodium and potassium.
Concentration of cationomycin in methanol [C]= 1.363 mM

Cationomycin(ml)	$w_{1/2}$/ Hz	Cat/PC x10^{-4}	Rate=$\pi.\Delta\omega$/Hz
0	13.61	0	0
10	14.55	3.81	2.95
20	15.39	7.62	5.59
30	16.61	14.13	9.42
40	20.01	15.24	20.11
50	21.60	19.05	25.10

Cationomycin vs [Na^+] at 25 mM

Cationomycin(ml)	$w_{1/2}$/ Hz	Cat/PC x10^{-4}	Rate=$\pi.\Delta\omega$/Hz
0	11.41	0	0
5	12.55	1.78	3.58
10	12.82	3.56	4.42
20	13.45	7.12	6.41
30	15.48	10.68	12.79
40	17.66	14.24	19.63
50	18.88	17.80	23.47
70	22.47	24.92	34.75
80	23.56	28.48	38.17
100	24.16	35.60	40.06

Cationomycin vs [Na^+] at 50 mM

Cationomycin(ml)	$w_{1/2}$/ Hz	Cat/PC x10^{-4}	Rate=$\pi.\Delta\omega$/Hz
0	14.19	0	0
10	15.60	3.19	4.43
20	15.66	6.38	4.62
30	17.14	9.57	9.27
40	18.46	12.76	13.41
60	21.82	19.14	23.97
80	23.99	25.52	30.78
100	26.36	31.90	38.28

Cationomycin vs [Na^+] at 75 mM

Cationomycin(ml)	$w_{1/2}$/ Hz	Cat/PC x10^{-4}	Rate=$\pi.\Delta\omega$/Hz
0	11.12	0	0
5	12.01	1.91	2.80
10	12.02	3.82	2.83
20	14.34	7.64	10.16
30	14.43	11.46	10.40
40	15.93	15.28	15.11
50	15.66	19.10	14.26
60	17.01	22.92	18.50
70	17.59	26.74	20.32
100	20.91	38.20	30.76

Cationomycin vs [Na^+] at 100 mM

Cationomycin(ml)	$w_{1/2}$/ Hz	Cat/PC x10^{-4}	Rate=$\pi.\Delta\omega$/Hz
0	11.55	0	0
10	12.47	3.82	2.89
20	14.28	7.64	8.58
40	15.09	15.28	11.12
60	16.11	22.92	14.32
80	18.43	30.56	21.61
100	22.39	38.20	34.05
120	23.78	45.84	38.42

Cationomycin vs [Na^+] at 100 mM

Cationomycin(ml)	$w_{1/2}$/ Hz	Cat/PC x10^{-4}	Rate=$\pi.\Delta\omega$/Hz
0	24.55	0	0
10	28.31	4.71	13.38
20	29.26	9.42	16.37
30	30.87	14.13	21.43
40	31.27	18.84	22.68
50	34.03	23.55	31.35
60	33.96	28.26	31.13
70	36.72	32.97	38.70
80	37.62	37.68	42.82
90	37.10	42.39	41.00
100	38.53	47.10	45.49

Cationomycin vs [Na^+] at 125 mM

Cationomycin(ml)	$w_{1/2}$/ Hz	Cat/PC x10^{-4}	Rate=$\pi.\Delta\omega$/Hz
0	13.16	0	0
2	15.36	2.68	6.88
5	16.08	6.70	9.17
10	19.74	13.40	20.67
15	21.56	20.10	26.39
20	28.51	26.80	48.22
25	31.80	33.50	58.56
30	45.32	40.20	101.03

Cationomycin vs [K^+] at 50 mM

Cationomycin(ml)	$w_{1/2}$/ Hz	Cat/PC x10^{-4}	Rate=$\pi.\Delta\omega$/Hz
0	10.01	0	0
10	10.50	3.36	1.54
15	10.74	5.04	2.29
20	11.23	6.72	3.83
30	14.89	10.08	15.33
40	17.58	13.44	23.78
50	18.80	16.80	27.61
70	21.48	23.52	36.04
80	25.63	86.11	49.07

Cationomycin vs [K^+] at 100 mM

Cationomycin(ml)	$w_{1/2}$/ Hz	Cat/PC x10^{-4}	Rate=$\pi.\Delta\omega$/Hz
0	8.79	0	0
10	12.70	4.01	12.30
20	12.94	8.02	13.03
30	15.38	12.04	20.07
40	14.16	16.05	16.87
50	18.31	20.06	29.91
70	17.58	28.08	27.61

Cationomycin vs [K^+] at 150 mM

Cationomycin(ml)	$w_{1/2}$/ Hz	Cat/PC x10^{-4}	Rate=$\pi.\Delta\omega$/Hz
0	12.70	0	0
5	14.60	1.80	5.97
10	15.62	3.60	9.17
20	17.09	7.20	13.79
25	17.09	9.00	13.79
30	18.55	10.80	18.37
40	18.55	14.40	18.37
50	17.09	18.00	13.79
60	18.07	21.60	16.87
70	21.97	25.20	29.12
80	20.51	28.80	24.53
100	25.39	36.60	39.86

Cationomycin vs [K^+] at 150 mM

Cationomycin(ml)	$w_{1/2}$/ Hz	Cat/PC x10^{-4}	Rate=$\pi.\Delta\omega$/Hz
0	15.14	0	0
5	16.11	2.45	3.05
10	18.55	4.90	10.71
20	19.53	9.80	13.79
30	22.53	14.70	24.54
40	21.48	19.60	19.92
50	21.97	24.50	21.46
60	23.93	29.40	27.61
70	23.93	34.30	27.61
80	26.86	39.20	36.82
100	26.37	49.00	35.28

Cationomycin vs [K^+] at 150 mM